UiT The Arctic University of Norway

Faculty of Engineering Science and Technology

Shell-based finite element modeling of Herøysund Bridge

Zeeshan Azad

Master's Thesis in Engineering Design, END-3900-1-23V, May 2023

Master thesis on Shell-based Finite element Modelling of Herøysund Bridge

University of Tromsø – The Arctic University of Norway

IVT, Faculty of Engineering Science and Technology Engineering Design

PO box 385, 8501 Narvik, Tlf: 76 96 60 00

Title: Shell based Finite element Modelling of Herøysund Bridge		***Date:*** 15.5.2023 ***Number of report pages:*** 54 ***Attachment pages:*** 33 ***Total number of pages:*** 87
Subject code: END-3900-1 23V	***Subject name:*** Masters thesis	
Author: Zeeshan Azad		
Department: Department of Computer Science and Computational Engineering	***Field of study:*** Master of science in engineering design	
Supervisors: Dr. Harpal Singh, UiT Narvik, Norway Professor Vanni Nicoletti, Marche Polytechnic University, Italy		
Partners: Statens Vegvesen, Nordland fylkeskommune, SINTEF, NTNU.		
Keywords: Herøysund Bridge, shell, 3d solid, fea, concrete, modal analysis, MAC, post-tensioned, structural health monitoring.		

Table of Contents

Software used	**Components**	**Skill (1-10)**
ANSYS 2023 R1	Space-claim, workbench, mechanical	9
Solidworks 2023	3D- parts and assembly modeling	10
Autodesk Civil 3D	2D- drawing analysis	8
Microsoft visio	Pictures and illustrations	10

List of Tables

List of Figures

M.Sc. in Engineering Design

This thesis study is a requirement of the END-3900-1 23V master thesis course, which serves as the final component of the engineering design master's programme at UiT Narvik. The course centers on completing an individual 30 ECTS master's thesis, thoroughly documented with a comprehensive report detailing the theoretical framework, computational aspects, and simulation results. The project aims to provide students with the opportunity to apply their knowledge and skills acquired from previous courses and to undertake an individual project relevant to the master's programme. Moreover, the course evaluates the learning outcomes, consisting of both theoretical and practical components. By conducting literature studies of previous works in the field and related disciplines and problem-solving, students acquire an extensive understanding of the subject matter.

Acknowledgment

I would like to express my sincere gratitude to the project partners of the Herøy FoU project [100397], that provided all the necessary resources for the successful completion of this master's thesis. I would also extend my appreciation to Per Ove Ravats (Advisor, Nordland Fylke) for his invaluable guidance, site visit, and exceptional availability throughout this masters thesis, Espen Dahl-Mortensen (Construction Manager at Norland Fylkeskommune), and Roy Eivind Antonsen for their kind assistance in providing the drawings and access to bridge archive data for Herøysund Bridge. I am also grateful to the supervisors, Dr. Harpal Singh and Dr. Vanni Nicoletti, who provided invaluable guidance and assistance throughout the project.

Additionally, the significant guidance and support provided by respectable faculty, including Andreas Seger, Guy Beeri Mauseth, and Per Johan Nicklasson are highly appreciated. The supervisors and partners provided unwavering support in an engaging, educational, and challenging thesis. Also, I would like to thank my classmate Patrick Norheim Berg working on Beam of the bridge, for collaboration on understanding the model, discussions and productive dialogue. Lastly, immense gratitude is expressed towards family, especially siblings and parents, for their genuine support throughout the academic journey.

Zeeshan Azad
Narvik 2023

Abstract

This master's thesis thoroughly examines the application of the Finite Element Method (FEM) to the numerical modal analysis of the Herøysund Bridge, focusing on the theoretical backdrop, construction process, FEM techniques, and Eurocode recommendations for concrete structures. This study aims to demonstrate the utility of FEM in bridge analysis by utilizing ANSYS 2023 R1 to conduct a full numerical investigation of the bridge's technical specifications and design features. The thesis discusses the theoretical background, including the context of applying FEM for bridge design and main bridge construction techniques. It then examines the specific FEM approaches applied and their advantages and disadvantages. The Herøysund Bridge analysis employs a two-pronged strategy consisting of a 3D-Solid Model and a Shell Model. To forecast the physical behavior of a structure, assumptions, modeling methodologies, and the incorporation of specific components such as pillars are applied to both approaches. The document describes the complexity of bridge design from the selection of units and materials through the development of connections and meshes.

The full report also emphasizes the importance of boundary conditions, examining the structural effects of standard earth gravity, post-tensioned load, and railing and asphalt load. The results section thoroughly explores the mode shapes and frequencies for the 3D-Solid and Shell models. The Modal Assurance Criteria analysis compares modal frequencies across several modes, including flexural, transverse bending, and twist modes. The conclusion of the thesis includes findings obtained from the study, implications for the Herøysund Bridge, detailed resonant frequencies of the structure, and a comparison of both modeling strategies. It also incorporates ideas for future research. It also guides employing FEM 3D-Solid and Shell methods to design and construct more efficient, resilient, and durable bridge structures.

1 Introduction

1.1 Background

The research concerning the Herøysund Bridge in Herøy municipality, Nordland County, has resulted in the thesis project titled "Shell-based Finite Element Modelling of Herøysund Bridge." The research project is financed by Nordland fylkeskommune(NFK) and Statens Vegvesen. The research on this project is being conducted in partnership with NFK, Statens Vegvesen (SV), UiT Narvik, NTNU, and SINTEF (Project partners). The Herøysund Bridge is a self-supporting post-tensioned casted girder bridge built-in 1966. It has been extensively studied by various organizations, including AAS-Jakobsen, Multi-Consult, and NTNU, to monitor its condition and maintenance needs [1].

During the 2017 inspection by Multi-consult, the presence of corrosive chlorides in the concrete structure was detected, and subsequent restoration efforts revealed additional deterioration, leading to the decision to construct a new bridge [2]. AAS-Jakobsen later conducted capacity calculation and maintenance work in 2020 [3]. Highlighting the need for ongoing monitoring of the bridge's condition, while HBK Norge AS built a monitoring system for the Herøysund Bridge in 2021 [4]. The old bridge will remain accessible for light traffic until the new bridge's completion in 2024, with a weight restriction of fifty tons. NTNU researched the bridge's post-tensioned reinforcement corrosion in 2022 as part of the Better Bridge Maintenance DP2 project [5]. The Herøy FoU project uses probabilistic approaches to obtain information on the bridge's structure and post-tensioned system, along with detailed superstructure modeling. The primary objectives are to acquire comprehensive data on the bridge's current structural condition and conduct structural health monitoring (SHM). Additionally, assessments will be carried out on the bridge's post-tensioning system to comprehend the corrosion process and examine optimal repair strategies. Structural appraisals are to be performed to analyze various damage scenarios, and probabilistic approaches are employed to assess the dependability of the findings. These aims ensure the continued safety and reliability of the bridge. R & D activities are planned to be executed in the following four work packages:

1. WP1: Structural health monitoring
2. WP2: Corrosion inspection, assessment, and repair
3. WP3: Structural assessment with damaged post-tension
4. WP4: Reliability and uncertainty quantification

This thesis study focuses on WP1 SHM, where modal analysis will be done through Solid and Shell structural techniques in the Finite element method (FEM). In the second phase of the Herøy FoU project under WP1, one of the objectives is to conduct operational modal analysis (OMA) using accelerometers on Herøysund Bridge. The goal is to improve our understanding of the Herøysund Bridge's structural condition and develop effective strategies for automating bridge health monitoring to streamline maintenance and operational activities while enhancing safety.

1.2 Aim and objectives of master's thesis

The primary objective of this thesis is to develop parametric 3D-Solid and Shell models for a numerical modal analysis using FEM. In this study, the numerical structural analysis using appropriate boundary conditions and loads will serve as a pre-stress condition for the study's primary aim, which is to calculate the mode shapes and resonant frequencies of Herøysund concrete bridge via ANSYS 2023 R1 modal analysis module numerically. This thesis also aims to equip the researcher with crucial data and knowledge related to the FEM of this bridge for structural health monitoring (SHM) under self-weight and asphalt load conditions providing valuable insights concerning bridge construction back in 1966. As part of the continuing Herøy FoU project under WP1- SHM, This study also aims to provide a comprehensive numerical modal investigation of the Herøysund concrete bridge to make a significant contribution to the second phase of Herøy FoU WP1 along with an enhanced understanding of vibration responses, performance, and suitable FEM modeling strategy for the post-tensioned concrete bridge. The findings of this study will assist in critical decisions concerning the future construction of similar constructions, preventive maintenance techniques, and the necessity for repair or rehabilitation.

1.3 Impact of this study

In Norway, bridges lack adequate inspection and maintenance, leading to severe damage in over a thousand structures. This issue is especially concerning in northern Norway and coastal areas where bridges serve as critical infrastructural components, such as the Herøysund Bridge, crucial to local fishing industries [5]. This thesis study intends to improve the future of bridge construction by developing better techniques and methods for autonomous monitoring of structural health, addressing the considerable resources currently dedicated to bridge maintenance until now.

The initiative involves creating a 3D finite element model to contribute to the experimental results comparison in the second half of 2023. The Herøysund Bridge, currently with limited structural health and maintenance documentation, will be the centerpiece of this study. Since no 3D Solid and Shell-based finite element model exists for the Herøysund Bridge, this thesis study adds novelty. These insights could transform the approach to monitoring structural integrity, streamlining the process, reducing costs, and facilitating quicker responses to other complex bridges.

1.4 Thesis description

The thesis study includes developing reliable models representing the Herøysund Bridge's physical behavior. As the bridge will undergo in-situ testing shortly, the model should be accurate enough to replicate the actual bridge's behavior, enabling the design and interpretation of experimental test outcomes with the numerical results obtained in this study. Therefore, a detailed 3D-Solid element model and a 3D Shell element model will be created using Solidworks and ANSYS Space-claim. Both models will undergo structural and modal analysis to determine their natural frequencies and mode shapes under realistic boundary conditions. The last step is a comparison of both models in terms of vibration using the Modal assurance criterion(MAC) to identify the similarity of mode shapes in the models. That would validate FEM for the Shell-based model identifying the resonant frequencies. The results in terms of mode shapes, total deformation, and natural frequencies of the system would be obtained.

1.5 Scope

The scope of this thesis is to comprehensively model a FEM for the Herøysund Bridge, which includes analysis of the documentation available from NFK and SV, a detailed CAD model of the bridge, followed by an in-depth FEM using Solid and Shell elements in ANSYS. The complete focus of this study shall include the following:

i. Developing a detailed 3D-Solid CAD bridge model with sections, subsections, joints, and contact regions.
ii. Developing a mass-controlled Shell model using an appropriate methodology for coherence with a 3D-Solid model.
iii. Assessment of material models, specifications, and boundary conditions for a relatable numerical structural and modal analysis.
iv. Analytical reference of the super-structure with necessary simplifications from previous calculations and numerical simulation.

v. Structural & Modal analysis of the detailed model using ANSYS 2023 R1.

vi. Discussion on results and proposition for future work.

1.6 Regulations

The regulations reference for this study would be based upon the following.

- Standard Norway, NS: 3473 Design of concrete structures - Calculation and construction rules, second edition, 1975.
- Norwegian Public Roads Administration: Handbook 239 Use classification, Load regulations 1920-1973 and bridge standards 1912-1958, 2003.
- Norwegian Public Road Administration: Handbook R-412 Classification of use, 2014, with NA circular 2017.
- EN 1992-1-1 (2004) (English): Eurocode 2: Design of concrete structures, (4)P, Eurocode 2 Part 2, Reinforced and prestressed concrete bridges, EN 1991-1.1 Densities, body mass and external loads.

1.7 Thesis Schedule

This study has been classified into three phases, Q1, Q2, and Q3, respectively, defining the complete workflow timeline for this thesis study.

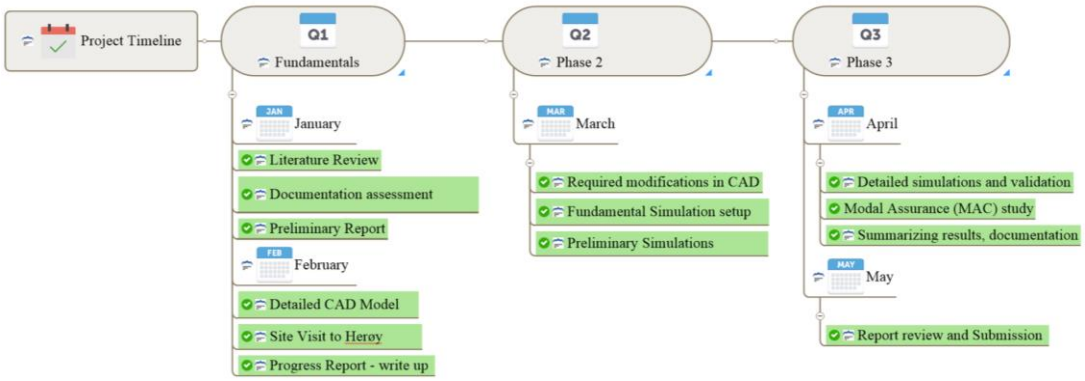

Figure 1. Thesis timeline

1.8 Herøysund Bridge specifications

The Herøysund Bridge (Construction no. 18-1069) is a post-tensioned cast-concrete bridge with variable heights, a bridge slab, underlying load-bearing beams, and pillars in Herøy, Helgeland-Nordland County that spans from south to north Herøy. It features seven axes, five columns, and two land vessels. It has a length of 154 m and an overall width of 5.30 m, with rock foundations. The categorization of the bridge's design is B-250 to B400, and its concrete density

is 2300 kilograms per cubic meter. The ratio of the weight of concrete to the importance of cement is 6.57. The load restrictions for the bridge are load class 2/1958, and the bridge was designed using the tension control method under the traffic load BK-10/50 [5].

Furthermore, the bridge has a cast-in-place pressure plate facing piers 4 and 5. The bridge between axes 3 and 6 is tension-reinforced, while the remainder is slack-reinforced. The bridge is constructed utilizing the stress control method [3], contrary to modern techniques, such as the partial factor method, which incorporates material and load factors;

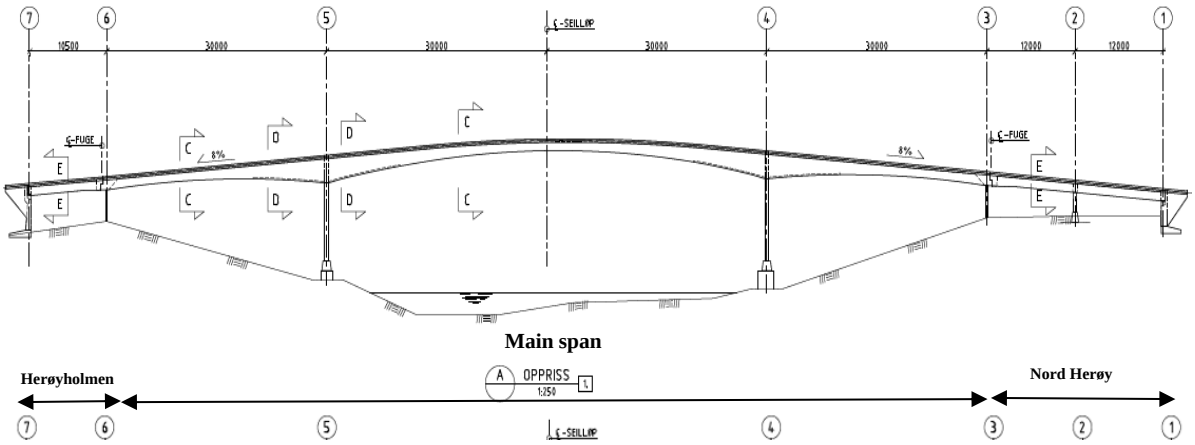

Figure 2. Herøysund Bridge layout [5]

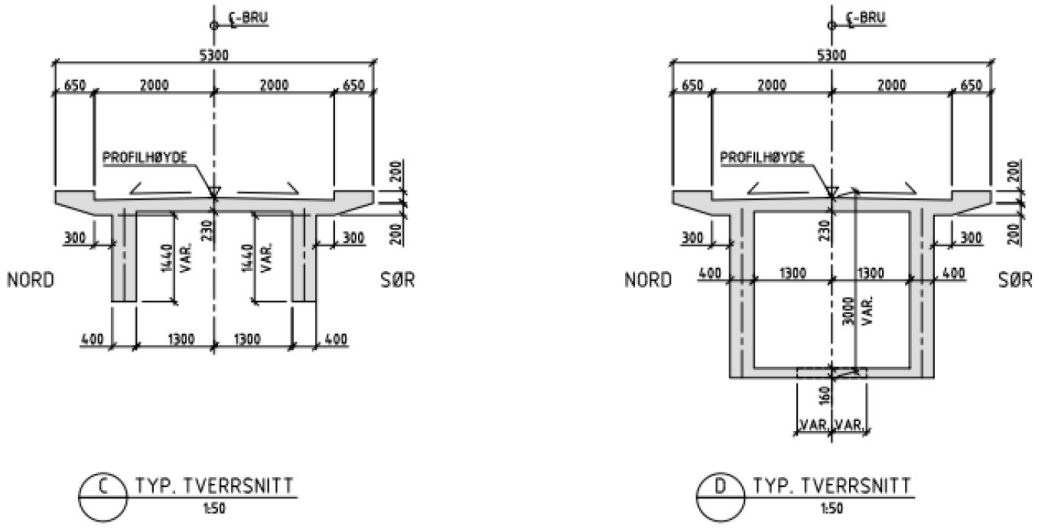

Figure 3. Section profiles variation from bridge span 1-7 [6]

2 Literature Review

2.1 Theoretical background

There are three primary types of contemporary concrete bridges: plain or unreinforced concrete, reinforced concrete, and prestressed concrete, as shown in Figure 4. The prestressing process is popular for a variety of reasons. For instance, precast beam bridges with straight tendons and single spans can reach up to 20 meters. The post-tensioning is frequently used for girders and decks that require longer spans, typically more than thirty meters, such as Herøysund Bridge. Concrete has high compressive but low tensile strength, so it involves reinforcement with high-tensile materials like steel to withstand tensile stresses. Steel is preferred due to its strength, thermal behavior, availability, and cost-effectiveness, but it rusts, reducing load capacity. Due to creep stresses, it also induces cracks as the bridge ages [7].

Prestressing enhances the flexural and tensile strength of concrete members beyond conventional concrete by tensioning the reinforcement within the concrete, generating compressive stress to counteract tensile stresses. It reduces materials usage and embodied energy and significantly reduces deflection. Members of prestressed concrete may include pre-tensioned or post-tensioned. Pre-tensioning is done during casting and transfers compressive stress through friction with the reinforcement [8].

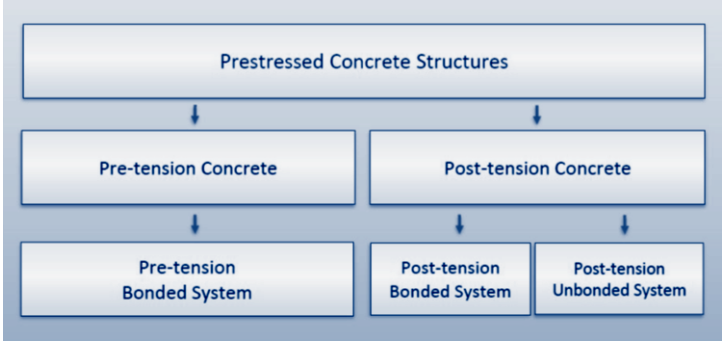

Figure 4. Prestressed concrete structure categories [9].

Post-tensioning involves developing After the concrete has hardened, the reinforcement experiences tension. It can be implemented in a bonded or unbonded system, with the unbonded system allowing for retightening of strands and the bonded system creating a connection between the strand and duct. Hydraulic jacks are used to stress the tendons, which are anchored to the surface of the concrete using mechanical anchorage devices.

The Herøysund Bridge is an unbonded post-tensioned structure with grouted anchors. It reduces the size and number of reinforcing bars in concrete members, resulting in material cost savings and lower maintenance and life-cycle costs. Additionally, the link formed between the strand and concrete in tension and compression and The interplay between tensional steel and compressional concrete contribute to a higher ultimate strength. Finally, post-tensioning permits complete section utilization, which aids in crack control [10].

2.2 Construction methodology

Concrete bridge-building techniques in Norway have been around since the early 20th century [11]. The most used bridge types are reinforced concrete bridges [12], [13], incremental launching method bridges [14], [15], precast concrete bridges [16], [17], and post-tensioned cast concrete bridges. The classification and construction methods for four general construction classes are in Appendix I and II. The main section discusses the appropriate construction method for a post-tensioned cast concrete girder bridge.

Cast concrete girder bridges evolved due to the limitations of older bridge designs [18]. They consist of concrete girders, horizontal beams that sustain the bridge's weight, and passing traffic. They are strengthened with steel bars to increase strength and longevity and are commonly precast or cast-in-place. The pillars and abutments are the vertical columns and supports that secure the girders and convey the bridge's weight to the ground. Decking is the surface of the bridge that traffic travels on, and bearings are the components that allow the bridge to move and expand or contract as the temperature changes [19]. A typical example of a post-tensioned girder bridge is demonstrated in Figure 5.

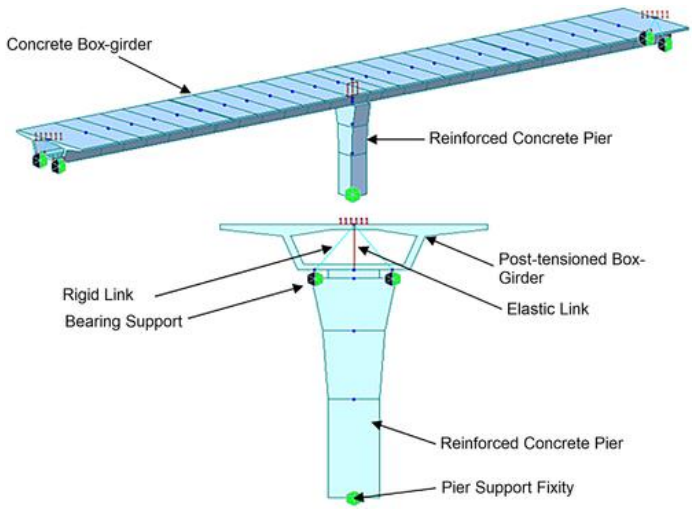

Figure 5. Post-tensioned cast box girder bridge [19]

2.3 Concrete bridges design in FEM

The following section signifies the importance of structural design methods for moments and forces distribution in bridges. It also reflects the theoretical background of FEM and its application in the concrete bridge industry. It is essential to mention that the base of numerical simulations heavily relies on the background aspects discussed in this section.

2.3.1 Background

FEM has revolutionized the analysis of concrete bridges, enabling engineers to develop models and assess their behavior under dead loads, live loads, wind, seismic loads, and varying boundary conditions. It provides vital information regarding the strength and stability of bridges, resulting in greater design precision, decreased dependency on physical testing, cost-effectiveness, and safety optimization. Case studies have shown the beneficial influence of numerical research on concrete bridges, leading to safer, more resilient, and long-lasting structures [20].

Researchers have conducted numerous case studies to solve a wide range of problems, such as a novel nonlinear analysis model created to examine the effects of creep and shrinkage on long-span prestressed concrete box girder bridges [21], construction of a prestressed concrete cable-stayed bridge by employing the progressive cantilever method in FEM [22], Shell model for the load-carrying capacity of prestressed concrete bridges under shear and torsion [23], and a new finite element model for analyzing the structural behavior of fiber-reinforced polymer (FRP)-strengthened steel-reinforced concrete (RC) beams under cyclic loading using FEM [24]. These case studies can be found in Appendix K for summarised for better correlation.

Using various FEM approaches, extensive research has examined concrete bridges' construction adaptability, serviceability, and reliability. The significance of the finite element approach for assessing concrete bridges is increasing with numerous advanced FEM models validated against the experimental results. It also indicates that FEM is one of the most reliable techniques for investigating superstructures.

2.3.2 Design methods

The choice of the FEM method for concrete bridge analysis depends on the complexity of the bridge geometry, accuracy, and loading conditions. 3D-Solid and Shell elements can be used to model long, slender structures with a low aspect ratio. Bridges with more complex geometry or slabs, walls, or other components with significant thickness, then 3D-Solid elements or 3D

Shell elements can be used in certain conditions. 3D-Solid element types are best suited for simulating thick components in bridges. In contrast, 3D Shell elements are best suited for simulating thin features, such as bridge decks and shear walls. The Herøysund Bridge has both types of components. Therefore, it is numerically evaluated using Solid and Shell element models in this study.

2.4 FEM Techniques

2.4.1.1 In Scope

The choice of analysis technique in FEM is of critical importance, as it directly affects the accuracy of results. This study involves structural and modal analysis of the bridge, and the methods that are used for FEM in such cases are:

- **Static linear analyses:** This method analyzes the structure under static loads and assumes linear behavior. The equations used are linear equations of equilibrium, which relate the applied loads to the corresponding stresses and strains.
- **Modal analysis**: Modal analysis examines the inherent frequencies and mode forms of a structure using FEM. At the system level, stiffness and mass matrices are formed after discretizing the structure into components. Solving the eigenvalue problem shows natural frequencies and mode shapes, aiding in the identification of resonance difficulties and high-stress vibrational zones [25].

Additionally, the design of concrete bridges inculcates approaches such as sensitivity analysis [26], optimization techniques [27], parametric modeling [28], probabilistic analysis [29], multi-objective optimization [30], and advanced material modeling [31] in FEM. These approaches are used to optimize the design of concrete bridges, assuring their safety, longevity, and efficiency, and FEM analysis provides significant insights into the bridge's behavior under varied loading circumstances. These relevant case studies are further explained for a deeper understanding in Appendix III Section A.

However, the scope of this study is required to comprehend the numerical vibrational behavior of the bridge. Therefore, proactive engineering design and optimization techniques using FEM are briefly introduced.

3 FEM Methodology

The following Section outlines six fundamental steps in the FEM analysis process for concrete structures. The section also details the accuracy and limitations of each step along-with the element orders, shapes, and degrees of freedom are also included for a deeper understanding of FEM.The computational implementation of FEM subsection provides the basis for fundamental equations, brief overview of linear and non-linear cases considerations and convergence differences [32]. A detailed explanation of these cases alongwith FEM process could be found in Appendix III section C.

3.1 FEM Process

The FEM Process generally includes idealization, discretization, element analysis, structural analysis, post-processing, and results phase, while numerous aspects concern the accuracy and limitations of each step. Therefore a brief layout of the process is shown in Figure 6 [33].

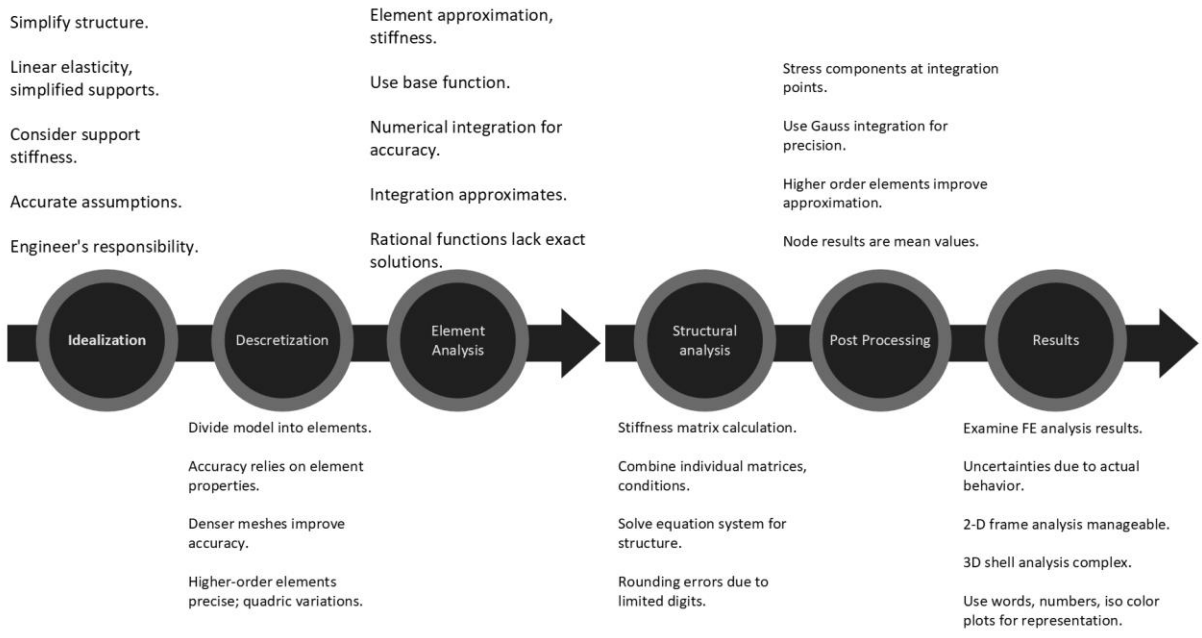

Figure 6. FEM methodology for concrete structures [33]

The detailed process of idealization, discretization, element analysis, structural analysis, post-processing, and results in concrete structures can be found in Appendix III Section C and for a deeper understanding of these topics (see, e.g. [34], [35], [36]).

3.1.1 Advantages and limitations of FEM

Each approach in FEM is unique depending on geometry, materials, configuration, and simplification. However, there could be circumstances where linear and non-linear analyses are

well suited. Some of the key advantages and disadvantages of both analysis types are discussed below (see e.g. [37]):

Table 1. Benefits and drawbacks of linear static analysis [37]

Advantages	Drawbacks
Simple linear equations	Only for linear elastic materials
Less computational time	Cannot account for transient conditions
Allows approximations to a certain extent	Inapplicable to large deformations/loads
Better for initial studies	Inaccurate approximations

Table 2. Advantages and drawbacks of non-linear static analysis [37]

Advantages	Drawbacks
Applicable to a vast range of materials	Complex and resource-intensive
Considers extreme deformations & loads	Requires specialized knowledge
Realistic boundary conditions	Convergence difficulties
Accurate results	High assumptions sensitivity

3.2 Eurocode recommendations for concrete structures

The standardization specifically for structural analysis of concrete structures sets a sound base in choosing an analysis type, such as linear or non-linear analysis. Moreover, it recommends methods for using 3D- Solid, beam, or Shell elements in FEM that provide valuable insight into problem definition and the correct approach toward understanding the behavior of concrete structures in experimental and numerical analysis. The guidelines in Eurocode 2, CEN (2001), recommend using linear or non-linear analysis methods for force distribution determination. Furthermore, EN 1992-1-1 Annex B refers to the scenarios for using 3D- Solid and Shell elements. The details and specifics of these regulations can be found in Appendix V [38].

3.3 Method selection for Herøysund Bridge

3.3.1 Type of analysis

The current study abides by the ULS in which the bridge is modeled in an uncracked and ideal state. As per the Eurocode recommendations, this study is focused on loading conditions such as self-weight and load from asphalt, while the joints are assumed to be frictionless. At the same time, the modal analysis would be performed for undamped conditions [38]. Considering the parameters of this study, Eurocode recommendations, and the absence of any non-linearity-

inducing parameters, the FEM for Solid and Shell models would be conducted in a linear elastic analysis using ANSYS 2023 R1.

3.3.2 Type of Elements

Furthermore, it is evident from the recommendations that specific parameters are best suited for a 3D- Solid and Shell element, respectively, for concrete structures. The scope of this study would cover both the element types and the comparison of models with Eurocode recommendations as a reference. Understanding the correct approach towards using elements for post-tensioned structures such as Herøysund Bridge would be beneficial.

4 Governing equations

The general governing equations for solid, shell models and modal analysis are discussed in this Section. The focus of this study is to perform a numerical simulation for Solid and Shell models, instead of development of new FE method for the structure. Therefore, for a general overview of governing equations will be discussed.

4.1 FEA Equations for solid body

In FEA, the governing differential equation is the equation of motion, based on Newton's law for the balance of forces acting on a Solid body,

$$\nabla . \sigma + F = \rho \ddot{u} \tag{4.1}$$

$\nabla . \sigma$ represents the divergence of stress tensor σ, i.e., the distribution of internal forces within the continuum, F represents external forces acting on the body, ρ is the density of the material, and the symbol u represents the displacement vector of the continuum, where $\ddot{u}$ Represents the acceleration of the material.

In the case of static analysis, the equation takes the form.

$$\nabla . \sigma + F = 0 \tag{4.2}$$

$$\frac{\partial \sigma_x}{\partial \mathrm{x}} + \frac{\partial \sigma_{xy}}{\partial \mathrm{y}} + \frac{\partial \sigma_{xz}}{\partial \mathrm{z}} + F_x = 0$$

$$\frac{\partial \sigma_{xy}}{\partial \mathrm{x}} + \frac{\partial \sigma_y}{\partial \mathrm{y}} + \frac{\partial \sigma_{yz}}{\partial \mathrm{z}} + F_y = 0$$

$$\frac{\partial \sigma_{xz}}{\partial \mathrm{x}} + \frac{\partial \sigma_{yz}}{\partial \mathrm{y}} + \frac{\partial \sigma_z}{\partial \mathrm{z}} + F_z = 0$$

The weak form of the governing equation is obtained using Galerkin's method [39]. That involves the multiplication of *equation (*4.2 by test functions, integration, and introducing

boundary conditions. From the weak form, we obtain the element formulation, which gives the stiffness matrix and force vector used in the FEM shown in the equation below:

$$[K]\{u\} = \{F\}. \tag{4.3}$$

where, K is the stiffness matrix, u is the displacement vector and F is the forces vector acting on the system. The FEM equation is then used for static analysis. The software initially calculates the displacements, and then the strains are determined. Finally, the stresses are computed from the strains, utilizing a constitutive equation below, Hooke's law for linear elastic materials.

$$\{\sigma\} = [D]\{\varepsilon\}. \tag{4.4}$$

where, $\{\sigma\}$ is the stress vector, $[D]$ is the elasticity matrix and $\{\varepsilon\}$ represents strain vector or matrix. Considering the primary focus of this study, i.e., Numerical prestressed modal analysis and governing equations provide insight into how the software computes the structure's displacements, stresses, and strains (see, e.g. [32] [40]).

4.2 Equations for Shell body

The Shell model in FEM is based on Kirchhoff–Love plate theory [41]. In this formulation, a position vector is defined on a mid-surface. A point in coordinates system is assumed and displacement corelation for point undergoes vector sum of mid-surface displacements, resulting into inplane deformation equations.

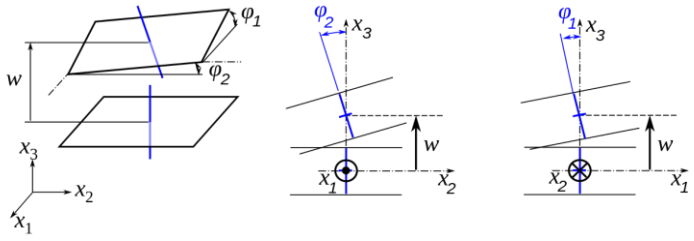

Figure 7. Kirchhof-Love plate theory for mid-surface shell elements

The position vector and point in cartesian coordinates in equations below.

$$x = x_1 e_1 + x_2 e_2 + x_3 e_3 = x_i e_i. \tag{4.5}$$

where, e_i is the cartesian basis, x_1, x_2 are cartesian coordinates of undeformed plate and x_3 is the coordinare in thickness direction and the displacement point of plate $u(x)$,

$$u(x) = u_1 e_1 + u_2 e_2 + u_3 e_3 = u_i e_{i,} \tag{4.6}$$

where, using vector sum of mid-surface displacements u_α^0, and out of plane displacement ω^0 in x_3 direction we can use in plane displacement of the mid surface of the following form, where $\alpha = 1,2$,

$$u^0 = u_1^0 e_1 + u_2^0 e_2 = u_\alpha^0 e_\alpha. \tag{4.7}$$

The Kirchhoff hypothesis takes the form for displacement field, as in equation below.

$$\frac{\partial \omega^0}{\partial x_\alpha} = u_\alpha^0 - \omega_\alpha^0 x_3 \; ; \; \alpha = 1,2 \tag{4.8}$$

The equilibrium equations of a thin plate under transverse load q, in x_3 direction can be observed in equations below,

$$\frac{\partial N_{11}}{\partial x_1} + \frac{\partial N_{21}}{\partial x_2} = 0 \tag{4.9}$$

$$\frac{\partial N_{12}}{\partial x_1} + \frac{\partial N_{22}}{\partial x_2} = 0 \tag{4.10}$$

$$\frac{\partial^2 M_{11}}{\partial^2 x_1} + 2\frac{\partial^2 M_{22}}{\partial x_1 \partial x_2} + \frac{\partial^2 M_{22}}{\partial^2 x_2^2} = -q \tag{4.11}$$

$$N_{\alpha\beta} = \int_{-h}^{h} \sigma_{\alpha\beta}\, dx_3 \text{ and } M_{\alpha\beta} = \int_{-h}^{h} x_3 \sigma_{\alpha\beta}\, dx_3$$

where, $\sigma_{\alpha\beta}$ are the stresses.

4.3 Equations FE Modal analysis

The modal analysis constitites of the following governing equations for free and forced vibration system. The free vibration equation for a structure can be expressed as:

$$[K]\{U\} + [M]\{A\}\,\omega^2\{U\} = \{0\} \tag{4.12}$$

where $[K]$ is the stiffness matrix, $[M]$ is the mass matrix, $\{U\}$ is the displacement vector, $\{A\}$ is the damping matrix, and ω is the angular frequency. The forced vibration equation for a system subjected to a dynamic load can be expressed as:

$$[K]\{U\} + [M]\{A\}\omega^2\{U\} = \{F(t)\} \tag{4.13}$$

where $\{F(t)\}$ is the time-dependent external force vector. The motion of a bridge can be described using the equation:

$$mx'' + cx' + kx = F(t) \tag{4.14}$$

m is the mass matrix, c is the damping matrix, k is the stiffness matrix, x is the vector of nodal displacements, $F(t)$ is the vector of external forces applied to the bridge at time t. To find the natural frequencies and mode shapes of the bridge, we can solve the eigenvalue problem:

$$(K - \omega^2 M)\,\varphi = -C\omega\varphi \tag{4.15}$$

K is the stiffness matrix, M is the mass matrix, C is the damping matrix, ω is the angular frequency (related to the natural frequency), φ is the eigenvector or mode shape of the bridge. The eigenvalues of this problem correspond to the natural frequencies squared, and the eigenvectors represent the mode shapes of the bridge [42].

4.4 Equation Modal assurance criteria(MAC)

The MAC analysis is used to determine the similarity between two mode shapes. These mode shapes can be obtained from two numerical simulations or between numerical and experimental data mode shapes. The similarity is based on percentage, if the two modes are ideally identical the of MAC is "one" and it has a value of "zero" if they have huge mode shape difference. Mathematically, the MAC value between two modes is the normalized dot product of the complex modal vector at each shared node (see e.g. [43] [44]).

Two modal vectors for mode shape I (φ_i) and mode shape J (φ_j) takes the following form to achieve similarity index for two modes.

$$\mathrm{MAC}(\{\varphi_\mathrm{i}\})(\{\varphi_\mathrm{j}\}) = \frac{\left|\{\varphi_\mathrm{i}\}^{*\mathrm{t}}\{\varphi_\mathrm{j}\}\right|^2}{(\{\varphi_\mathrm{i}\}^{*\mathrm{t}}\{\varphi_\mathrm{i}\})(\{\varphi_\mathrm{j}\}^{*\mathrm{t}}\{\varphi_\mathrm{j}\})} \tag{4.16}$$

The *Equation (*4.16 shows that the It is important to note that the the equation is normalizing the two mode shape vectors, makes the mode shapes insensitive to scaling, i.e., if modes are multiplied by a common factor the MAC will not change. Also, if the there exists a linear correlation of both vectors, higher MAC value is achieved. The percentage match depends on the nodes allignment throughout the structure. Also, the participation factor and effective mass are two criterias to critically analyze the mass movement in x, y and z direction for each mode. A higher value indicates that the mode exites by any oscillations in that direction.

$$\gamma_i = \{\varphi\}_i^T [M]\,\{D\} \tag{4.17}$$

where, $\{\varphi\}_i^T$ represents the mode shape, $[M]$ is the mass matrix and $\{D\}$ is the excitation direction vector. The effective mass can simply be written as

$$M_{eff,i} = {\gamma_i}^2 \tag{4.18}$$

5 CAD Model Methodology

The study models Herøysund Bridge using 3D- Solid and Shell finite elements based on 1966 technical drawings. A 3D CAD model is created in Solidworks, and FEA is conducted in ANSYS, following a specific workflow.

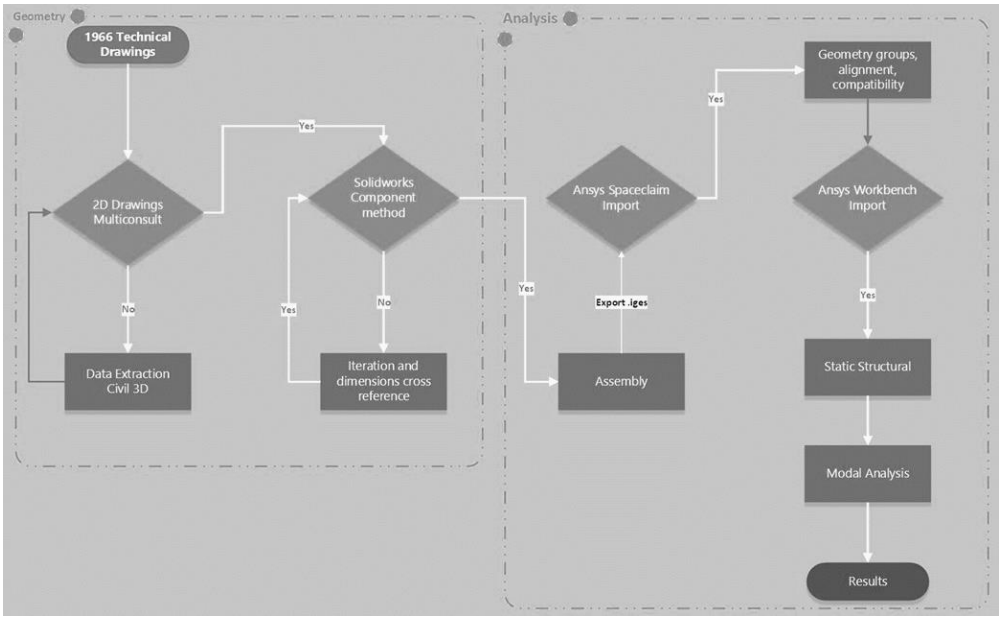

Figure 8. Methodology for bridge study

The Herøysund Bridge's parametric CAD model features complex geometry, including horizontal and vertical curvatures, as illustrated in Figure 2. To geometrically recreate the bridge using a FEM, certain low-sensitivity simplifications must be implemented without affecting the study's objectives. Specifically, bridge section 1-3 possesses both vertical and horizontal curvature, while section 6-7 exhibit slight horizontal curvature. The main span has minimal horizontal curvature, varying primarily in the vertical direction. As indicated by the original 1971 drawing, the top deck incorporates banking, with elevations in point data form at each pillar, i.e., alphabetical elevation points in Figure 9.

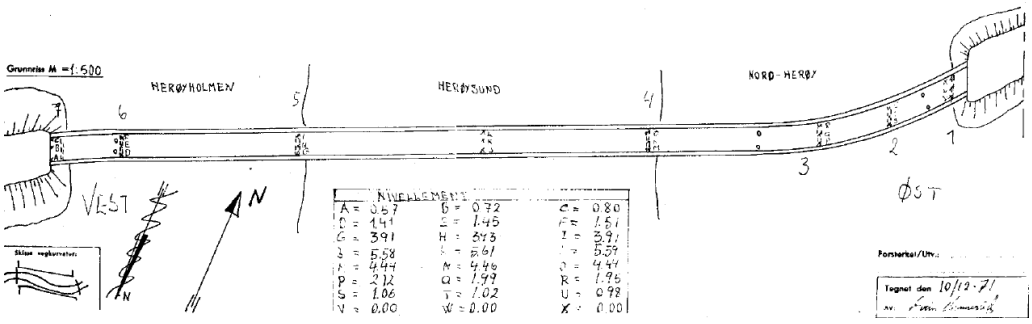

Figure 9. Herøysund Bridge transverse curvature [2]

A notable characteristic of the structure is the varying cross-section across spans, as shown in section view D of Figure 3. It features a 16 mm pressure plate at the bottom, depicted as a single body but independent.

5.1 Methodology of 3D-Solid Model

5.1.1 Assumptions

The Solid model is created in Solidworks and has been simplified as per the needs of this project. The simplifications are as follows:

1. The transverse curvature in bridge spans 1-3 and 6-7, as shown in Figure 9, has been assumed without curvature since it would add complexity to the geometry. Also, this assumption would not affect the mid-span 3-6, i.e., the primary area of concern.
2. The elevation of the top deck adds complexity to FEM geometry, as shown in Figure 9, it is assumed to be perfectly in-plane.
3. Post-tensioning in the bridge involves tendons embedded within the structure, making them difficult to track physically. Due to limited geometrical information in the drawings, an inward compressive force of $12{,}083{,}400N$ is assumed on either side of the main span 3-6.
4. The top deck features a 60 mm asphalt layer, according to the SV handbook V-412 [6], that exerts additional load. To avoid FEM contact region errors, a uniform pressure of 7 kN/m is applied to the entire top deck from pillars 1-7 instead of modeling a layered geometry.
5. This study does not consider reinforcements or rebars in pillars and other spans.

5.1.2 Modeling procedure

AutoCAD 2D- drawings of the bridge were requested from AAS-Jakobsen. The AAS-Jakobsen report identified the bridge's cross-section variations across bridge spans [3]. Original hand drawings from the multi-consult were analyzed to understand main span dimensions [2]. Using the section profile obtained from the archive data provided by NFK, the model was dimensioned using Autodesk Civil 3D student version annotation tool. The details on pillars, bridge spans, pressure plates, and beam curvatures were also extracted from the drawing in Figure 10 below.

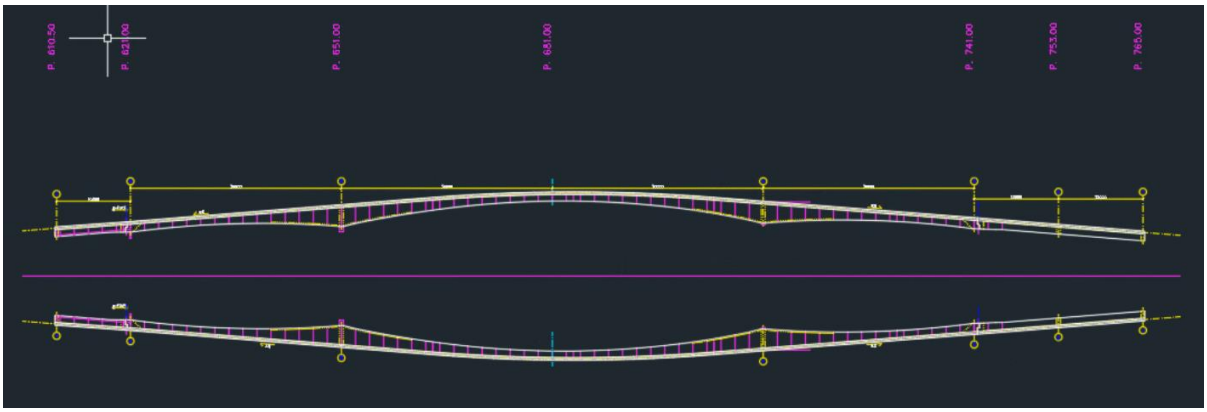

Figure 10. Herøysund Bridge layout drawing [45]

5.1.3 Method and Considerations

This sub-section depicts all the necessary considerations for drawing the bridge structure as close to the actual structure as possible. Therefore, it includes steps where no further assumptions were made to capture the behavior realistically.

1. Top deck cross-sections for each section were drawn across the curved path from the .dwg file as in Figure 10 and swept across the drawn path to create the top deck for spans 1-3, 3-6, and 6-7, respectively.
2. Individual spans 1-3, 3-6, and 6-7 were assembled using coincident planes with the top deck.
3. The pressure plate profile in Figure 11(c) was dimensioned as per the original drawing to capture the behavior of the bridge.
4. Support beams and the top deck's vertical gradients were identified using a spline tool in Civil 3D. These points were drawn in Solidworks and extruded to predefined thicknesses from the drawings. Using the drawing shown in Figure 10 ensured exact curve matching.
5. Bridge span 1-3 and 6-7 rest on a 16 mm structural steel plate at the top of the pillars, where beams are simply-supported.
6. Identical beams on either side of the bridge were mirrored across the mid-plane. Beams for sections 1-3 and 3-6 are 200 mm thicker than those in mid-span 3-6.
7. Pillar dimensions were extracted from archive drawings obtained from the bridge archive in the database of SV known as Brutus.
8. The slope at the top of pillar two strictly followed the drawing, as shown in Figure 11(a). It replicates the exact profile of pillar 2.

9. The bases of the pillars were also drawn as per the drawings shown in Figure 11(b) without any assumptions.
10. All pillars' protrusions extend 50 mm on either side of the beams shown in Figure 11(b).
11. The assembly view of the bridge can be seen in Figure 12.

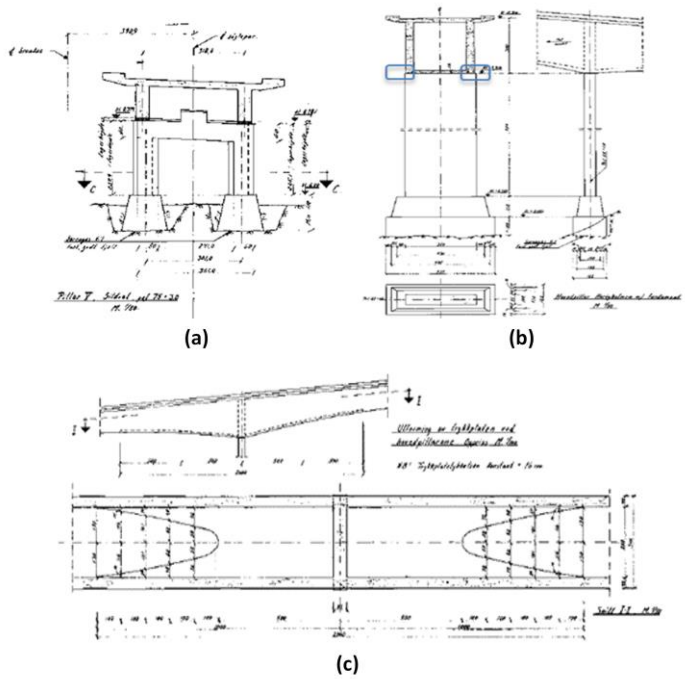

Figure 11. Pillar 2, 4 and pressure plates in 1971 drawings [2]

5.1.4 SolidWorks Assembly

Drawings from the Brutus document directory, provided by SV and NFK, served as a foundation for understanding the bridge structure. The technical drawings extracted key information on support mechanisms, pillars, superstructure section connectivity, and curvature dimensions. Given the hand-drawn nature of these drawings, details appeared blurred. A cross-reference approach was adopted by consulting recreated drawings using Autodesk Civil 3D. The superstructure deck, piers, and curvatures were cross-referenced and dimensioned to minimize anomalies in interpreting the original base drawings.

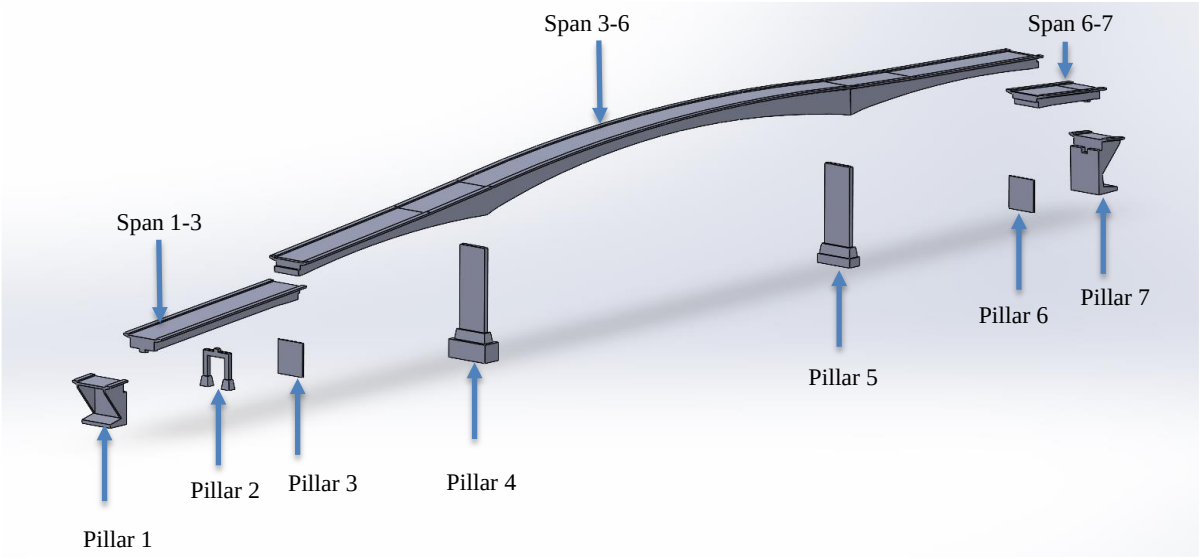

Figure 12. Solidworks Assembly exploded view for bridge components.

5.1.5 Pillars Integration

The model is an assembly with each pillar connected to the deck and beams, as shown in Figure 13 below. The configuration shown for pillar 3 is followed for all other pillars having load-bearing structural steel plates. The pressure plates discussed above are also visible in pillar 4 and 5 configurations.

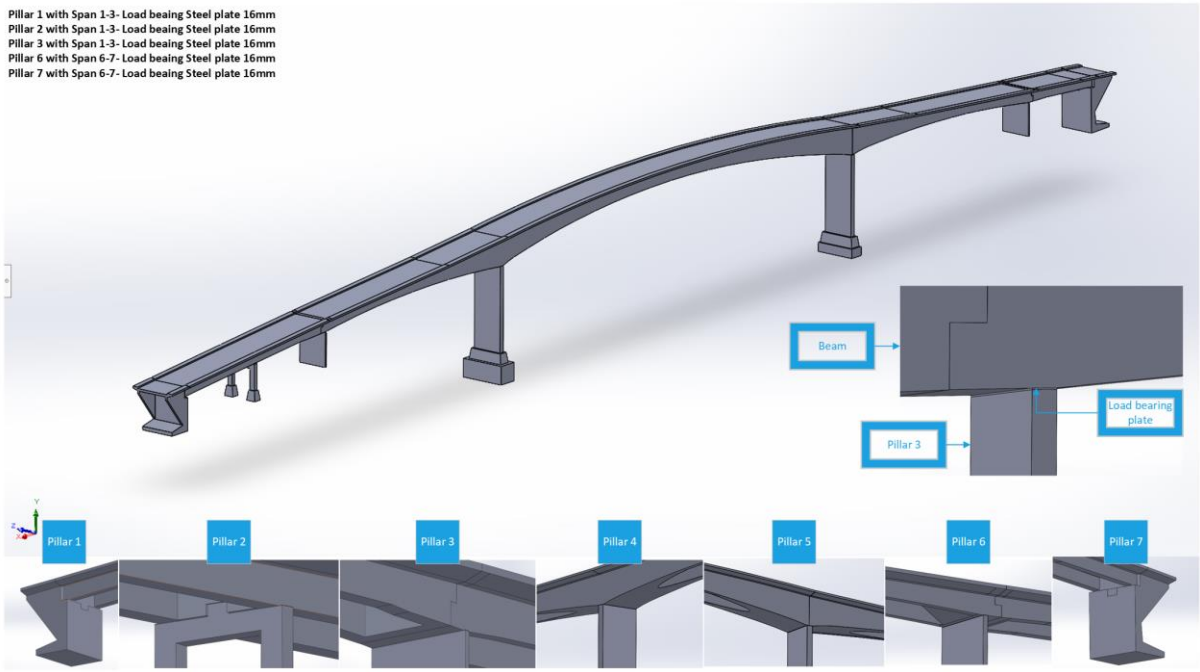

Figure 13. Solidworks Assembly for bridge components

5.2 Methodology of Shell Model

5.2.1 Assumptions

The Shell model is created in ANSYS Space-claim using the 3D-Solid model. As discussed in theory, the Shell model needs several considerations as it is based on a mid-surface method where each Solid body is represented as a single mid-surface. Therefore, it has been simplified as per the needs of the required model. The simplifications are as follows:

- Since the surfaces are to be extracted from a 3D-Solid model, it automatically induces the assumption of transverse curvature in Figure 9. The same is applied to spans 1-3 and 6-7 and is considered perfectly straight.
- As done for the Solid model, the banking or elevation of top deck asphalt is small in magnitude and has been assumed to be completely planar.
- The post-tensioning CAD integration is not possible for a Shell model since it is a planar representation of all Solid features. Therefore, compressive inward forces on the main span replicate the effect of tendons.
- The top deck has an asphalt layer of 60 mm, like the Solid model described in the handbook V-412 [6]. Modeling two coincident surfaces cause mesh errors as it duplicates surfaces in the Shell model. Therefore, instead of modeling mid-surface for asphalt, a uniform pressure of 7 kN/m has been applied to the top deck from pillars 1-7.
- The reinforcements or rebars in pillars and other spans are neglected for the Shell model.
- The top deck step profile is considered flat as a mid-surface to simplify the pedestrian walkways. If drawn as a separate surface, the pedestrian walkways cause surface disconnectivity.
- The pressure plates have varying profiles, as shown in Figure 11(c). For a Shell model, exceedingly small curvatures at the end of the profile make them highly undesirable due to the large deflection and stress concentration possibility. Also, these singularities disrupt the meshing. Therefore, the pressure plates are not included in the Shell model.

5.2.2 Modeling procedure

The Shell model is extracted from the Solid model with afore mentioned assumptions. The following steps are adopted to model the geometry.

- The Solid model assembly of the bridge was first imported to Ansys space-claim as a .iges file.
- The space-claim geometry was then renamed into the sub-assemblies, such as the deck, beams, and pillars for each section.
- Space-claim allows the Solid models to be mid-surfaced from a Solid body. The mid-surface represents the geometry's cross-section(Shell), given a section thickness representing a Solid body. Using the mid-surface command, the features of the bridge, such as the top deck, beams in +z and -z directions, transverse beams, and pillars, were transformed into individual mid-surfaces.
- The control of surfaces was conducted by stitching each surface with the adjacent to avoid connectivity issues. If there is disconnectivity in the mid-surfaces, the internal forces and stresses are not appropriately translated, affecting the results.
- The longitudinal and transverse beams on either side of the bridge were drawn on independent surfaces to be given a thickness equal to the top deck width since the main span rests on these beams.
- Once the mid-surfaces were connected, the topology was shared individually for each span to define the contact edges in surfaces. It again is an important step, as the distribution of loads between members during analysis plays a significant role.
- The Shell model was also drawn section by section for each span and pillar. The load-bearing plates were also mid-surfaced.
- Space-claim built-in geometry checks were conducted to investigate extra edges, dis-continuities in surface, tangencies, gaps, and duplicates. The model was then imported to ANSYS for further analysis.

5.2.3 Shell model Assembly

The Shell model components transformation can be seen in the figure below. The shared topology in space-claim was done for each component individually. The definition of individual topologies dis-associate these components as an assembly; therefore, the joints between bridge spans were analyzed in detail to represent the real bridge connections correctly.

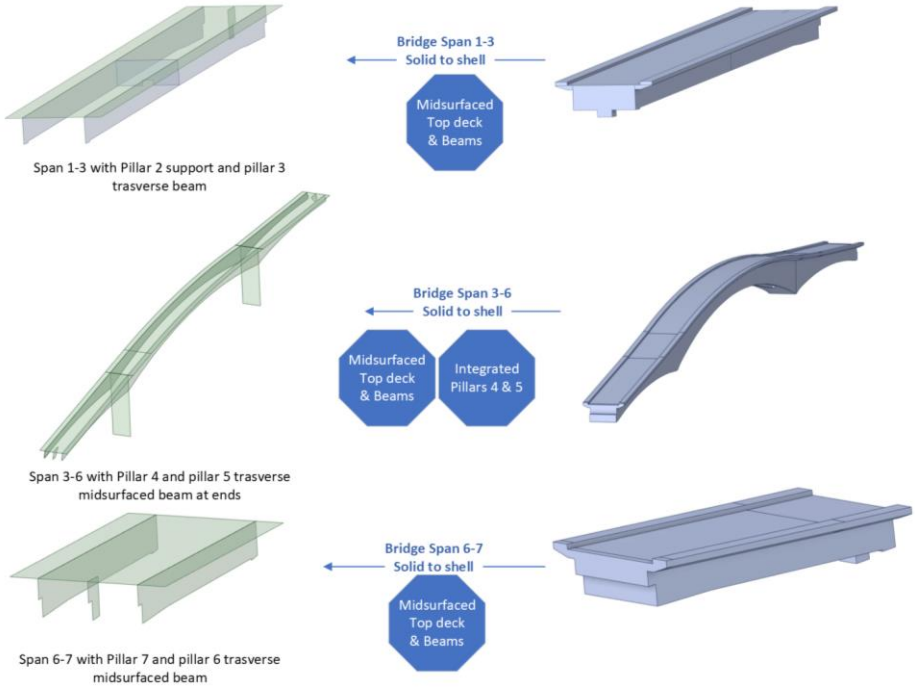

Figure 14. Shell and Solid model transformation

The Shell model from spans 1-3, 3-6, and 6-7 share the topology between respective span surfaces. Each surface in the Shell, as shown in Figure 16 has been assigned thickness per the technical drawings. The thickness parameter plays a vital role in mass control for the bridge geometry. Since the model is to be compared to the Solid model the mass distribution across its span should be as close to the Solid model as possible. The components of spans 1-3 are shown in Figure 15; the same terminology follows in other bridge spans.

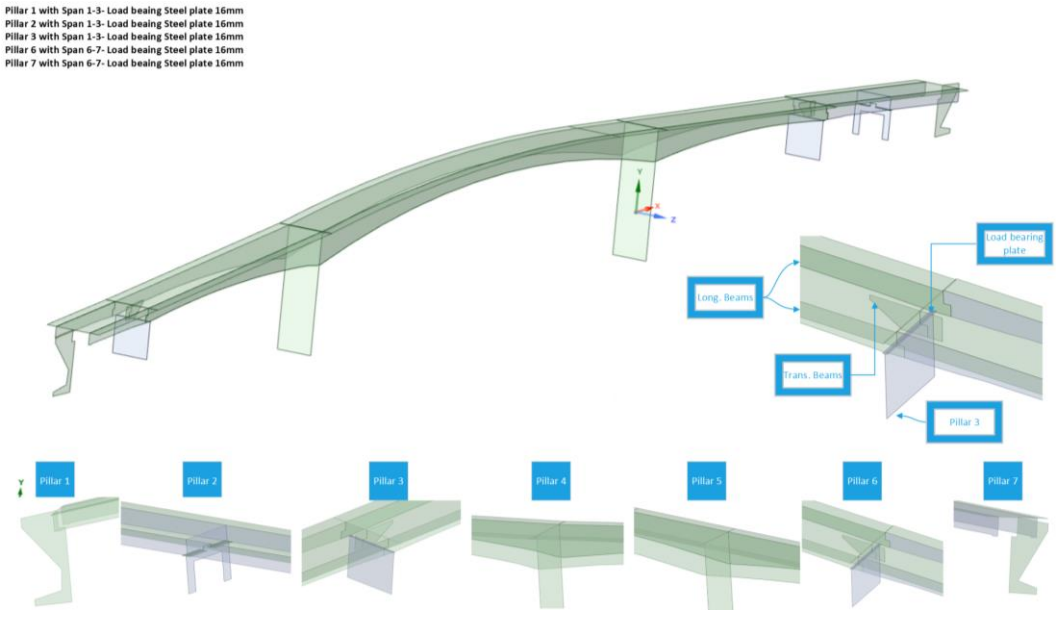

Figure 15. Shell model pillars configuration

5.2.4 Section thicknesses

Each bridge section has longitudinal beams, transverse beams at pillars, top deck, and pillar surfaces.

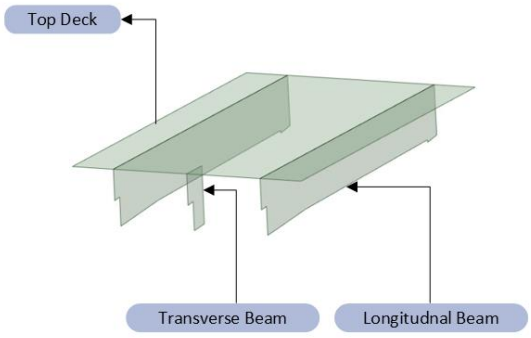

Figure 16. Surface identification for thickness assignment

These surfaces are placed in the middle of the bridge and have a thickness, as shown in Table 3. Section thickness for surfaces in the Shell modelTable 3 below. Once the thicknesses are defined in the Shell model in ANSYS, the geometry takes the form, as shown in Figure 17. Overlapping 3D-Solid and Shell model, where Shell appears like a Solid model.

Table 3. Section thickness for surfaces in the Shell model

Section	Nordherøy, (mm)	Main Span, (mm)	Herøyholmen, (mm)
Plane	Midsurfaces	Midsurfaces	Midsurfaces
Longitudinal beams	600	400	600
Transverse beams	2200	2600	2200
Top Deck	250	250	250
Pillar 1(Land vessel)	4000	-	-
Pillar 2	450	-	-
Pillar 3	-	200	-
Pillar 4	-	550	-
Pillar 5	-	550	-
Pillar 6	-	-	200
Pillar 7(Land vessel)	-	-	4000

5.2.5 CAD Models coherence

The overlapping models can be seen in Figure 17, where the 3D-Solid model overlaps the Shell model. The coherence in these models plays a vital role in results comparison. The primary control parameters are mass control and geometric constraints similarity. As discussed in the FEM section, the Shell model allows faster computation than a Solid model with fewer

elements. However, due to mid-surfacing limitations and the bridge's complex geometry, it would be interesting to compare the structural and modal deformations.

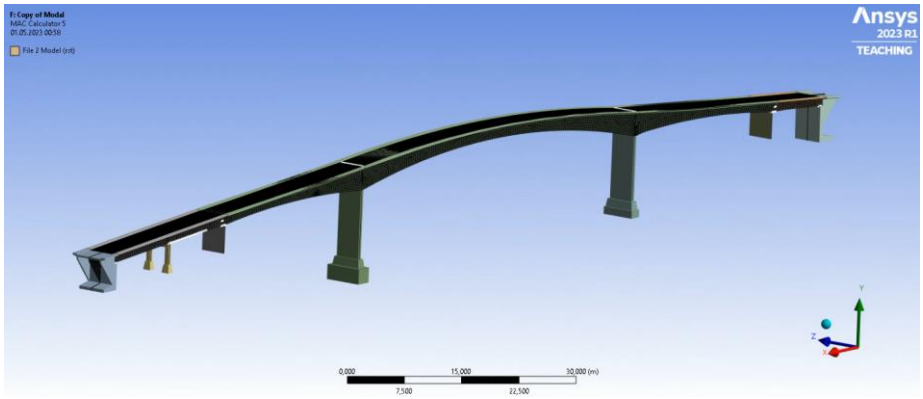

Figure 17. Overlapping 3D-Solid and Shell model

Furthermore, the mass and volume control for constrained prestressed structures shall be as close as possible for 3D-Solid and Shell models. To compare the vibration modes effectively controlling these parameters is significantly important. These parameters can be seen listed in Table 4. Mass and volume control for models

Table 4. Mass and volume control for models

Properties	**3D-Solid Model**	**Shell model**	**Abs. Percentage error**
Mass, kg	$1.3848e+006$	$1{,}3512e+006$	1.0248%
Volume, mm^3	$5.7891e+011$	$5{,}6478e+011$	1.0248%

6 Numerical Simulations

This Section includes workflow of ANSYS static structural and modal analysis with all the cosiderations for materials, coneections, mesh attributes and sulotion metrics.

6.1 Units

The numerical analysis has been performed using SI units, the governing parameters to be studied in the structural and modal analysis are total deformations (mm), normal stresses (MPa), modal frequencies (Hz), mass (kg), and volume (m^3).

6.2 Geometry

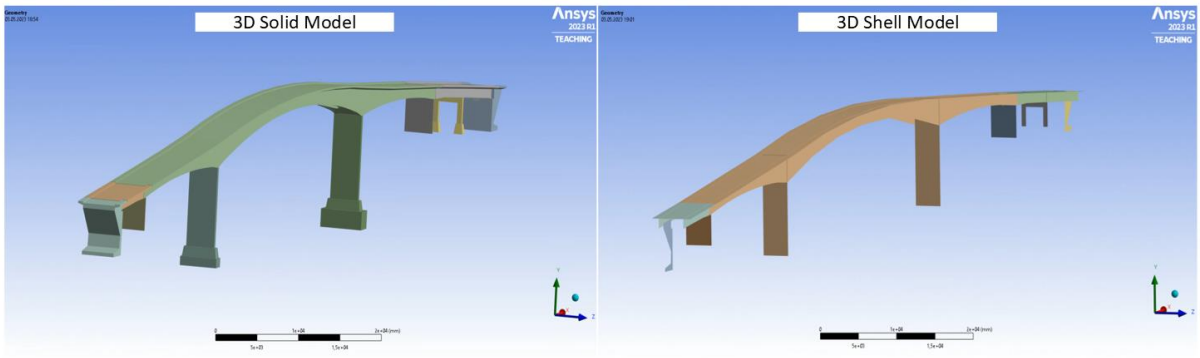

Figure 18. 3D-Solid and 3D Shell bridge geometry

6.3 Materials

Concrete is used for pillars and span 1-7, while structural steel is used for the load-bearing plates on pillar 1, 2, 3, 6 & 7. The material properties are based on the Granta materials library in ANSYS 2023 R1 are shown in Table 5.

Table 5. Material properties for models in numerical simulations[46]

Properties	Concrete	Structural Steel
Density, Kg/mm^3	2.39e-06	7.85e-06
Young's Modulus, MPa	19360	2.00e+05
Poisson's Ratio	0.1414	0.3
Bulk Modulus, MPa	8998	1.67e+05
Shear Modulus, MPa	8480.8	76923
Tensile Ultimate Strength, MPa	1.1960	460
Tensile Yield Strength, MPa	1.0950	250
Isotropic Thermal Conductivity, $W/mm°C$	0.002071	0.06050
Specific heat constant pressure, $mJ/Kg°C$	9.36e+05	4.34e+05
Isotropic Resistivity, $ohm-mm$	5.85e+07	-
Secant Thermal Expansion Coeff.	-	1.20e-05

6.4 Connections

6.4.1 3D-Solid model Connections

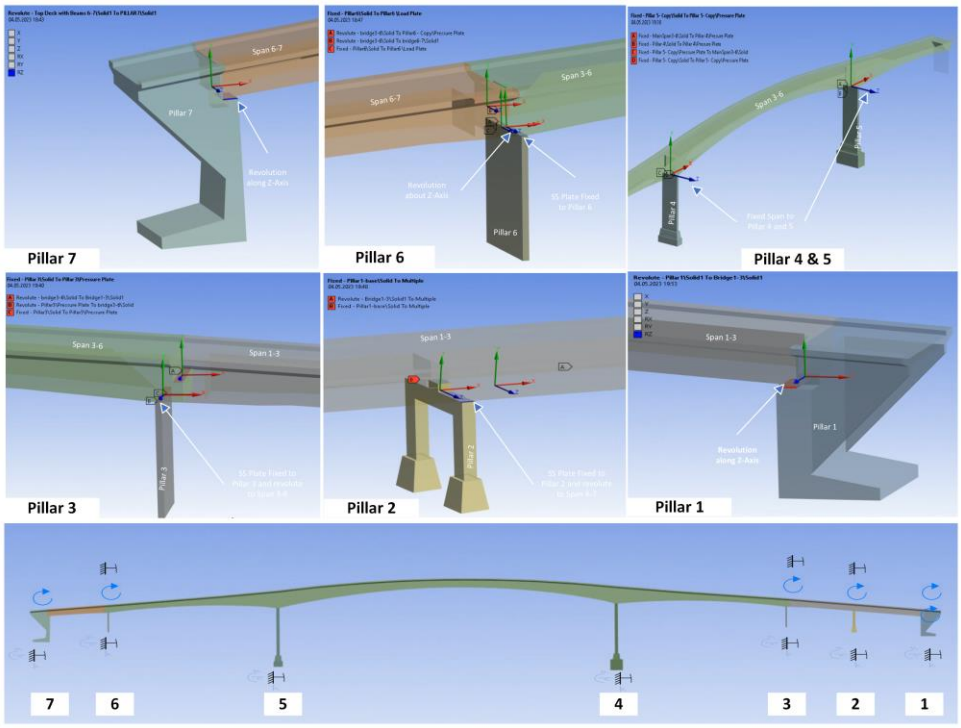

Figure 19. 3D-Solid model joints across all pillars

6.4.2 Shell model Connections

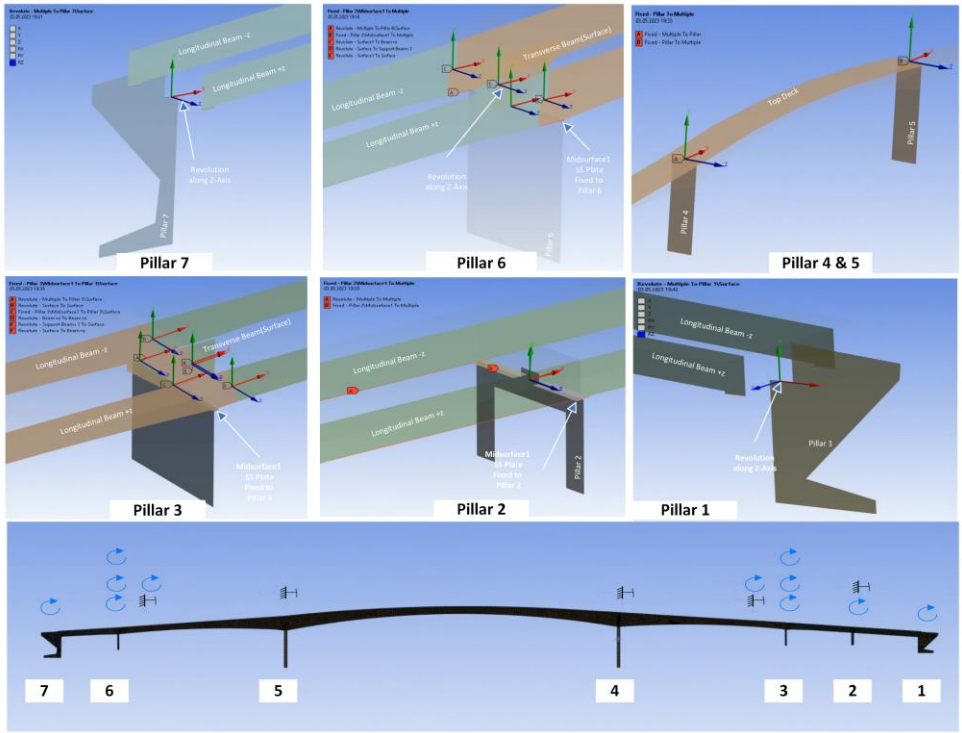

Figure 20. Shell model joints across all pillars

6.5 Mesh

Solid 186 and 187 elements are used in the FEM for the Solid model. Solid 186 has reduced integration and is suitable for linear analyses of structures with moderate to low aspect ratios[47]. However, the element best suited for each geometry section, solid 187, is an improved version of solid 186 with full integration and is suitable for modeling thin-walled structures with high aspect ratios, accurately capturing bending and shear stresses[48]. Therefore, both element types are program controlled by ANSYS in areas where needed in the Solid model. For the Shell model, Shell 281 has been used. Shell 281 is a 6-node FE type used in ANSYS for the structural analysis of thin to moderately thick Shell structures. It accurately captures shear deformation effects and has three degrees of freedom per node[48]. Its ability to capture shear deformation effects makes it a preferred choice for accurately analyzing and designing structures such as Herøysund Bridge under investigation. The choice of element type for quad mesh is also program controlled. The mesh attributes can be seen in Figure 21.

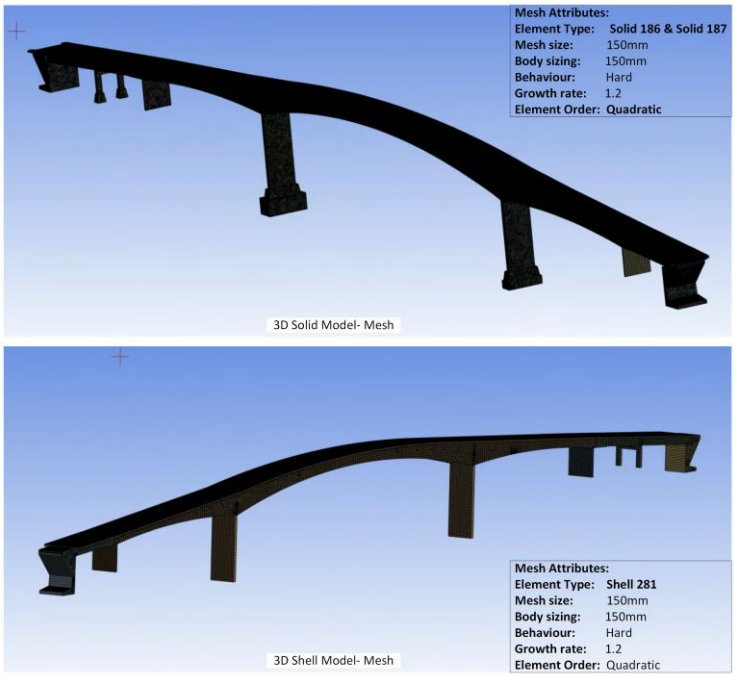

Figure 21. Mesh illustration for Solid and Shell models

6.5.1 Mesh Convergence

The optimum agreement between mesh size, computational time, and accuracy of results is achieved by selecting the best suitable number of elements; it is a well-known approach to studying mesh convergence for more reliable, accurate, and consistent results. As discussed in the Methodology Section, the 3D-Solid and Shell models differ in stiffness, geometry creation,

and element types. Therefore, to compare the mesh sizes concerning normal stress and total deformation, two nodes were selected at the bridge midspan 3-6, where section planes were drawn along the x and z-axis.

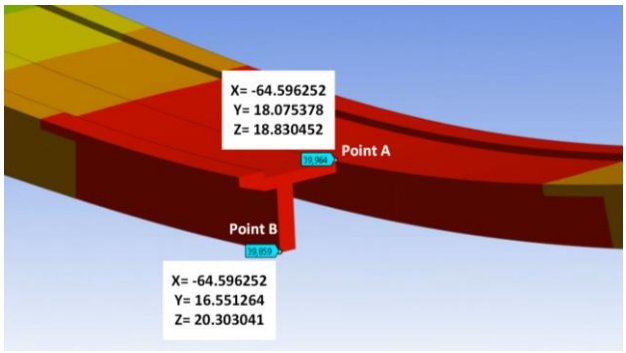

Figure 22. Mesh convergence check locations

Using the maximum normal stress ($\sigma_{n_{max}}$) and total deformation method for mesh convergence, the points were selected based on the region of maximum vulnerability (center of midspan 3-6), restricted the element location by section planes. In contrast, the mesh resolution changes the location of the top deck (point A) and bottom at (point B) in global coordinates, which can be seen in Figure 22. The maximum stress (MPa) and total deformations(mm) were obtained at the specified points for mesh sizes of 800, 600, 400, 250, 150, and 80 mm for both 4-node quadratic and 8-node quadratic mesh element types. The mesh size was then plotted against the relative error for max. Normal stress and total deformation were used to observe the order of convergence for both locations with additional parameters of mesh element types. Using the absolute values for normal stress (σ_n) and total deformation the percentage error was calculated. For instance, the percentage error can be computed as in the equation below for a mesh size of 800 mm in a Solid model 8-node quadratic mesh having 22,381 elements.

$$Percentage\ error_{\sigma_n} = \frac{\left|\sigma_{n_{80}} - \sigma_{n_{800}}\right|}{\left|\sigma_{max\ n_{80}}\right|} = 18.79\% \tag{6.1}$$

Identifying the optimum condition for the percentage error, it reduces to 0.01% at a mesh size of 150 mm, with 150,6931 elements. Moreover, the error percentage reduces to 0.0% for a mesh size of 80 mm, however, at 98,000,895 elements. The increase in the number of elements with respect to the effect on error reduction is negligible as shown in Figure 23.

3D Shell Meshing										
	Top Deck					Beam Bottom				
	Mesh Size mm	Normal Stress MPa	% error	Deformation mm	% error	Normal Stress MPa	% error	Deformation mm	% error	Elements
8-Node Shell	800	-5.650	2.637%	56.051	8.631%	3.150	5.243%	58.817	4.373%	2646
	600	-5.750	0.910%	60.556	1.288%	3.210	3.438%	59.507	3.252%	4628
	400	-5.787	0.274%	60.796	0.897%	3.220	3.138%	60.707	1.301%	10742
	250	-5.798	0.090%	61.236	0.179%	3.299	0.761%	61.247	0.423%	24801
	150	-5.799	0.065%	61.346	0.000%	3.320	0.129%	61.357	0.244%	67408
	80	-5.803	0.000%	61.346	0.000%	3.324	0.000%	61.507	0.000%	236064
4-Node Shell	800	-5.987	3.210%	55.221	9.984%	2.980	11.423%	56.458	8.209%	2752
	600	-5.999	3.417%	58.476	4.678%	3.005	10.680%	58.717	4.536%	4612
	400	-5.890	1.538%	60.286	1.728%	3.166	5.894%	60.757	1.219%	10998
	250	-5.854	0.917%	60.416	1.516%	3.473	3.240%	60.927	0.943%	24775
	150	-5.806	0.086%	61.266	0.130%	3.424	1.783%	61.407	0.163%	6680
	80	-5.801	0.000%	61.346	0.000%	3.364	0.000%	61.507	0.000%	236007
3D Solid Meshing										
	Top Deck					Beam Bottom				
	Mesh Size mm	Normal Stress, MPa	% error	Deformation mm	% error	Normal Stress, MPa	% error	Deformation mm	% error	Elements
8-Node Solid	800	-4.058	18.79%	32.474	18.742%	1.685	19.34%	29.789	25.264%	22381
	600	-4.158	16.79%	33.024	17.366%	1.785	14.55%	33.929	14.877%	40062
	400	-4.547	9.01%	36.964	7.507%	1.852	11.35%	37.929	4.842%	96265
	250	-4.908	1.78%	39.894	0.175%	1.985	4.98%	40.029	0.427%	335412
	150	-4.998	0.02%	39.914	0.125%	2.085	0.19%	39.929	0.176%	1506931
	80	-4.997	0.00%	39.964	0.000%	2.089	0.00%	39.859	0.000%	9800895
4-Node Solid	800	-3.019	39.59%	25.670	32.052%	1.255	31.27%	25.934	31.576%	33581
	600	-3.218	35.60%	29.279	22.499%	1.350	26.07%	28.165	25.690%	65286
	400	-3.705	25.86%	31.239	17.311%	1.445	20.87%	32.229	14.968%	110795
	250	-4.164	16.67%	34.614	8.378%	1.652	9.53%	34.999	7.659%	352254
	150	-4.884	2.26%	36.139	4.341%	1.805	1.15%	36.029	4.942%	1528521
	80	-4.997	0.00%	37.779	0.000%	1.826	0.00%	37.902	0.000%	9923658

Figure 23. Mesh convergence with increasing mesh resolution

The percentage errors were plotted against decreasing mesh resolution, as shown in Figure 24 below for both 3D-Solid and Shell models. Figure 24(a) and (b) represent normal stress at the top deck and bottom location, while (c) and (d) represent total deformation for both locations. The relative error can be seen decreasing with an increase in mesh resolution. The solution for both parameters appears to converge from a mesh size of 200 mm.

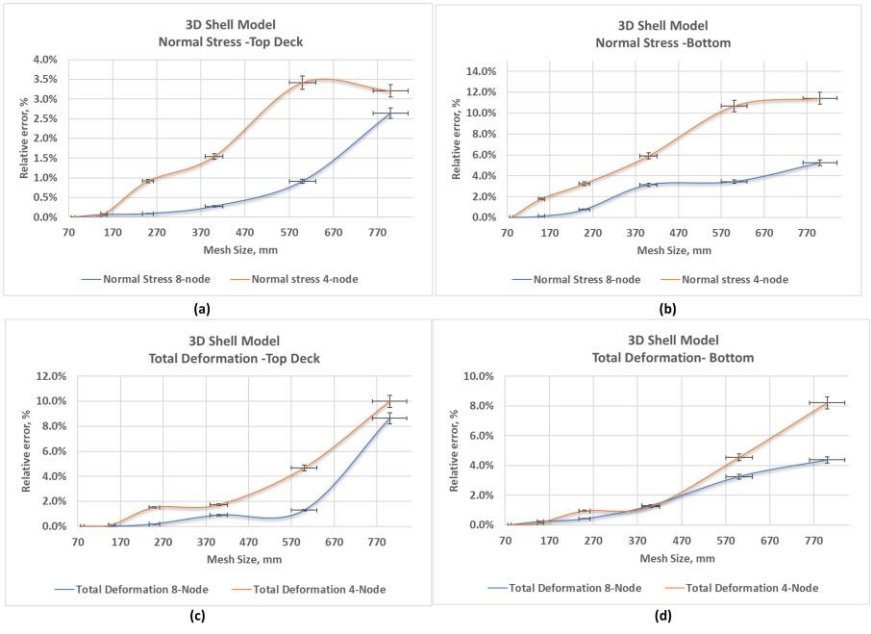

Figure 24. Convergence plots for 3D Shell at the top deck and bottom

Similarly, for the 3D-Solid model, Figure 25(a) and (b) represent normal stress at the top deck and bottom location, while (c) and (d) represent total deformation for both locations. As compared to the Solid model similar pattern for both parameters appears to converge from a mesh size of 200 mm in the Shell model.

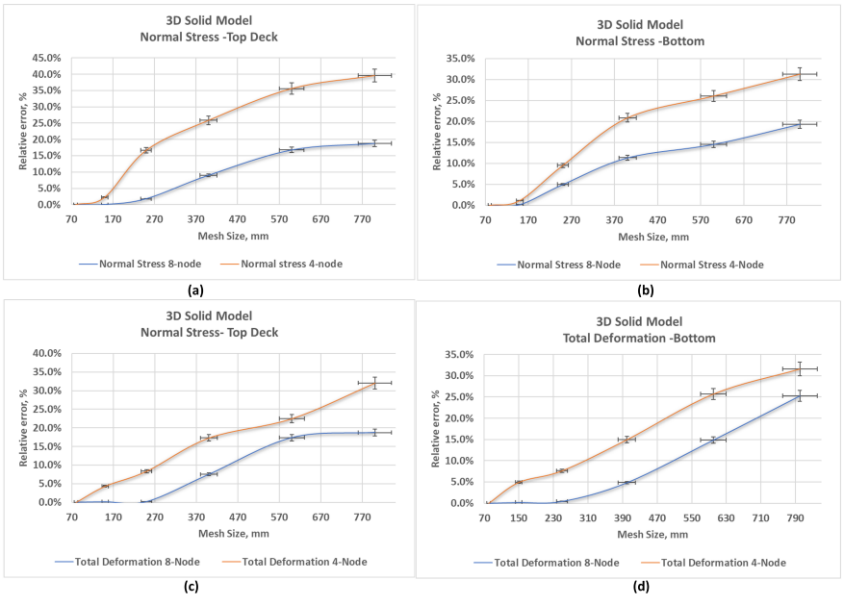

Figure 25.Convergence plots for 3D-Solid at the top deck and bottom

It is important to note that the mesh convergence for a 4-Node quadratic mesh type convergence rate is of the first order, while for an 8-Node quad mesh is of the second order. Therefore an 8-Node Quad method, i.e., second-order convergence, was preferred based on the accuracy and stability of the solution. The quadratic shape function was chosen because it considers linear stress variation, accurately represents curved surfaces, and is less distortion-sensitive. The computational time for both cases was 1 minute 34 seconds for the Shell model and 5 minutes 54 seconds for the Solid model. The mesh convergence check, accuracy of the result, and computational time were in good agreement for a mesh size of 150 mm.

7 Boundary Conditions

Proper boundary conditions, including supports, loads, temperature, and soil, are essential for safe and reliable bridge analysis. This study considers self-weight, ambient temperature, and foundation supports for prestressed modal analysis from structural to modal analysis.

7.1 Standard earth gravity

The whole bridge structure is under the action of 9880 g/mm^2 along $-$ve (Y-axis). Standard earth gravity is used to calculate internal forces and stresses caused by the weight of the bridge structure and loads, and its constant value is used to calculate the self-weight of the bridge structure.

7.2 Post Tensioned Load

The post-tensioning in the Herøysund Bridge consists of tendons along the longitudinal beams, as shown in Figure 26. The tendons in the bridge structure are tensioned while exerting a compressive force on the bridge structure. Due to the unavailability of tendons' exact locations across the geometry, as an approximation, a compressive load is applied at the front face on either side of span 3-6.

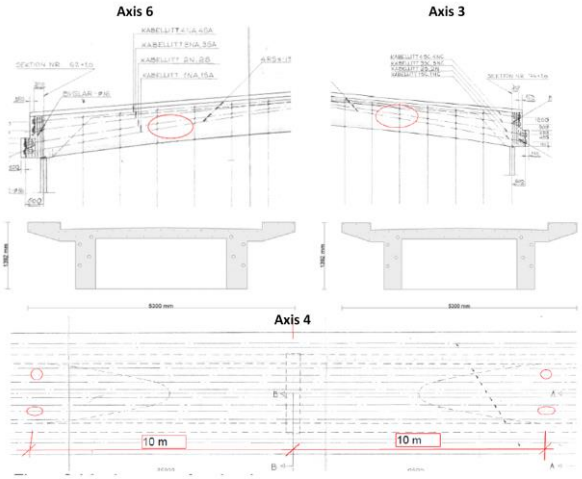

Figure 26. Post-tensioned system across axis 3 to 6(DEKRA 584522)

Each cable per the SV document is tensioned with a load of 137 tonnes along the x-axis, i.e., Span 3-6 in the longitudinal direction. There are 18 tendons providing post-tensioning force F_{PT} (see, Equation (7.1). Therefore, on each end of the main span, a compressive force C_{PT} acts at the pillars 3 and 6 directing towards the center. The force can be seen in the equation below.

$$F_{PT} = tension\,per\,cable \times no.of\ cables \times gravitaional\,acceleration \quad (7.1)$$

$$F_{PT} = 137 \times 1000 \times 18 \times 9806.6 = 24{,}166{,}800\ N,$$

$$C_{PT} = 12{,}083{,}400\ N$$

7.3 Railing and asphalt load

The bridge under study has $200mm$ railing, i.e., $0.5kN/m$ along with asphalt at the top with a thickness of $60mm$ throughout the span with a load of $25kN/m^3$ as per the SV V412 Load capacity classification of bridges, loads[6]. Based on the classification, the loads across the bridge in accumulated form can be calculated as a resultant load at the top deck. For $4m$ transverse span, asphalt load exerted by asphalt is $6kN/m$ while the side rails on both sides exert a load of $1kN/m$. Therefore, the accumulated load becomes $7\ kN/m$. For the whole span this load could be transformed to a result force of 1078000 N for bridge length of 154 m.

7.4 Applied Boundary Conditions

The illustrations of 3D-Solid and Shell model boundary conditions are presented in and Figure 28, respectively. The base of all seven pillars is fixed to the ground, and a force of $1078kN$ exerted at the top deck. A compressive force of $12{,}083{,}400N$ is applied as a compressive load across pillar 3-6. The body in global coordinate system in under the action of standard earth gravity, i.e., $9806.6\ mm/s^2$.

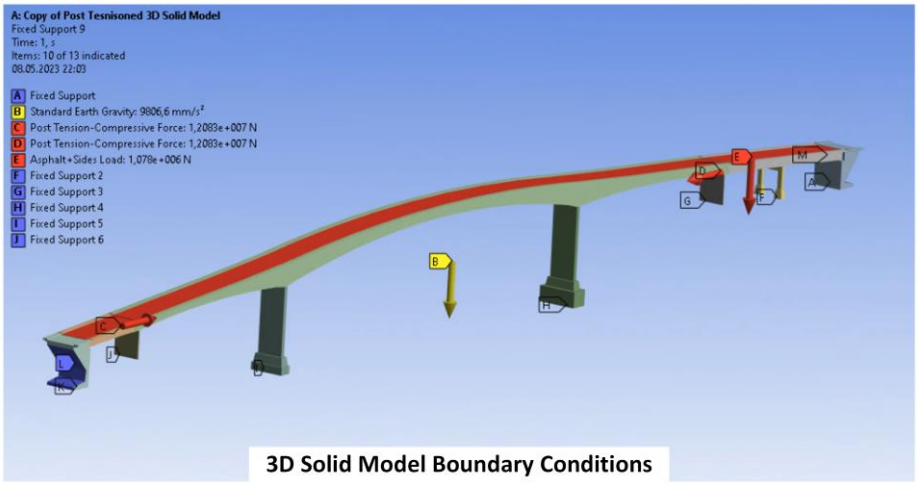

Figure 27. Boundary conditions for 3D Solid model

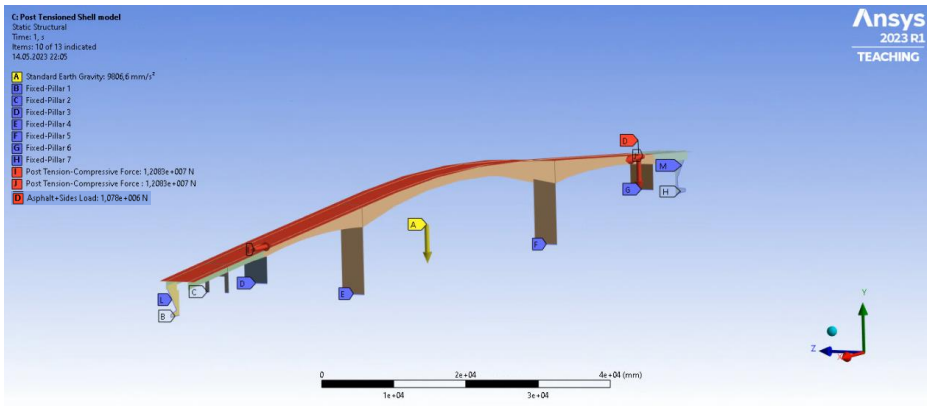

Figure 28. 3D Shell model boundary conditions

7.5 Solution metrics

Numerical simulations can accurately predict the behavior of a structure, but it requires a careful approach to selecting the right parameters and finding a balance between reliable results, efficient simulation time, and level of detail. The following Table 6 shows the computational resources used to achieve reliable results in Solid and Shell models.

Table 6. Numerical simulation resources used in ANSYS 2023 R1

Parameters	3D- Solid	Shell
Unit system	metric	metric
RAM available, GB	128	128
I/O to disk, GB	19.5	9.43
No. of Nodes	1,086,945	118,903
DOFs	3198967	643243
Solver type	Direct	Direct
Time to solve	5m 54s	1m 34s

The resource utilization in Solid and Shell numerical models in Table 6 shows that the Shell based model requires significantly fewer resources than the 3D- Solid model. The simulation for the Shell model takes 4.13 times less time to solve as the number of nodes and DOFs are significantly lower; however, the model needs more assumptions than solid. It can also be validated that the general element formulation theory of resource utilization is prominently visible in the metrics.

8 Results & discussion

This Section presents the structural and modal analysis results that were carried out using ANSYS 2023 R1. The numerical modal analysis was carried out for twenty modes, most relevant data for structural deformation, mode shapes and modal frequencies are discussed in detail for first six modes. It also, incorporates a widely used modal assurance criterion (MAC) based comparison of Solid and Shell models. This section will also identify the numerical suitability of both modeling strategies for structures of the scale of Herøysund Bridge.

Reiterating that the study aimed to develop a Shell-based FEM of a post-tensioned Herøysund concrete bridge. As part of the ongoing WP1- Structural health monitoring of research project, Herøy FoU, the objective was to equip the researchers with numerical modal analysis data to compare with on-site experimental vibration data. Therefore, a 3D- Solid and a Shell model were created for numerical modal analysis. The investigative parameters under evaluation were total deformation, resonant frequencies, and corresponding mode shapes of the Herøysund concrete bridge. Deformation analysis

Under the action of loads, as specified in the boundary conditions Section, the maximum deformation occurred in the middle of both 3D- Solid and Shell models. The loads deform the top deck where there is the maximum distance from the fixed supports; therefore, the general location of deformation is as anticipated. The maximum total deformation obtained in linear static structural analysis of the Solid model was 39.978 mm, while in the Shell model, it was 61.724 mm at the center of the mid-span 3-6 of the bridge shown in Figure 29. Since the mid-span 3-6 was 60 m long, i.e., more than any other pillar-to-pillar length.

As the post-tensioned tendons in the mid-span 3-6 of the bridge are in tension, they exert a compressive force on the concrete, allowing resistance to deformation due to self-weight. Furthermore, geometrically positive curvature along +y-axis assists in resisting deformation as well. The deformation pattern for Solid and Shell models was tested by applying significantly low post-tension force. It was observed that the deformation tends to rise from 132.5 mm to 146 mm, respectively, at 18 times lower post-tension force of 671,253 N than the actual. Therefore, it can be deduced that the post-tensioning in the bridge induces more stiffness to the structure hence more resistance towards deformation.

However, it is important to note that the Shell model's maximum deformation is 35.23% more than the Solid model's. Numerous aspects, such as geometry, DOFs, stiffness, load distribution,

and mesh density, can influence the total deformation in both models. A comparison of models for the Herøysund Bridge can be seen in Table 7.

Table 7. Factors influencing the deformation in Solid and Shell models

Factors	3D- Solid model	Shell model
Simplified geometry	Volume based elements	Thin surface elements
DOFs	3198967 DOFs	643243 DOFs
Stiffness Distribution	Higher	Lower
Boundary conditions	Applied to surfaces	Applied to edges
Load distribution	Higher loads on surfaces	Higher loads on edges

The 3D- Solid model is 4.97 times stiffer than the Shell model based on DOFs. Therefore Shell model has lower overall deformation as compared to the Solid model. Also, the load distribution, joints, and constraints across both model types differ in their application to surfaces and edges for Solid and Shell models, which is another reason for the deformation magnitude difference.

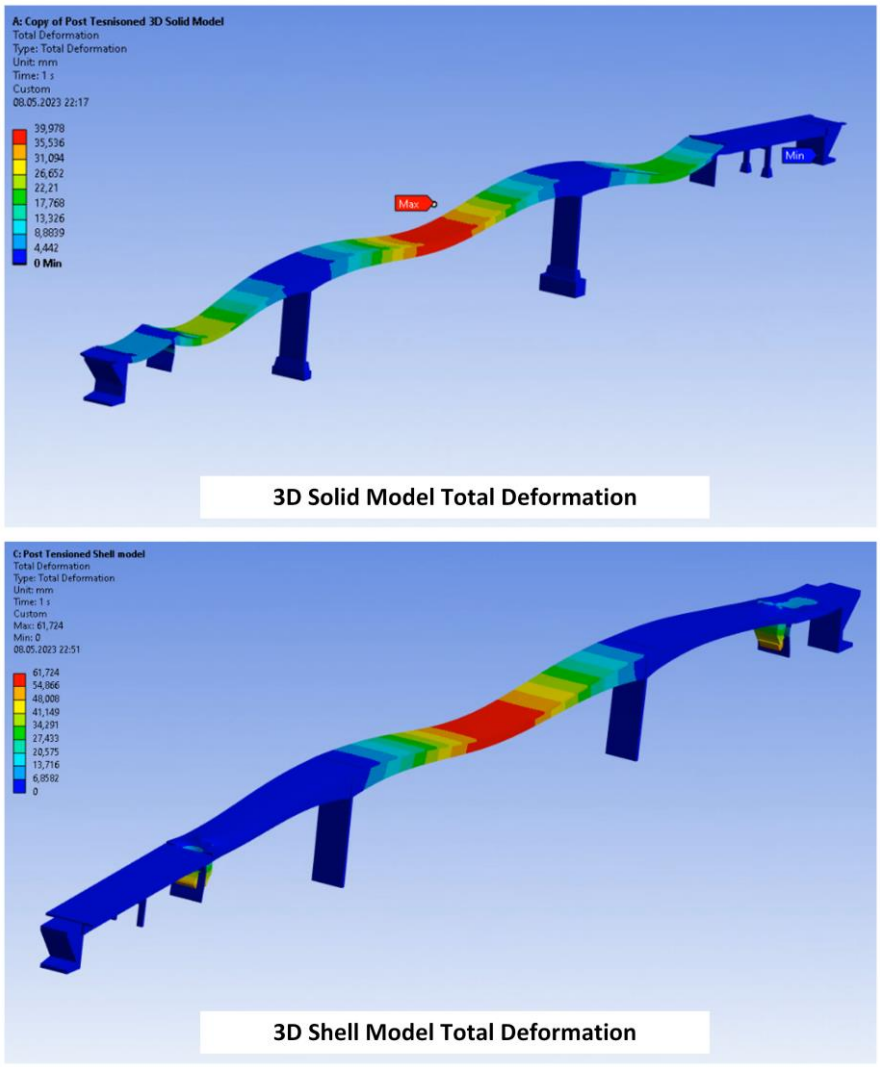

Figure 29. Maximum total deformation for 3D- Solid and Shell model

8.1 Modal Analysis

The numerical modal analysis generates mode shapes and natural frequencies. The lowest energy modes, i.e., mode one to six, are discussed in this section, the mode shapes for mode 7 to mode 20 for solid and shell models could be found in Appendix IV. In numerical modal analysis, mode shapes characterize the displacement pattern, whereas natural frequencies represent the oscillation frequency at each mode. For complicated constructions like the Herøysund Bridge, FEM calculates the natural frequency and identifies mode shapes. There are three primary mode shapes; flexural (bending), transverse, and torsional, also known as the twist. The significance of each mode type can vary substantially based on the bridge's design, materials, location, and load types. For the Herøysund Bridge, a severity matrix can be seen in Table 8 based on the importance of each mode in the design criteria. A brief overview of all three mode shapes for Solid and Shell models can be seen listed in Table 9.

Table 8. Severity mode shape matrix against design parameters

Design factor / Mode shape	Flexural (bending)	Transverse	Torsional (twist)
The integrity of the structure	High	High	Medium
Pedestrian comfortability	High	High	Medium
Complexity of design	High	Medium	Medium
Monitoring and maintenance	High	High	High

Table 9. Mode types and affected characteristics

Characteristics \ Mode Type	Flexural (Bending)	Transverse	Torsional (Twist)
Nature of Motion	Up and down	Side to side	Twisting
Primary Causes	Self-weight and load	Self-weight and load	Uneven weight distribution
Impact on Structure	Deflection, cracking	Lateral instability	Twisting, warping
Frequency	Lowest	Higher than flexural	Higher than flexural and transverse
Design Considerations	Material selection, geometry	Wind barriers, damping	Symmetry, torsional stiffness

8.1.1 Mode shapes and frequencies of 3D- Solid model

The Herøysund Bridge also shows the primary mode shapes for the 3D- Solid model in Figure 30. The nature of modes shows a similar general pattern of modes for structures. The first mode of Herøysund Bridge is also the flexural mode (first fundamental mode). The reason is that the flexural mode is a primary vibrational mode that requires the least energy for excitation with equal mass distribution, resulting in the whole structure exciting cohesively. Since the natural frequency is inversely proportional to the square root of mass, as described by the equation below;

$$\omega_n = \frac{1}{2\pi}\sqrt{\frac{k}{m}}, \tag{8.1}$$

where, ω_n represents the natural frequency of the system, k is the spring constant, and m represents the mass of the system. The overall frequency magnitude required to cause longitudinal bending or flexure is low. The first flexural mode shown in Figure 30a is the first fundamental mode with the least resonant frequency magnitude of 1.3486 Hz, i.e., with the highest wavelength. The high wavelength means a slight variation in modal displacements across the structure. Therefore, the first flexural mode shape also depicts deformation in one section only, i.e., mid-span. Similarly, the second and third flexural modes represent two and three crests oscillating in opposite directions.

The lowest energy state is the energy required to oscillate a structure [25]. In the bridge structure under investigation, the second lowest excitation energy state occurred for transverse bending mode at 1.6808 Hz in Figure 30b. The third and fourth lowest energy states were found for the second flexure at (2.5177 Hz) and the first twist mode at (3.3022 Hz) in Figure 30(c &d). Moreover, the fifth and sixth lowest energy states occur for the second twist at (3.4874 Hz) and the third flexural mode at (3.6568 Hz) in Figure 30(e & f). In general, the excitation frequency for each mode shape increases while the wavelength decreases. Thus, it was deduced that the displacement variation is multiplying, i.e., more upward (crests) and downward (troughs) oscillations with increasing frequency. Another significant finding was that the mode shapes at higher frequencies showed flexure, transverse, and torsional modes combinations.

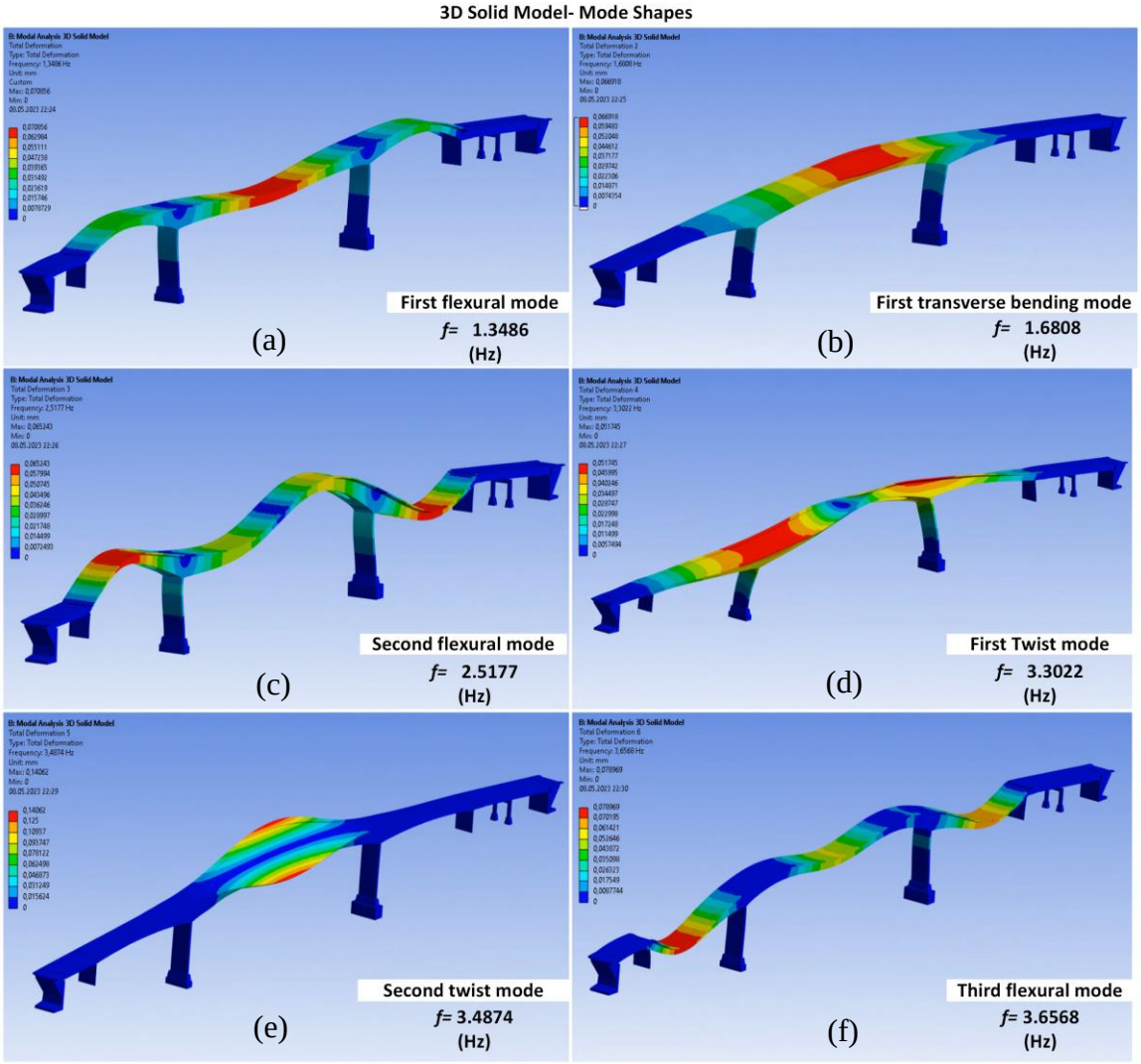

Figure 30. 3D- Solid model first six mode shapes

However, the most vulnerable frequencies for a structure are the lowest achievable frequencies, so the first six mode shapes are shown in Figure 30. The resonant frequencies for the first twenty modes can be seen in Table 10.

Table 10. 3D- Solid model first twenty modes with corresponding resonant frequencies

Modes and Frequencies					
Modes	**1**	**2**	**3**	**4**	**5**
Frequency (Hz)	1.3486	1.6808	2.5177	3.3022	3.4874
Modes	**6**	**7**	**8**	**9**	**10**
Frequency (Hz)	3.6568	4.4578	4.7402	6.1745	6.7829
Modes	**11**	**12**	**13**	**14**	**15**
Frequency (Hz)	7.0255	7.3416	7.3879	7.6387	9.6832
Modes	**16**	**17**	**18**	**19**	**20**
Frequency (Hz)	9.6869	10.143	10.612	12.005	13.08

8.1.2 Mode shapes and frequencies for the Shell model

Similar to the Solid model, the excitation frequency for each mode shape increases while the wavelength decreases. In the bridge Shell model under investigation, the first flexural mode shown in Figure 32 is also the first fundamental mode with the lowest resonant frequency magnitude of 1.2773 Hz in Figure 31a, i.e., with the highest wavelength. The second lowest excitation energy state was also found to occur for transverse bending mode at a frequency of 1.5415 Hz in Figure 31b. The third and fourth lowest energy states for the first twist mode (2.5447 Hz) and second flexure (2.5613 Hz) are in Figure 31(c&d). Moreover, the fifth and sixth lowest energy states for the second twist (3.0333 Hz) and third flexural mode (3.7280 Hz) are in Figure 31 (e&f), respectively.

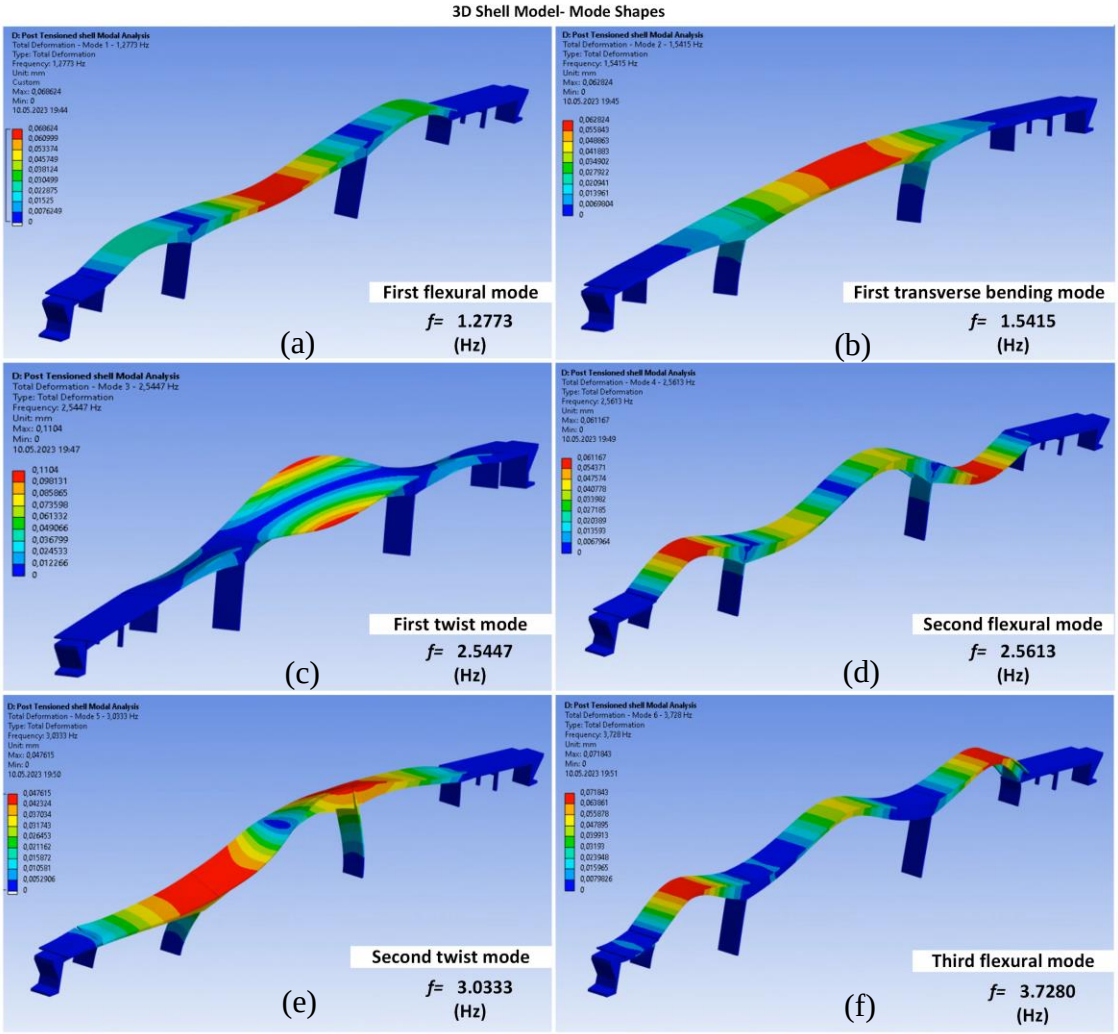

Figure 31. Shell model first six mode shapes

The mode shapes at higher frequencies again show a combination of flexure, transverse and torsional modes in the Shell model. However, the sequence of mode shapes in the Shell model

does not undergo exact modal excitation as in the Solid model. It was found that the first twist mode in the Shell model occurs at a frequency of 2.5447 Hz, and it has the third lowest frequency, followed by the second flexure at 2.5613 Hz and then the second twist at 3.0333 Hz. Since a structure needs much more energy to twist than it needs for bending, it is deduced that the lower stiffness of the Shell model has a primary contribution to this variation. The frequency at which the Solid model undergoes the second flexure and the Shell model undergoes the first twist. The differences will be further analyzed in the modal assurance criteria comparison Section. Moreover, the first twenty resonant frequencies for the Shell model can be seen in Table 11.

Table 11. Shell model first twenty modes with corresponding resonant frequencies

Modes and Frequencies					
Modes	**1**	**2**	**3**	**4**	**5**
Frequency (Hz)	1.2773	1.5415	2.5447	2.5613	3.0333
Modes	**6**	**7**	**8**	**9**	**10**
Frequency (Hz)	3.728	3.9371	4.2565	4.5244	4.9784
Modes	**11**	**12**	**13**	**14**	**15**
Frequency (Hz)	5.502	6.584	6.9045	7.4243	7.5512
Modes	**16**	**17**	**18**	**1**	**20**
Frequency (Hz)	7.6499	8.5219	8.7959	9.8551	9.9871

9 Modal assurance criteria analysis

The Modal Assurance Criterion (MAC) is a quantitative/statistical method of comparing mode shapes. It produces a similarity matrix that compares mode shapes for different numerical models or quantifies the similarity between numerical and experimental data. Its ability to normalize the mode shapes to a common scale provides a sound base for a reliable comparison of two models using FEM [43].

This study implemented the MAC to compare the mode shapes for 3D-Solid and Shell models. The MAC value of "one" represents a perfect match between modes, meaning the modes have identical shapes and phases, while "zero" represents no correlation between mode shapes. The scalar comparison depicts the similarity percentage between modes establishing "one" & "zero" as match percentage maxima and minima, respectively. The MAC matric for the Solid vs. Shell model is generated using ANSYS 2023 R1 NVH MAC Toolkit. That is plotted against their corresponding modal frequencies, as in Figure 32. MAC Index matrix for Solid and Shell model matched modes. In the matrix, each modal frequency of the Solid model (along the y-axis) corresponds to the Shell model (along the x-axis) with similarily index ranging from 0 to 1.

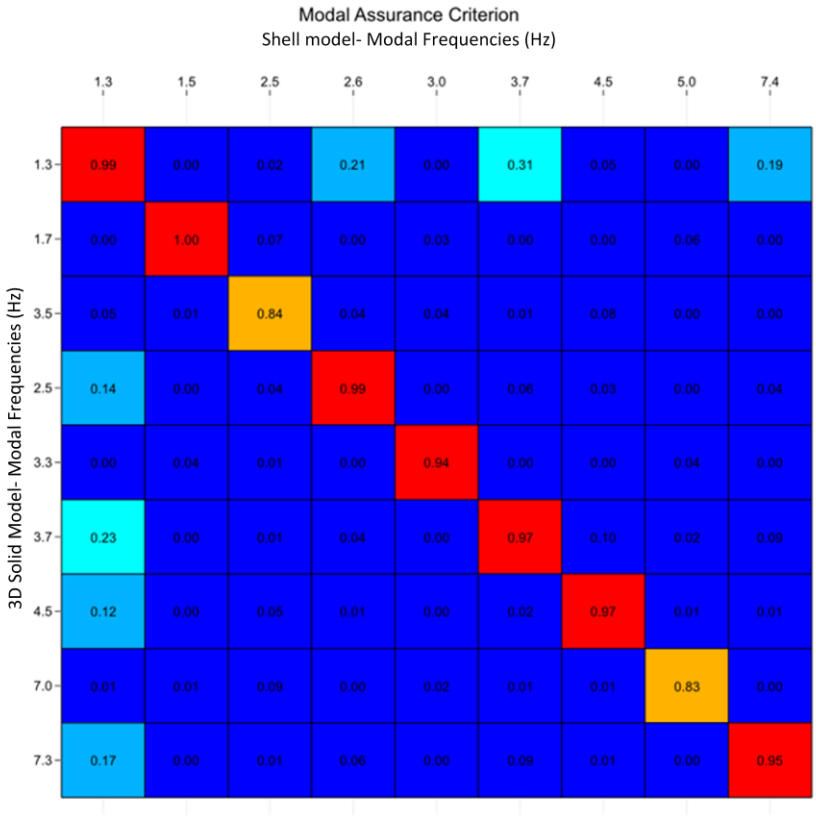

Figure 32. MAC Index matrix for Solid and Shell model matched modes

The similarity percentages for each mode can be seen listed in Table 12 for a better understanding of the MAC matrix. The similarity percentage in MAC between 0.8 - 1 is considered a good agreement between the two numerical models in the MAC analysis.

Table 12. MAC Index of Solid and Shell mode shapes

Freq. Solid model (Hz)	**Mode No.**	**Freq. Shell model (Hz)**	**Mode No.**	**Abs. Freq. error (Hz)**	**Rel. Freq. error (%)**	**MAC**	**Relative Similarity**
1.35	1	1.28	1	0.07	5.58	0.99	High
1.68	2	1.54	2	0.14	9.04	1	Max.
3.49	5	2.54	3	0.94	37.05	0.84	Lower
2.52	3	2.56	4	-0.04	-1.7	0.99	High
3.3	4	3.03	5	0.27	8.86	0.95	High
3.66	6	3.73	6	-0.07	-1.91	0.97	High
4.46	7	4.52	9	-0.07	-1.47	0.98	High
7.03	11	4.98	10	2.05	41.12	0.83	Lower
7.34	12	7.42	14	-0.08	-1.11	0.95	High

The MAC values are highly sensitive to large differences in shapes. The comparison shows very low discrepancies in the mode shapes for the models being compared. Similar to the finding in the total deformation, the mode shapes for the Shell model show a difference in mode shape sequence for the 3rd, 4th, and 5th modes. However, it is found that despite having a

difference in the sequence of mode shape occurrence, the modal frequencies are in good agreement for both the models, with a maximum similarity of 100% for mode 2 (Solid and Shell) and minimum similarity of 83% for mode 11 & 10 in Solid and Shell models respectively. A decent agreement was found for nine mode shapes in total among the first twenty modes.

It is important to note that for structures such as Herøysund Bridge, the lowest frequencies are of the highest importance. The reason is that the energy of excitation required for these modes is low, which can primarily cause the induced frequencies by external loads and environmental conditions to coincide with the system's natural frequencies [43]. It can result in resonance or even structural failure; however, a detailed study is required to identify the system's experimental frequencies to interpret the possibility of resonance.

The comparison of mode shapes shows that despite having approximations and assumptions in the Shell model, the MAC for both models shows good agreement for the concerned mode shapes and corresponding modal frequencies. The built-in property of normalizing the deformation vectors at each node of models in MAC allows reaching this conclusion. Normalization means the sum of squares of element deformation values equals 1 [43]. This characteristic makes MAC independent of mode magnitudes and compares mode shapes. A 3-D representation of mode shapes similarity can be seen in Figure 33.

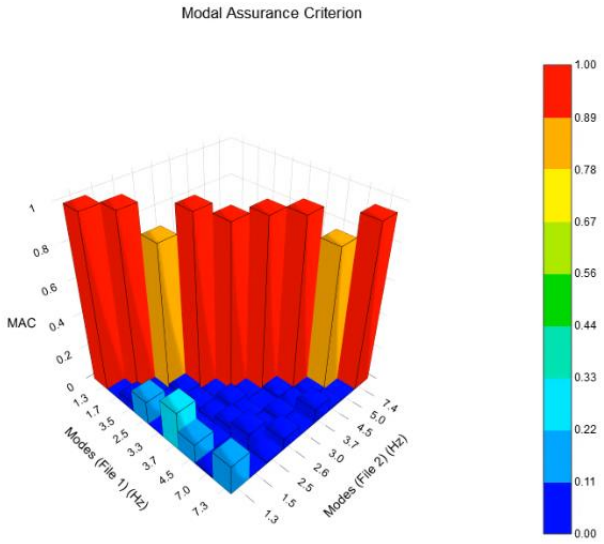

Figure 33. 3D MAC representation for Solid and Shell models

9.1 Comparison of modal frequencies

This sub-section discusses the MAC comparison of 3D-Solid and Shell models. The mode shapes listed in Table 8. Severity mode shape matrix against design parameters will be compared for models, to identify the similarity index.

9.1.1 First Flexural mode

The first flexural mode for Solid and Shell models occurs at 1.3486 Hz and 1.2773 Hz, respectively, shown in Figure 34 below. The fundamental or first bending mode frequencies depict the deformation at the lowest excitation energy, with a match percentage of 99% and an absolute frequency error of 0.07 Hz. The first mode for Solid and Shell models is almost identical and has a high degree of similarity.

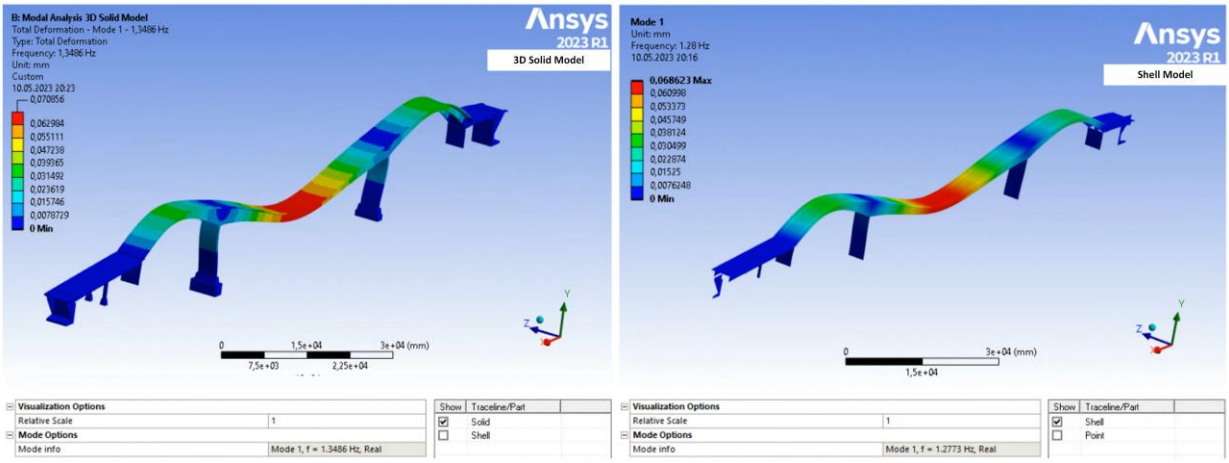

Figure 34. Flexure mode comparison for Solid and Shell model

9.1.2 First transverse bending mode

For Solid and Shell models, the transverse mode (bending perpendicularly to the longitudinal axis) occurs at frequencies of 1.6808 Hz and 1.5415 Hz, respectively, as shown in Figure 35 below. The frequencies depict the deformation at the second lowest excitation energy, with a match percentage of 100% and an absolute frequency error of 0.14 Hz. It means the second mode for the Solid and Shell models is identical and has maximum similarity.

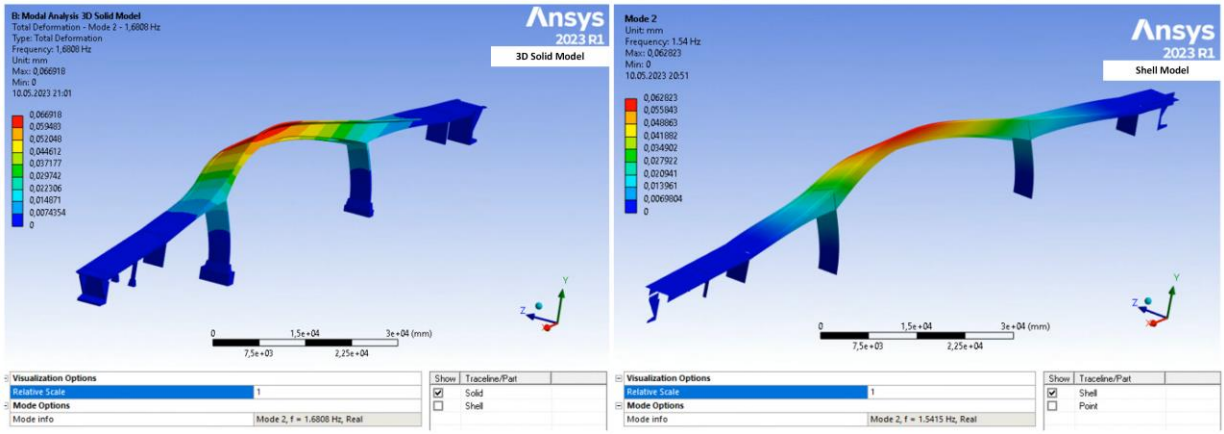

Figure 35. Transverse mode comparison for Solid and Shell model

9.1.3 Twist mode

The twist mode for both models occurs at frequencies of 3.4874 Hz (mode 5) and 2.5447 Hz (mode 3), respectively, as sown in Figure 36, with a match percentage of 84% and an absolute frequency error of 0.94 Hz. It is important to mention that the order of mode shape sequence is affected by modeling differences, numerical precision, and complexity of modes(cite). It implies that the twist mode for Solid and Shell models has significant similarity but is lower than other mode shapes.

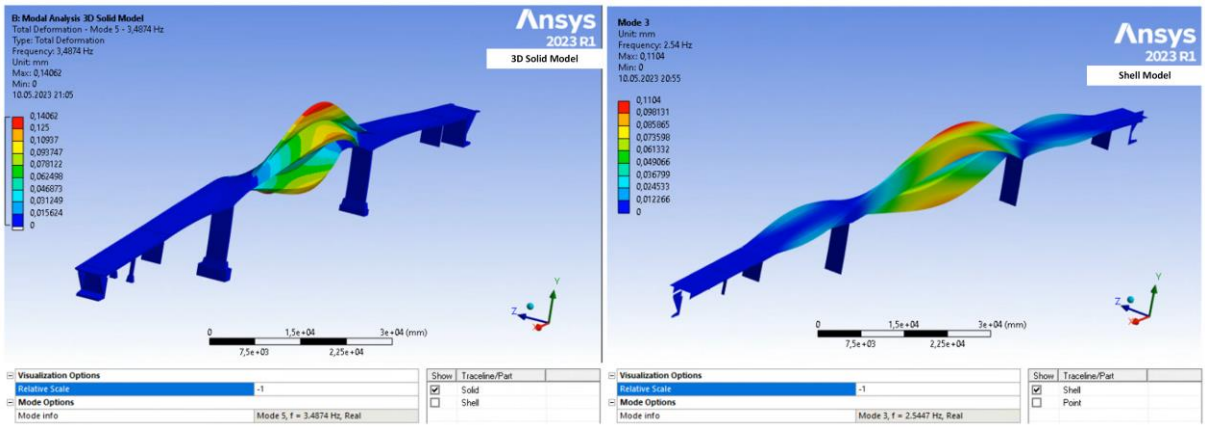

Figure 36. Twist mode comparison for Solid and Shell model

9.1.4 Second flexural mode

The second flexure mode for both models occurs at 2.5177 Hz (mode 3) and 2.5447 Hz (mode 4), respectively, as shown in Figure 37, with a match percentage of 84% and an absolute frequency error 0.94 Hz. It means that the second flexure mode for Solid and Shell models is almost identical and has a high degree of similarity in the behavior of the physical structure. A similar sequential mode shape difference exists for the second flexure mode.

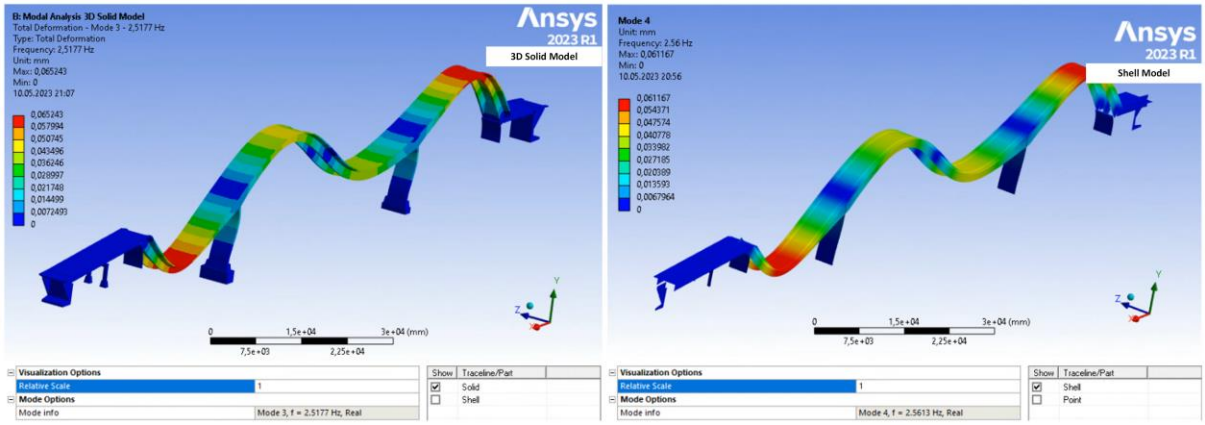

Figure 37. Second Flexure mode comparison for Solid and Shell model

9.1.5 Second twist mode

The second twist mode for both models occurs at 3.3022 Hz (mode 4) and 3.3033 Hz (mode 5), respectively, as shown in Figure 38, with a match percentage of 95% and an absolute frequency error 0.27 Hz. The second flexure mode for Solid and Shell models is also almost identical. A similar sequential mode shape difference exists for the second twist mode.

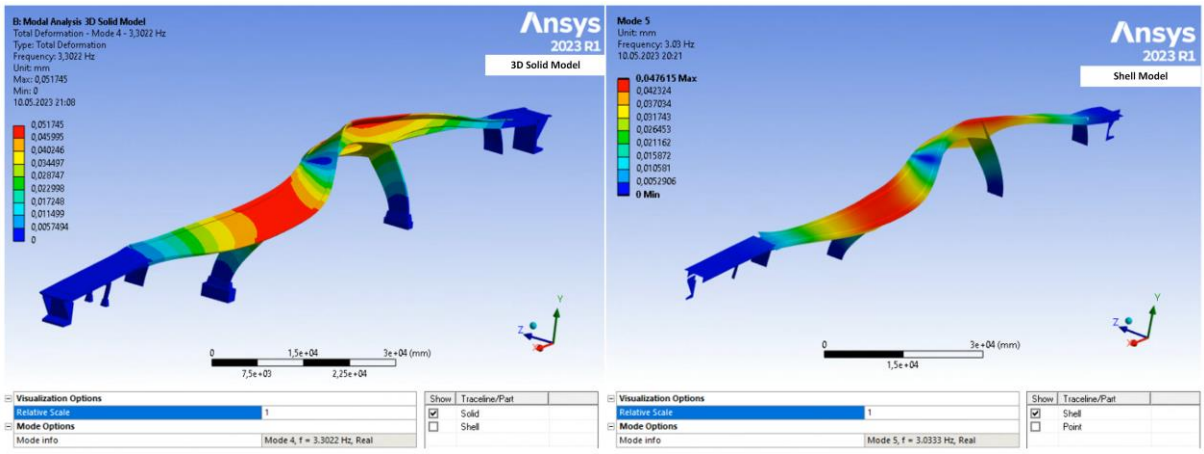

Figure 38. Second twist mode comparison for Solid and Shell model

9.1.6 Third flexural mode

The third flexure mode for both models occurs at 3.6568 Hz (mode 6) and 3.7280 Hz (mode 6), respectively, as shown in Figure 39, with a match percentage of 97% and an absolute frequency error 0.94 Hz. That implies that the second flexure mode for Solid and Shell models is almost identical and highly similar.

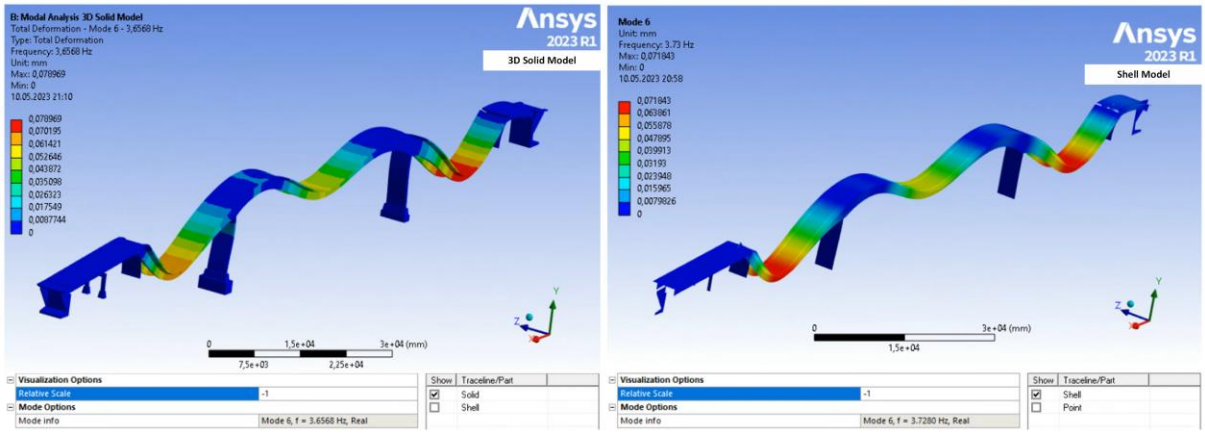

Figure 39. Third flexure mode comparison for Solid and Shell model

Further results with normal stress, modes seven to twenty and MAC comparison for other mode shapes can be seen attched in Appendix IV.

9.2 Conrtibution of modes in Solid and Shell model

The participation factor and effective mass are two metrics for assessing the mass movement of each mode along the x, y, and z axes. A bigger number indicates that oscillations in that direction may be able to leave the mode. Both the parameters actually identify the same mode that has maximum contribution in modal analysis.

9.2.1 3D Solid model excitation participation modes

The modes identifed in the numerical simulations for solid 3D model can be seen in the Table 13.

Table 13. Participartion modes for translational and rotatonal participation of modes

Excitation	Participating modes	Effective mass ratio
X-Direction	1, 3, 4, 7, 8, 9, 14, 15, 17, 19	84.11%
Y-Direction	1, 3, 4, 7, 8, 9, 14, 15, 17, 19	40.67%
Z-Direction	2, 6, 8, 9, 10, 11, 12, 13, 16, 18, 20	65.41%
X-Direction	2, 7	56.02%
Y-Direction	2, 8	56.38%
Z-Direction	2, 5, 6, 10, 11, 12, 18, 20	37.92%

Overall, the combined modal mass, kinetic energies and translational effective masses show significant contribution from mode 2 and mode 8, followed by mode 9, 16, 18 and 20 respectively, and can be seen in Figure 41.

***** MODAL MASSES, KINETIC ENERGIES, AND TRANSLATIONAL EFFECTIVE MASSES SUMMARY *****

				EFFECTIVE MASS					
MODE	FREQUENCY	MODAL MASS	KENE	X-DIR	RATIO%	Y-DIR	RATIO%	Z-DIR	RATIO%
1	1.232	185.2	5550.	5.642	0.41	96.99	7.00	0.8248E-06	0.00
2	1.690	238.1	0.1343E+05	0.2531E-07	0.00	0.4384E-06	0.00	536.5	38.74
3	2.568	237.0	0.3085E+05	22.05	1.59	0.2101	0.02	0.1349E-04	0.00
4	3.015	565.7	0.1015E+06	863.7	62.36	66.20	4.78	0.2584E-10	0.00
5	3.291	404.9	0.8656E+05	0.3047E-03	0.00	0.6177E-03	0.00	0.9759E-02	0.00
6	3.457	51.29	0.1210E+05	0.1185E-04	0.00	0.7093E-05	0.00	0.2393	0.02
7	3.629	176.3	0.4583E+05	211.8	15.29	251.4	18.16	0.1292E-03	0.00
8	4.696	331.0	0.1441E+06	4.447	0.32	0.2524	0.02	243.3	17.57
9	4.698	242.2	0.1055E+06	34.95	2.52	1.878	0.14	31.12	2.25
10	6.175	119.8	0.9019E+05	0.4181E-05	0.00	0.1118E-03	0.00	0.9238	0.07
11	6.776	148.1	0.1343E+06	0.7974E-05	0.00	0.7959E-03	0.00	1.836	0.13
12	7.068	33.30	0.3284E+05	0.3045E-06	0.00	0.1824E-04	0.00	6.167	0.45
13	7.329	38.76	0.4110E+05	0.2345E-03	0.00	0.1224E-01	0.00	0.7398	0.05
14	7.384	201.0	0.2164E+06	3.217	0.23	57.13	4.12	0.2921E-04	0.00
15	9.310	247.3	0.4232E+06	17.10	1.23	9.058	0.65	0.1548E-01	0.00
16	9.381	323.9	0.5626E+06	0.4673E-02	0.00	0.7052E-03	0.00	64.05	4.62
17	9.655	99.82	0.1837E+06	1.944	0.14	0.3788	0.03	0.1983E-02	0.00
18	10.14	80.66	0.1636E+06	0.2951E-07	0.00	0.2102E-03	0.00	14.05	1.01
19	10.66	155.9	0.3497E+06	0.1085	0.01	79.71	5.76	0.5622E-04	0.00
20	11.49	319.8	0.8338E+06	0.1297E-08	0.00	0.2201E-01	0.00	6.950	0.50
sum				1165.	84.11	563.3	40.67	905.9	65.41

Figure 40. Effective masses summary for extracted modes

9.2.2 Shell model excitation participation modes

The modes identifed in the numerical simulations for solid Shell model can be seen in the table

Table 14. Shell model participartion of modes

Excitation	Participating modes	Effective mass ratio
X-Direction	1, 4, 6, 9, 13, 14, 16, 17, 19, 20	72.79%
Y-Direction	1, 4, 6, 9, 13, 14, 16, 17, 19, 20	43.23%
Z-Direction	2, 3, 5, 7, 8, , 10, 11, 12, 13, 16, 15, 18	70.30%
X-Direction	2, 6	58.33%
Y-Direction	2, 8	60.76%
Z-Direction	2, 10, 11, 12, 15	36.05%

Overall for shell model as well, the combined modal mass, kinetic energies and translational effective masses show significant contribution from mode 2 and mode 8, followed by mode 10, 12, 17 respectively.

***** MODAL MASSES, KINETIC ENERGIES, AND TRANSLATIONAL EFFECTIVE MASSES SUMMARY *****

				EFFECTIVE MASS					
MODE	FREQUENCY	MODAL MASS	KENE	X-DIR	RATIO%	Y-DIR	RATIO%	Z-DIR	RATIO%
1	1.277	212.4	6840.	0.4750E-01	0.00	76.68	5.67	0.1095E-03	0.00
2	1.541	272.0	0.1276E+05	0.3652E-05	0.00	0.1073E-04	0.00	583.6	43.19
3	2.545	82.06	0.1049E+05	0.5927E-04	0.00	0.8206E-05	0.00	0.7804	0.06
4	2.561	271.6	0.3517E+05	12.79	0.95	0.4582	0.03	0.5679E-05	0.00
5	3.033	480.4	0.8725E+05	0.2409E-04	0.00	0.4148E-04	0.00	0.2870	0.02
6	3.728	194.1	0.5325E+05	4.574	0.34	388.7	28.77	0.1425E-03	0.00
7	3.937	215.7	0.6601E+05	0.1120E-04	0.00	0.6190E-04	0.00	0.9331E-01	0.01
8	4.257	231.5	0.8278E+05	0.3793E-03	0.00	0.4906E-04	0.00	274.8	20.34
9	4.524	308.1	0.1245E+06	93.04	6.89	0.8741	0.06	0.4701E-03	0.00
10	4.978	80.37	0.3932E+05	0.5345E-04	0.00	0.1388E-05	0.00	12.74	0.94
11	5.502	136.7	0.8167E+05	0.5110E-05	0.00	0.2972E-07	0.00	0.1306	0.01
12	6.584	332.8	0.2848E+06	0.1227E-03	0.00	0.1290E-03	0.00	3.170	0.23
13	6.905	74.39	0.7001E+05	746.5	55.25	2.745	0.20	0.9502E-04	0.00
14	7.424	45.50	0.4951E+05	27.76	2.05	35.34	2.62	0.5929E-07	0.00
15	7.551	141.9	0.1597E+06	0.4468E-03	0.00	0.1771E-03	0.00	0.2265	0.02
16	7.650	57.33	0.6623E+05	74.92	5.54	67.79	5.02	0.8064E-04	0.00
17	8.522	19.69	0.2823E+05	13.94	1.03	0.1197	0.01	0.1061E-04	0.00
18	8.796	247.8	0.3784E+06	0.3358E-04	0.00	0.7141E-05	0.00	73.92	5.47
19	9.855	153.5	0.2944E+06	7.394	0.55	5.612	0.42	0.1260E-04	0.00
20	9.987	33.76	0.6646E+05	2.585	0.19	5.775	0.43	0.1132E-05	0.00
sum				983.5	72.79	584.1	43.23	949.8	70.30

Figure 41. Effective masses summary for extracted modes

The detailed participation factors extracted from ANSYS for both models can be seen in Appendix VII.

10 Conclusion

The primary aim of this thesis was to provide an in-depth numerical prestressed modal analysis of 3D Solid and Shell models utilizing finite element modeling for Herøysund Bridge design. FEM was used to accurately predict structural deformations, modes, shapes, and modal frequencies in a post-tensioned concrete bridge structure. Developing a 3D solid model and extracting the Shell model through mid-surfacing yielded high similarity between models. Developing a 3D solid model and extracting the Shell model through mid-surfacing yielded high similarity between models. The Shell model requires geometrical simplifications due to the different element types used in numerical simulation. The mass and volume control for models resulted in a percentage difference of 1.028% which was negligible; however, the Shell model resulted in a mass distribution difference across the structure.

Structural analysis revealed distinct deformations for 3D Solid and Shell models, with Shell models allowing more deformation than the solid model. Another significant finding was that the defined joints, instead of default bonded joints, allowed the bridge connections to deform realistically. The total deformation for the Solid model was in good agreement with the structural calculations from AAS Jacobsen validating the Solid model. The total deformation of the 3D Solid model yielded a better representation of the physical structure. The prestressed modal analysis revealed distinct mode shapes and modal frequencies for 3D Solid and Shell models. The study also explored differences in the modal frequencies across various modes, including flexural, transverse bending, and twist modes. The MAC correlation for Shell vs. Solid found that the MAC correlation for nine modes out of twenty was in good agreement. 80-100%. Although the mode shapes were identical, it was also revealed that they appeared in different sequences for the shell model because of the mass distribution difference across different spans. Despite the comprehensive analysis, the study had limitations such as limited post-tensioned tendons details leading to assumption, shell model geometrical limitations leading to mass distribution difference, time constraints to dive deeper, and approximations in applying boundary conditions in ANSYS. The findings are significant for Herøysund Bridge since the data obtained for both models will significantly contribute to comparing experimental vibration data with numerical results. This study also signifies the credibility of the 3D Solid model strategy for complex concrete structures such as the Herøysund Bridge. Finally, the insights derived in this study underscore the importance of FEM in revolutionizing bridge design, leading to efficient and more reliable structures.

11 Future work

Future work could extend the current research by incorporating different load scenarios, exploring other types of FEM modeling, or applying the methods to other bridge structures. A few suggestions are as follows:

1. The numerical results obtained in the thesis study could be compared OMA activity to validate the resonant frequencies of the physical structure.
2. The numerical analysis of Herøysund Bridge could be conducted incorporating the dynamic loading conditions such as wind, siesmic, traffic loads.
3. The geometric methodology used in this study could be used for other concrete bridges to identify the best methodology for comparable bridge constructions.

4. A parametric study for Herøysund Bridge could be carried out to identify the sentivity of parameters affecting mode shapes, deformation and modal frequencies of post-tensioned tendons.
5. An in-depth numerical model of the bridge could be developed with consideration of non-linear affects caused by friction, post-tensioned tendons and dynamic loads.
6. A dynamic simulation of bridge could be performed with induced cracks currently present

References

[1] ‘Herøysund bru’, *SINTEF*, Nov. 02, 2022. https://www.sintef.no/prosjekter/2022/heroysund-bru/ (accessed Apr. 30, 2023).

[2] L. H. Fredheim, ‘18-1069 HERØYSUND BRU SPESIALINSPEKSJON’. Statens vegvesen, oktober 2017.

[3] A. Sveen, ‘18-1069 Herøysund bru. Bæreevneberegninger’. Statens vegvesen, Nov. 09, 2020.

[4] M. Selmurzaev, ‘Rapportering av måleregistringer for tidsrom September 2021’. HBK Norge AS, Oct. 15, 2021.

[5] M. Holmqvist, ‘Locating voids in grouted tendon ducts with NDT’. (DEKRA Industrial AB), Feb. 18, 2020.

[6] ‘Bruer, ferjekaier og andre bærende konstruksjoner’, *Statens vegvesen*. https://www.vegvesen.no/fag/publikasjoner/handboker/handboker-etter-hovedtema/bruer-ferjekaier/ (accessed May 06, 2023).

[7] Z. P. Bažant and M. Jirásek, *Creep and Hygrothermal Effects in Concrete Structures*, 1st ed. 2018. in Solid Mechanics and Its Applications, no. 225. Dordrecht: Springer Netherlands : Imprint: Springer, 2018. doi: 10.1007/978-94-024-1138-6.

[8] H. Süleymanoğlu, A. Uzel, and G. Arslan, ‘Use of Post-tensioned Concrete Slabs for Sustainable Design of Buildings’, in *High Tech Concrete: Where Technology and Engineering Meet*, D. A. Hordijk and M. Luković, Eds., Cham: Springer International Publishing, 2018, pp. 2390–2395. doi: 10.1007/978-3-319-59471-2_272.

[9] ‘Post-Tensioning Institute > Education > PT Applications > PT 101’. https://www.post-tensioning.org/education/ptapplications/pt101.aspx (accessed Apr. 30, 2023).

[10] J. Abdelhalim, ‘Prestressed Concrete Slabs with Bonded and Unbonded Tendons’, *Theses and Dissertations*, May 2021, [Online]. Available: https://fount.aucegypt.edu/etds/1658

[11] J. Tørset, ‘Thesis Master of Technology Management’, Sep. 2003. [Online]. Available: https://www.konstruksjon.com/manuel/gammel/NorwayBridgeHistory.pdf

[12] R. M. Barton, ‘Prestressed Precast Concrete Railroad Bridges’, *Journal of the Structural Division*, vol. 94, no. 12, pp. 2885–2912, Dec. 1968, doi: 10.1061/JSDEAG.0002146.

[13] W. on H. Ltd, ‘Composite Bridges | Design & Construction’. https://www.steel-bridges.com/composite-beam-bridge.html (accessed Apr. 21, 2023).

[14] A. Pipinato, ‘30 - Bridge construction equipment’, in *Innovative Bridge Design Handbook (Second Edition)*, A. Pipinato, Ed., Butterworth-Heinemann, 2022, pp. 827–852. doi: 10.1016/B978-0-12-823550-8.00022-6.

[15] M. Hassanein, Y. Shao, and M. Zhou, ‘Chapter 2 - Development of bridges with corrugated webs’, in *Behavior and Design of Trapezoidally Corrugated Web Girders for Bridge Construction*, M. Hassanein, Y. Shao, and M. Zhou, Eds., in Woodhead Publishing Series in Civil and Structural Engineering. Woodhead Publishing, 2022, pp. 3–17. doi: 10.1016/B978-0-323-88437-2.00008-3.

[16] L. Aurier, M. Hassan, J. Jaworski, and L. Guizani, ‘Review of Accelerated Bridge Construction Systems for Bridge Superstructures and Their Adaptability for Cold Weather’, *CivilEng*, vol. 4, no. 1, Art. no. 1, Mar. 2023, doi: 10.3390/civileng4010007.

[17] midasBridge Team, ‘Construction Analysis of Precast Bridge’. http://www.midasbridge.com/en/blog/casestudy/construction-analysis-of-precast-bridge (accessed Apr. 21, 2023).

[18] ‘Historical development and description of box girder - Shanghai Metal Corporation’. https://www.shanghaimetal.com/929-929.htm (accessed Apr. 22, 2023).

[19] M. A. Haider, M. Batikha, and T. Elhag, ‘Precast versus cast in-situ concrete in the construction of post-tensioned box-girder bridges: Span effect’, *Structural Concrete*, vol. 21, no. 1, pp. 56–64, 2020, doi: 10.1002/suco.201800263.

[20] T. Cakebread, ‘The role of finite element analysis in bridge assessment and design’, pp. 2433–2439, Jul. 2010, doi: 10.1201/b10430-369.

[21] S. Li, Y. Yang, Q. Pu, D. Yang, B. Sun, and X. Li, ‘Three-dimensional nonlinear creep and shrinkage effects of a long-span prestressed concrete box girder bridge’, *Structural Concrete*, vol. 20, no. 2, pp. 638–649, 2019, doi: 10.1002/suco.201800148.

[22] I. Souza Hoffman, B. Manica Lazzari, A. Campos, P. Manica Lazzari, and A. Rodrigues Pacheco, ‘Finite element numerical simulation of a cable-stayed bridge construction through the progressive cantilever method’, *Structural Concrete*, vol. 23, no. 2, pp. 632–651, 2022, doi: 10.1002/suco.202100662.

[23] H. Broo, M. Plos, K. Lundgren, and B. Engström, ‘Non-linear finite-element analysis of the shear response in prestressed concrete bridges’, *Magazine of Concrete Research*, vol. 61, no. 8, pp. 591–608, Oct. 2009, doi: 10.1680/macr.2008.61.8.591.

[24] P. Pathak and Y. X. Zhang, ‘Nonlinear finite element analyses of fiber-reinforced polymer-strengthened steel-reinforced concrete beams under cyclic loading’, *Structural Concrete*, vol. 18, no. 6, pp. 929–937, 2017, doi: 10.1002/suco.201600122.

[25] G. Szeidl and L. P. Kiss, *Mechanical vibrations: an introduction*. in Foundations of engineering mechanics. Cham, Switzerland: Springer, 2020.

[26] T. Nishat and R. Ahsan, *Sensitivity analysis of cost optimized solution of post-tensioned pre-stressed concrete i-girder bridge system*. 2018.

[27] E. O. L. Lantsoght, A. de Boer, C. van der Veen, and D. A. Hordijk, ‘Optimizing Finite Element Models for Concrete Bridge Assessment With Proof Load Testing’, *Frontiers in Built Environment*, vol. 5, 2019, Accessed: Apr. 22, 2023. [Online]. Available: https://www.frontiersin.org/articles/10.3389/fbuil.2019.00099

[28] C. Shim, S. Dang, S. Lon, and C. Jeon, ‘Development of a bridge maintenance system for prestressed concrete bridges using 3D digital twin model’, *Structure and Infrastructure Engineering*, vol. 15, pp. 1–14, Jun. 2019, doi: 10.1080/15732479.2019.1620789.

[29] R. Vrijdaghs and E. Verstrynge, ‘Probabilistic structural analysis of a real-life corroding concrete bridge girder incorporating stochastic material and damage variables in a finite element approach’, *Engineering Structures*, vol. 254, p. 113831, Mar. 2022, doi: 10.1016/j.engstruct.2021.113831.

[30] T. García-Segura, V. Yepes, and D. Frangopol, ‘Multi-objective design of post-tensioned concrete road bridges using artificial neural networks’, *Structural and Multidisciplinary Optimization*, vol. 56, pp. 139–150, Jul. 2017, doi: 10.1007/s00158-017-1653-0.

[31] E. Bruun, A. Kuan, G. Proestos, E. Bentz, and M. Collins, *Advanced Nonlinear Finite Element Modelling of Reinforced Concrete Bridge Piers*. 2018. doi: 10.1201/9781315189390-167.

[32] O. C. Zienkiewicz, R. L. Taylor, and J. Z. Zhu, *The finite element method: its basis and fundamentals*, 6th ed. Burlington (Mass.): Elsevier/Butterworth-Heinemann, 2005.

[33] Samuelsson, A, *Finite Element Method- Basics*. Lund, Sweden: Studentlitteratur AB, 1998.

[34] R. J. Cope, 'Structural concrete: finite-element analysis for limit state design: M. D. Kotsovos and M. N. Pavlović Thomas Telford, London, 1995, 550pp. £70 UK and Europe, £78 elsewhere, ISBN: 0 7277 2027 9', *Engineering Structures*, vol. 18, no. 8, p. 655, Aug. 1996, doi: 10.1016/0141-0296(96)87031-3.

[35] S. Tanev, 'Introduction to Finite Element Method, Niels Ottosen, Hans Petersson', *Materials Science and Engineering: B*, vol. 39, no. 1, p. 72, May 1996, doi: 10.1016/0921-5107(96)01551-6.

[36] 'BROSAMVERKAN VÄST. Strukturanalys av brokonstruktioner med finita elementmetoden. Fördelning av krafter och moment. - PDF Free Download'. https://docplayer.se/69470458-Brosamverkan-vast-strukturanalys-av-brokonstruktioner-med-finita-elementmetoden-fordelning-av-krafter-och-moment.html (accessed Apr. 23, 2023).

[37] B. D. Davidson, A. Bansal, Q. Bing, and X. Sun, 'Linear and nonlinear finite element analyses of unidirectional, symmetric single leg four-point bending tests', *Engineering Fracture Mechanics*, vol. 75, no. 8, pp. 2130–2143, May 2008, doi: 10.1016/j.engfracmech.2007.10.009.

[38] 'Eurocode 2: Design of concrete structures | Eurocodes: Building the future'. https://eurocodes.jrc.ec.europa.eu/EN-Eurocodes/eurocode-2-design-concrete-structures (accessed Apr. 30, 2023).

[39] 'Galerkin Method - an overview | ScienceDirect Topics'. https://www-sciencedirect-com.mime.uit.no/topics/physics-and-astronomy/galerkin-method (accessed May 10, 2023).

[40] 'How are governing equations formulated in FEM?', *Quora*. https://www.quora.com/How-are-governing-equations-formulated-in-FEM (accessed May 07, 2023).

[41] 'Kirchhoff–Love plate theory', *Wikipedia*. Aug. 25, 2021. Accessed: May 14, 2023. [Online]. Available: https://en.wikipedia.org/w/index.php?title=Kirchhoff%E2%80%93Love_plate_theory&oldid=1040623925

[42] *Vibrations and Waves in Continuous Mechanical Systems*, 1st ed. John Wiley & Sons, Ltd, 2007. doi: 10.1002/9780470518434.

[43] *Structural Health Monitoring*, 1st ed. John Wiley & Sons, Ltd, 2006. doi: 10.1002/9780470612071.

[44] 'Modal Assurance Criterion (MAC)'. https://community.sw.siemens.com/s/article/modal-assurance-criterion-mac (accessed May 14, 2023).

[45] 'Forvaltning', *Statens vegvesen*. https://www.vegvesen.no/fag/teknologi/bruer/forvaltning/ (accessed May 07, 2023).

[46] 'Ansys | Engineering Simulation Software'. https://www.ansys.com/ (accessed May 07, 2023).

[47] ‘SOLID186’. https://www.mm.bme.hu/~gyebro/files/ans_help_v182/ans_elem/Hlp_E_SOLID186.html (accessed May 06, 2023).

[48] ‘SOLID187’. https://www.mm.bme.hu/~gyebro/files/ans_help_v182/ans_elem/Hlp_E_SOLID187.html (accessed May 06, 2023).

[49] H. Khawaja, ‘Applicability extent of 2-D heat equation for numerical analysis of a multiphysics problem’, presented at the ICNPAA 2016 WORLD CONGRESS: 11th International Conference on Mathematical Problems in Engineering, Aerospace and Sciences, La Rochelle, France, La Rochelle, France, 2017, p. 020075. doi: 10.1063/1.4972667.

[50] ‘Finite Element Analysis’, *MULTIPHYSICS*. https://www.multiphysics.org/finite-element-analysis (accessed Apr. 23, 2023).

[51] ‘Linear Static Analysis’. https://2021.help.altair.com/2021/hwsolvers/os/topics/solvers/os/analysis_linear_static_c.htm (accessed Apr. 23, 2023).

[52] P. P. Górski, ‘Structural analysis and design of concrete bridges Current modelling procedures and impact on design Master of Science Thesis in the Master's Programme Structural Engineering and Building Performance Design’, Accessed: Apr. 22, 2023. [Online]. Available: https://www.academia.edu/8122216/Structural_analysis_and_design_of_concrete_bridges_Current_modelling_procedures_and_impact_on_design_Master_of_Science_Thesis_in_the_Masters_Programme_Structural_Engineering_and_Building_Performance_Design

Site Visit

A Master's thesis is an important step in a student's career as it highlights their expertise and ability to conduct independent research. I was given the opportunity to collaborate with Nordland fylkeskommune and Statens Vegvesen on the Shell type Finite Element Modelling of Herøysund Bridge, and to visit Nordland fylkeskommune in Vefsn Municipality, Mosjøen. During their two-day visit, they met with an exceptional team of experts dedicated to improving the structural health monitoring of bridges in Norway. I was motivated by the zeal and vigor of the Nordland fylkeskommune team as a whole, and is confident that with a strong relationship between university and industry and sufficient funding, we can develop safe, reliable, and innovative bridges across Norway.

The visit helped me gain a thorough look at the Herøysund Bridge. It helped understanding the structure better in terms of joints, configuration, design understanding and overall structural repair zones. The visit also, contributed in the development of a comprehensive CAD model, that was one of the core requirements of this study.

BADagen Presentation

At UiT Norway The Arctic University's Building and Architecture (BA) Day, Patrick and I presented our master's thesis to the industry leaders, including Multi-Consult and SINTEF. The event, aimed at fostering sustainability in the construction sector, provided an opportunity for me to emphasize on the importance of bridge health monitoring. The presentation emphasized the need for formal investigations and specialized skills in the numerical analysis of bridges, resonating with the EU's mandate for 70% recyclability or reusability of construction waste. Feedback from these industrial leaders was constructive and instrumental in fostering dialogue around efficient and sustainable solutions in construction.

Appendix I

Construction classification and methods

Construction in Sections

The Balanced Cantilever Method It entails erecting box girder segments on each side of the pier table in order to balance them. During construction, the segments act as a cantilever supported at the site of the pier table. This is a frequent way for constructing bridges with large spans that are difficult to reach. It is appropriate for usage in regions with limited access and offers superior segment alignment control.

The Incremental Launching Method enables the longitudinal construction of box girder bridges by casting parts on the ground and launching them into place using a launching nose. This approach is ideal for the building of straight bridges, since the mechanism used to move the bridge segments needs a clean, straight surface. In addition, the approach can only be employed in places where the launching nose has adequate clearance. It entails constructing each bridge span sequentially, beginning with one abutment and progressing to the next.

Construction in spans

Full Staging Method, Until the concrete has adequate strength, the whole dead weight of concrete, formwork, and falsework is supported throughout the complete spans of the bridge. This approach is often used for bridges with intermediate spans and restricted clearance, while the usage of continuous tendon is restricted for bridges with lengthy spans.

The Movable Scaffolding Method is a variation of the Span-by-Span Method in which the scaffold moves as each span is constructed. This approach is well suited for the construction of long-span bridges that need continuous support. The approach offers excellent segment alignment control and is especially beneficial in regions with restricted clearance. On the basis of building phases defined by construction joints, structural analysis is performed.

Appendix II

Construction methods

Reinforced concrete bridges:

The use of reinforced concrete was another significant advance in the history of concrete bridge construction in Norway. The addition of steel reinforcing to the concrete boosted the strength and durability of the bridge construction dramatically. During the 1920s and 1930s, reinforced concrete became increasingly popular in Norway, and it was used to build many significant bridges[12].

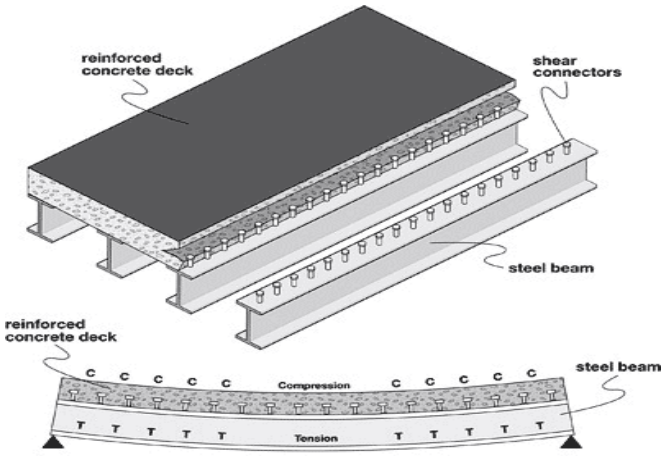

Figure 42. Reinforced concrete bridge [13]

Incremental launching method bridges

The incremental launching method of concrete bridge construction was developed in Norway in the 1960s and 1970s. This method entailed building the bridge in parts on one side of the river and then lifting each component out over the water with hydraulic jacks. This resulted in speedier and more efficient construction and less traffic disturbance during the development period.

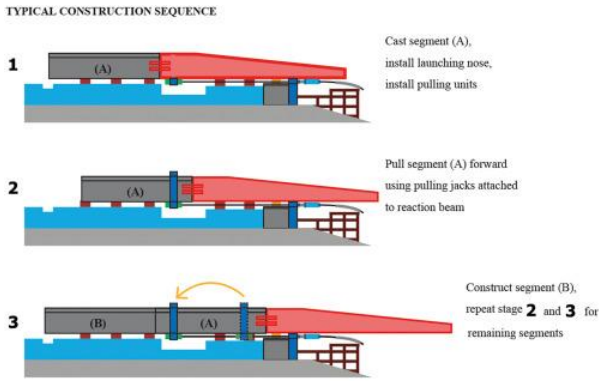

Figure 43. Incremental launching method [14]

Norway now employs a variety of sophisticated concrete bridge construction methods, including cable-stayed bridges, segmental construction, and innovative formwork systems. These approaches enable the building of longer, more complicated, and aesthetically beautiful bridge constructions while keeping the strength and durability demanded by the severe Norwegian climate[15].

Precast concrete bridges

The use of precast concrete parts was one of the early technologies of concrete bridge construction in Norway. Off-site precast materials, such as beams and slabs, were built and delivered to the construction site, where they were combined to form the bridge framework. This technology facilitated faster construction and minimized on-site labor[16]. Cast concrete girder bridges emerged in the early 20th century as a response to the limitations of earlier bridge designs. The first known example was built in San Francisco in 1907. They became increasingly popular during the mid-20th century due to demand for infrastructure and advancements in construction technology. Today, they are a common type of bridge used in a wide range of applications due to their durability, strength, and ease of construction.

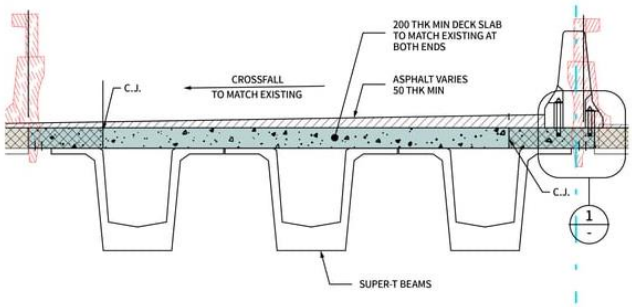

Figure 44. Precast concrete bridge schematics [17]

Appendix III

Section A

FEM case studies in bridge industry

FEM techniques play a vital role in the precise analysis of concrete bridges by accurately modeling their complex structure and predicting their behavior under various loading scenarios. In addition, FEM can assess the effects of deterioration due to environmental factors, including corrosion and loss of material strength, to ensure the longevity and safety of these critical infrastructure assets.

Researchers at Southwest Jiaotong University developed a novel nonlinear analysis model that was created to examine the effects of creep and shrinkage on long-span prestressed concrete box girder bridges in a comprehensive manner. This model incorporated the three-dimensional (3D) features of the structure and the progression of girder degradation. To test the accuracy of the model, a user defined ABAQUS model was used to create a corresponding numerical analysis approach, which was then compared to conventional experimental data. As an engineering example, the concept was applied to a continuous rigid frame bridge with a primary span of 220 meters. The analytical results were compared to long-term deflection data acquired on site. The investigation determined that the 3D characteristic and nonlinear property of creep had a substantial effect on the prediction of long-term deflection[21].

Federal University of Rio Grande do Sul, Brazil researchers studied the simulation of the various phases of the construction of a prestressed concrete cable-stayed bridge by employing the progressive cantilever method, the Finite Element Method (FEM), and ANSYS with a modified USERMAT3D subroutine to introduce viscoelastic models that account for creep and shrinkage, and concrete cracking. The FEM model accurately reflects the pylon, deck, and stay-cables of the bridge. The findings of the vertical displacements of the deck and the history of forces in the stay-cables were compared to measurements taken during the actual building of a bridge, revealing a high degree of consistency. In addition, the analysis revealed the horizontal displacements of the pylon and the stress-strain history in the concrete during the building sequence, which, despite the addition of viscous effects, exhibiting good agreement[22].

The researchers at Chalmers University of Technology developed a method for analyzing the load-carrying capacity of prestressed concrete bridges under shear and torsion. The method used Shell elements with embedded reinforcement and nonlinear material models, and its ability

to predict shear-type cracking and failure were verified. The evaluation of a box-girder bridge demonstrated accurate estimates of shear response and capacity. The proposed method outperformed conventional evaluation techniques, and semi-probabilistic forms were recommended for non-linear finite-element analysis. This study provides evidence for the reliability of the proposed method in assessing the load-carrying capacity of prestressed concrete bridges under shear and torsion.[23].

University of New South Wales Canberra researchers proposed a new finite element model for analyzing the structural behavior of fiber-reinforced polymer (FRP)-strengthened steel-reinforced concrete (RC) beams under cyclic loading. The model considered all beam components and accounted for the nonlinear material properties of concrete and steel rebars. The developed model was validated against experimental results and was found to be effective for analyzing FRP-strengthened RC beams under cyclic loading. Parametric studies were conducted to investigate the effects of FRP types, thicknesses, and lengths on the structural behavior of beams using the new model. The research findings were summarized, and the proposed finite element model provided a reliable tool for analyzing the structural behavior, supporting the development of design guidelines for FRP strengthening applications in practice[24].

Section B

FEM Process

Idealization

In FE analysis, a structural model is created by simplifying the actual structure, including geometry, boundary conditions, and loads. Concrete structures often assume linear elasticity and simplified supports, but considering support stiffness is crucial for realism. The engineer must make accurate modeling assumptions to avoid significant impact on results[34].

Discretization

is a variant of the Span-by-Span Method in which the scaffold moves as it constructs each span. This approach is ideal for constructing long-span bridges that need constant support during construction. The approach offers precise control over segment alignment and is especially beneficial in places with restricted clearance. On the basis of construction joints, structural analysis is performed depending on building phases [35].

Element analysis

In the third phase, element approximation and element stiffness are calculated using a base function and numerical integration to achieve accurate integration across the specified integration points. Even with sufficient integration points, the integration is an approximation since the integration of rational functions does not produce accurate answers [34].

Structural analysis

A stiffness matrix is computed in the fourth phase by integrating the stiffness matrices of individual components with equilibrium conditions and geometry criteria. The equation system is solved for the full structure, however rounding mistakes may arise due to the limited amount of significant digits that computers can use.

Post-processing

In the fifth phase, stress components are estimated for all elements in the integration points, which are often not positioned at the element nodes but rather at a distance within the element using techniques such as Gauss integration. The most accurate results may be obtained at the integration points, however they are often shown at the element nodes. Using the element base functions, integration point outcomes are extended to nodes. An element with a higher order approximates a linear elastic analysis more accurately. Typically, each node is linked to many elements, and the node result is determined as the mean of each element's contribution. Consequently, the aforementioned post-processing findings are imprecise and include rounding mistakes [35].

Results

In the last phase, the FE analysis findings are submitted to further scrutiny. Due to the consideration of the actual behavior of the structure, this may result in substantial uncertainty. Generally, the output data from 2-D frame analysis is manageable for big models, however it is commonly challenging and occasionally impossible to examine the output data from 3D Shell analysis. A mix of words, numbers, and iso color charts may offer a more accurate description of the data [36].

Section C

Finite element model formulations

Link elements are 1-D elements with two or three nodes, while Shells are 2-D elements with triangular or quadrilateral forms and three or four nodes. If the element has mid nodes, triangular elements may include up to six nodes and quadrilateral elements may contain up to eight nodes. The maximum number of nodes for tetrahedrons, hexahedrons, and pentahedrons are ten, twenty, and fifteen, respectively. Although engineering structures are generally classified as 1-D, 2-D, or 3-D, the majority of structures have a finite value in all three dimensions. For example, a string is a 1-D structure, but it has a finite cross-sectional area, and paper is a 2-D structure, but it has a limited thickness. Specific physical measures, like strength, may not have meaningful values in certain dimensions. For example, a string may be strong when tugged, yet it provides little support in other directions [49].

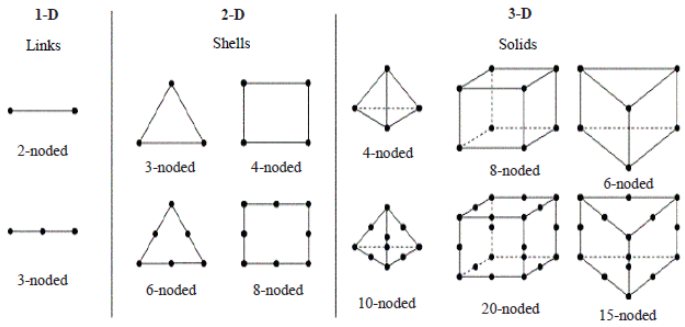

Figure 45. Elements and nodes representation in terms of dimensions [49]

The premise behind the finite element approach is that a complex structure may be broken down into a limited number of smaller "elements." These components have predictable or conceptually predictable behaviour and may be used to replicate the behavior of the structure. This notion is intuitively plausible, yet it poses important questions that need a certain degree of mathematical accuracy to answer. Consequently, the development of finite element approaches requires a rigorous mathematical strategy.

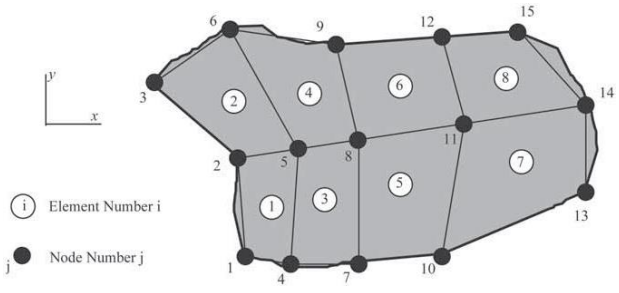

Figure 46. Finite element formulation basis in a mesh space[49]

The finite element approach divides the physical world into discrete elements, as seen in Figure 8's bold line. The location and connection of nodes establish the form of the elements, and for basic triangle elements, three nodes are needed to specify the shape and position. The placements of the four corner nodes form quadrilateral items, while additional nodes may be used to construct components with more complexity. Each node has six degrees of freedom in three dimensions, including translation and rotation along each of the three global axes, when the structure is loaded. The amount of active degrees of freedom at each node is dependent on the formulation of the connecting components; for the membrane depicted in the x-y plane, each node has two active degrees of freedom: translation in the x and y directions. Therefore, the exhibited finite element model has 30 degrees of freedom, which is equivalent to 15 nodes with two degrees of freedom apiece, or 30 DOFs [50].

Computational implementation of FEM

Linear static analysis

The fundamental equation to be solved by the finite element method for structures under static loads is expressed as follows.

$$[K]\,[u] = [f]$$

Here, K denotes the stiffness matrix of the structure, which is a combination of the stiffness matrices of the constituent elements. The vector u represents the displacement vector, whereas the vector f represents the vector of loads applied to the structure. This equation represents the balance between external and internal forces. For instance, in case of a 3 DOF the matrix notation could be written in the form of a 6×6 stiffness matrix representing horizontal, vertical, and in-plane rotation.

$$\begin{bmatrix} f_{x1} \\ f_{y1} \\ m_{z1} \\ f_{x2} \\ f_{y2} \\ m_{z2} \end{bmatrix} = \begin{bmatrix} k_{11} & k_{12} & k_{13} & k_{14} & k_{15} & k_{16} \\ k_{21} & k_{22} & k_{23} & k_{24} & k_{25} & k_{26} \\ k_{31} & k_{32} & k_{33} & k_{34} & k_{35} & k_{36} \\ k_{41} & k_{42} & k_{43} & k_{44} & k_{45} & k_{46} \\ k_{51} & k_{52} & k_{53} & k_{54} & k_{55} & k_{56} \\ k_{61} & k_{62} & k_{63} & k_{64} & k_{65} & k_{66} \end{bmatrix} \begin{bmatrix} u_{x1} \\ u_{y1} \\ \theta_{z1} \\ u_{x2} \\ u_{y2} \\ \theta_{z2} \end{bmatrix}$$

If displacement boundary conditions are not used to fix the rigid body degrees of freedom of the model, the stiffness matrix is singular. Direct or iterative solvers are commonly used to solve the equilibrium equation. By default, the direct solver concurrently solves the unknown

displacements using a Gauss elimination approach that optimizes computing performance by using the sparsity and symmetry of the stiffness matrix, K. Alternately, a preconditioning conjugate gradient iterative solver may be used. In terms of speed, the iterative solver may outperform the direct solution, particularly for thick-walled structures. Solid structures [51].

Once the unknown displacements at the nodal locations of the elements are identified, the constitutive relations of the material may be used to compute the stresses. For linear static analysis, when deformations lie within the elastic range, it is assumed that stresses,, are linear functions of strains,, according to Hooke's law.

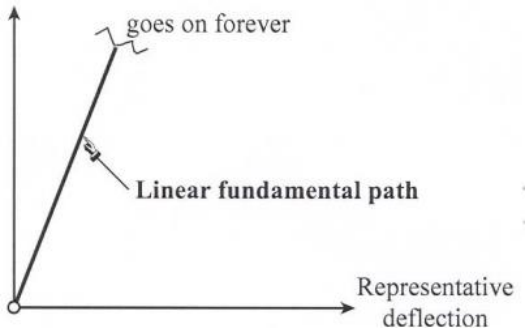

Figure 47. Hooke's law for linear behaviour

Hooke's law can be stated as

$$\sigma = C\,\varepsilon$$

where C represents the elasticity matrix of the material. The strains, ε, are a function of the displacements.

$$\begin{bmatrix}\sigma_{xx}\\ \sigma_{yy}\\ \sigma_{zz}\\ \sigma_{yz}\\ \sigma_{zx}\\ \sigma_{xy}\end{bmatrix} = \begin{bmatrix}C_{11} & C_{12} & C_{13} & C_{14} & C_{15} & C_{16}\\ C_{21} & C_{22} & C_{23} & C_{24} & C_{25} & C_{26}\\ C_{31} & C_{32} & C_{33} & C_{34} & C_{35} & C_{36}\\ C_{41} & C_{42} & C_{43} & C_{44} & C_{45} & C_{46}\\ C_{51} & C_{52} & C_{53} & C_{54} & C_{55} & C_{56}\\ C_{61} & C_{62} & C_{63} & C_{64} & C_{65} & C_{66}\end{bmatrix}\begin{bmatrix}\varepsilon_{xx}\\ \varepsilon_{yy}\\ \varepsilon_{zz}\\ \varepsilon_{yz}\\ \varepsilon_{zx}\\ \varepsilon_{xy}\end{bmatrix}$$

It is convenient to represent the computational algorithm for a linear static case however, the nonlinear static case involves higher order equations and mathematical notations. The scope of this study is to numerically analyse the linear and nonlinear cases for Solid and Shell models of concrete bridge. Therefore, the brief mathematical model is summarised below.

Non-Linear Static analysis

Nonlinear analysis in the context of finite element methods involves solving structural problems that exhibit nonlinear behavior. Nonlinear behavior refers to the situation where the response of a structure is not proportional to the applied load, and may include large deformations, material nonlinearity, geometric nonlinearity, or contact nonlinearity. Hooke's law illustration in the following figure represents the non-linear behavior.

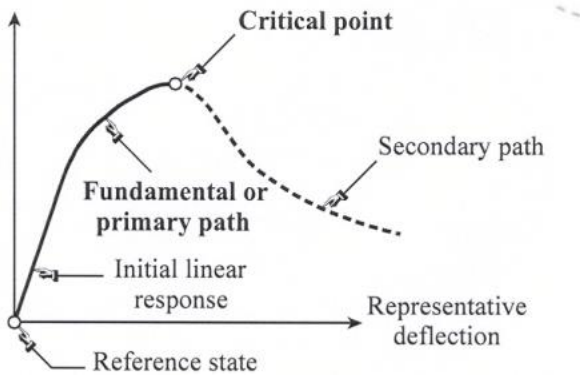

Figure 48. Hooke's law illustration for non-linear behavior

To obtain an accurate solution for a nonlinear problem, the analysis is typically performed in small increments. At each increment, the equilibrium equation is solved using a suitable numerical method, such as Newton's method, and a corresponding increment size is selected. The incremental approach allows for the nonlinearity of the problem to be captured and for a more accurate solution to be obtained. An important consideration in nonlinear analysis is the choice of time increment. Many finite element software systems, including ANSYS, have an automated time increment control that assesses the difficulty of convergence at the current increment. If the determined number of iterations matches the ideal number of iterations for convergence, the following increment uses the same increment size. If fewer iterations are necessary, the increment size is raised; if too many iterations are necessary, the current increment is tried again with a lower increment size. ANSYS can do nonlinear analysis using either small displacement or large displacement analysis. Commonly employed to solve nonlinear equilibrium equations, the Newton technique permits a quadratic rate of convergence for smooth solutions. Additionally, ANSYS gives extra user control choices for configuring automated time increments, providing for greater analysis process flexibility.

Appendix IV

3D Solid model results

Normal Stress

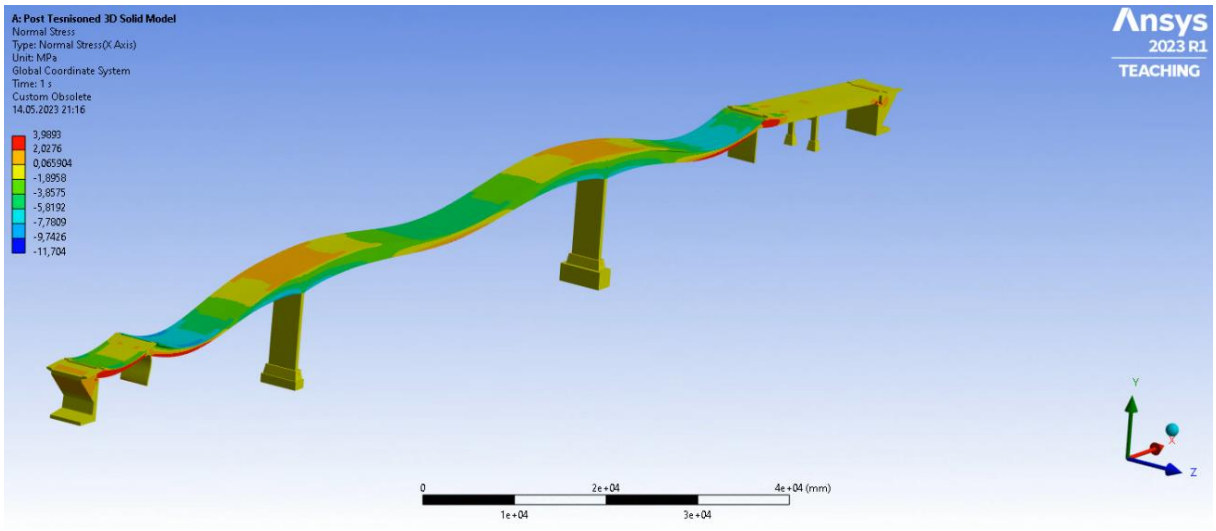

Modal Analysis remaining modes

Mode 7

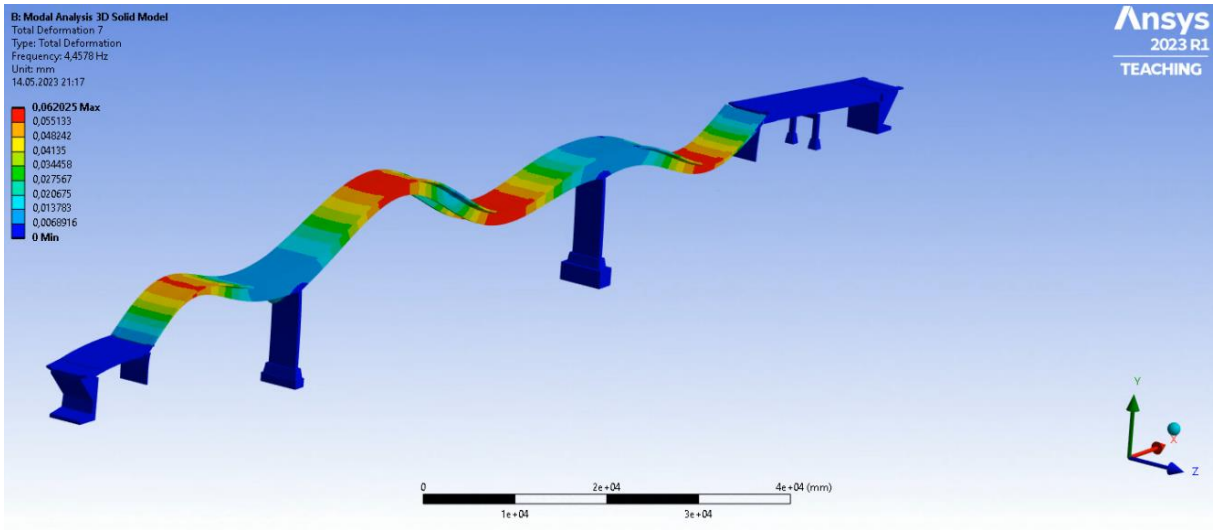

Mode 8

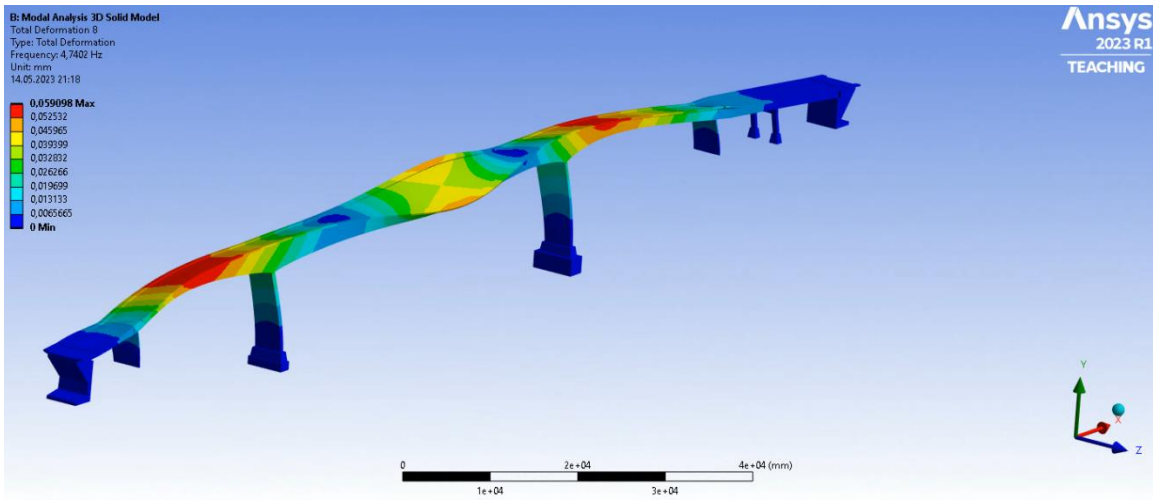

Mode 9

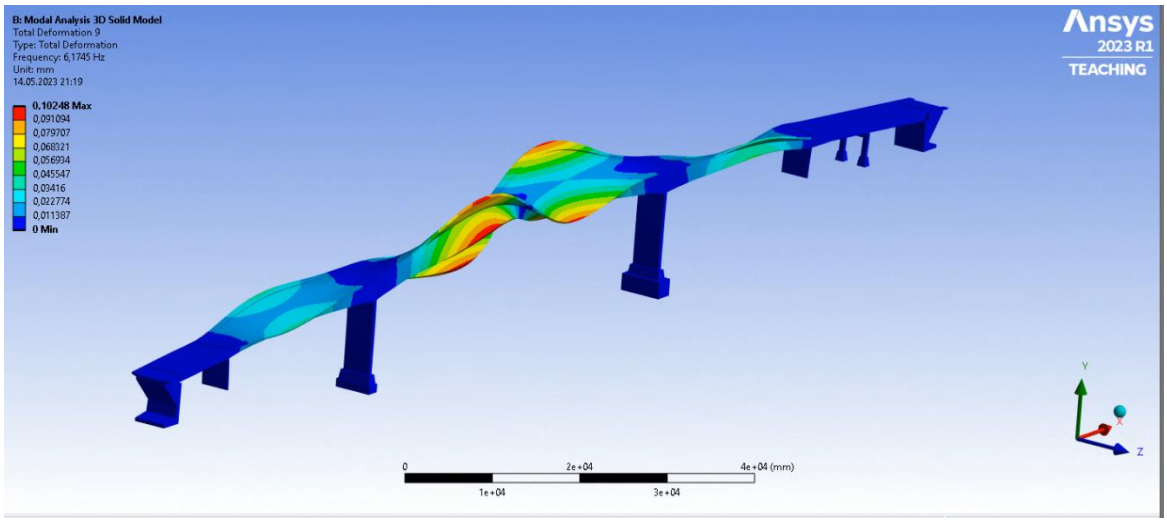

Mode 10

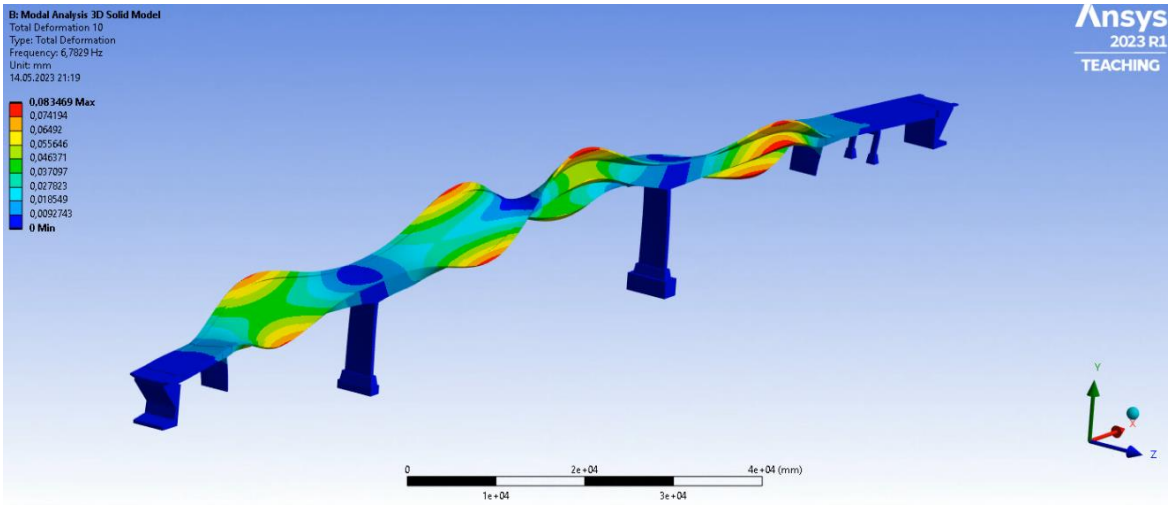

Mode 11

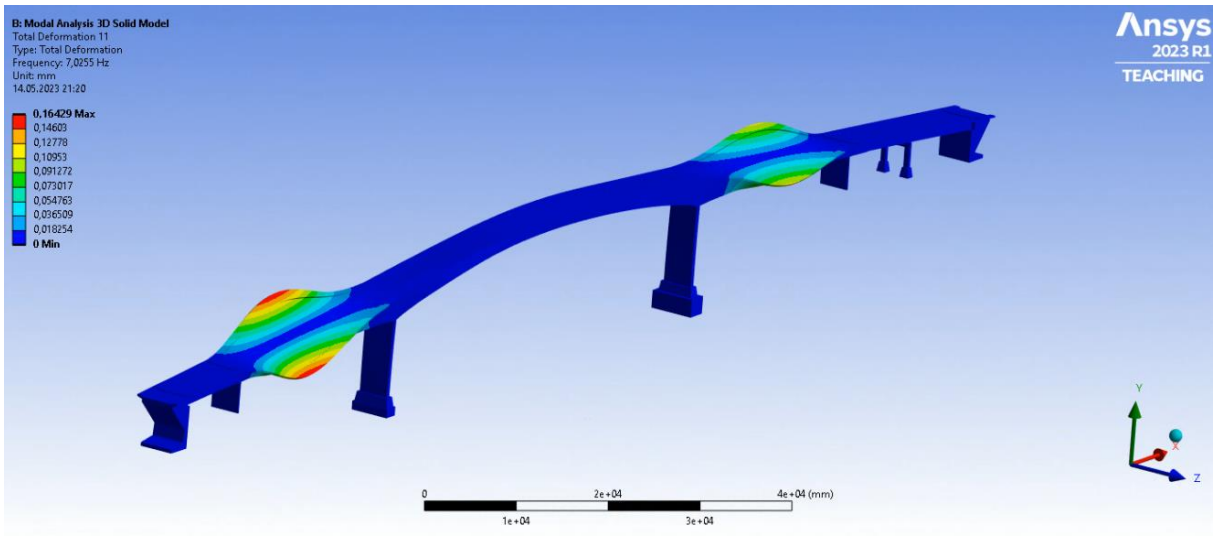

Mode 12

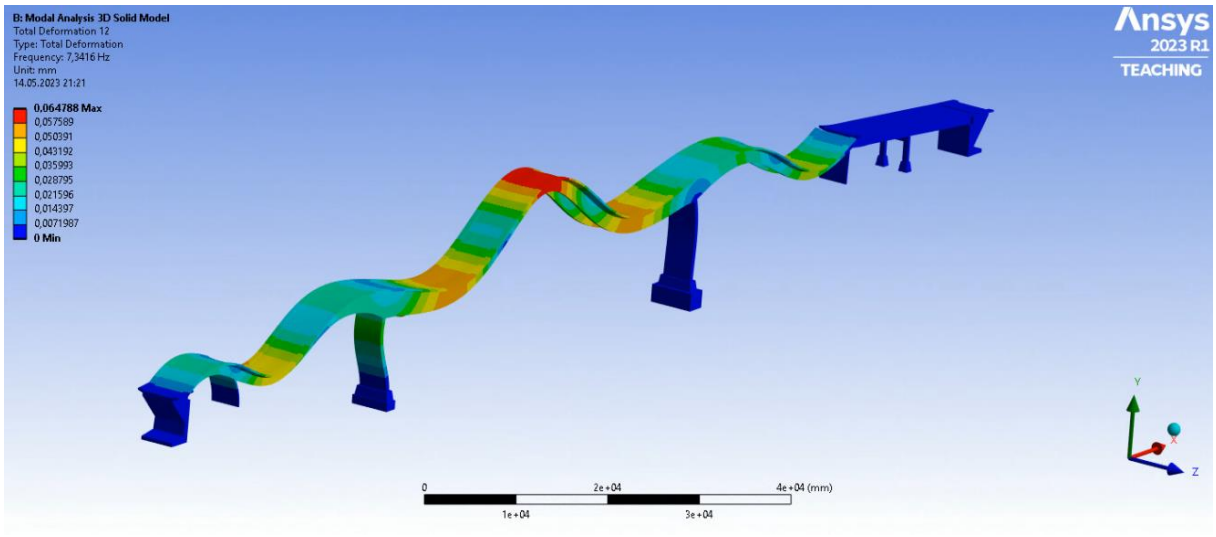

Mode 13

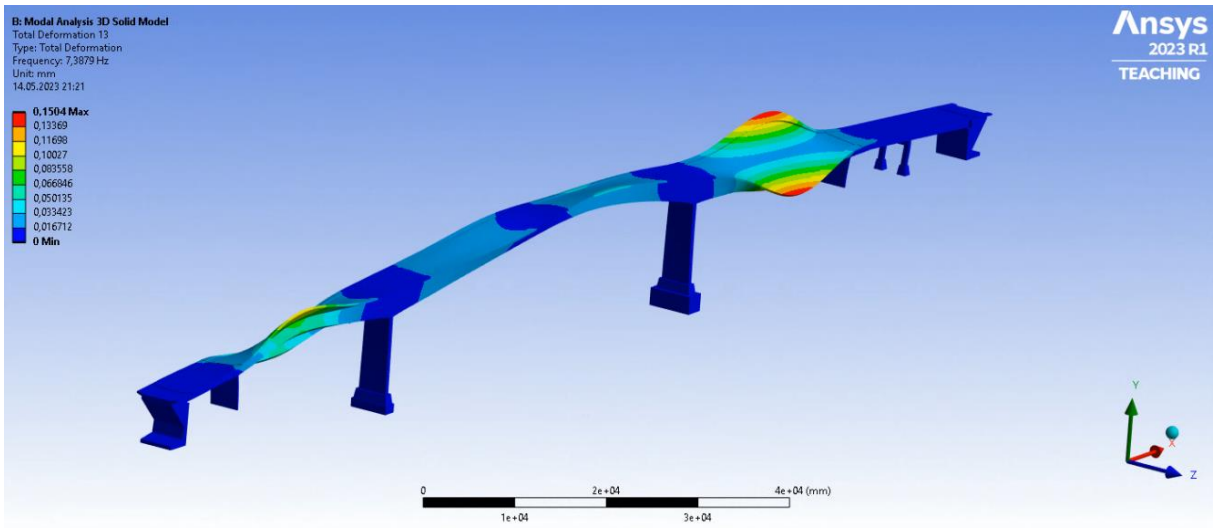

Mode 14

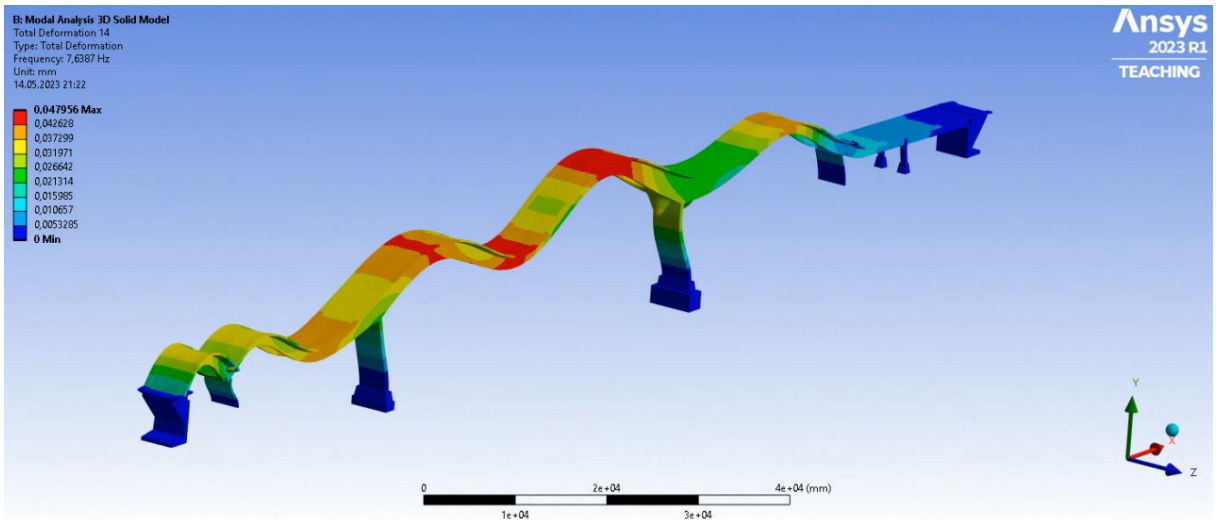

Mode 15

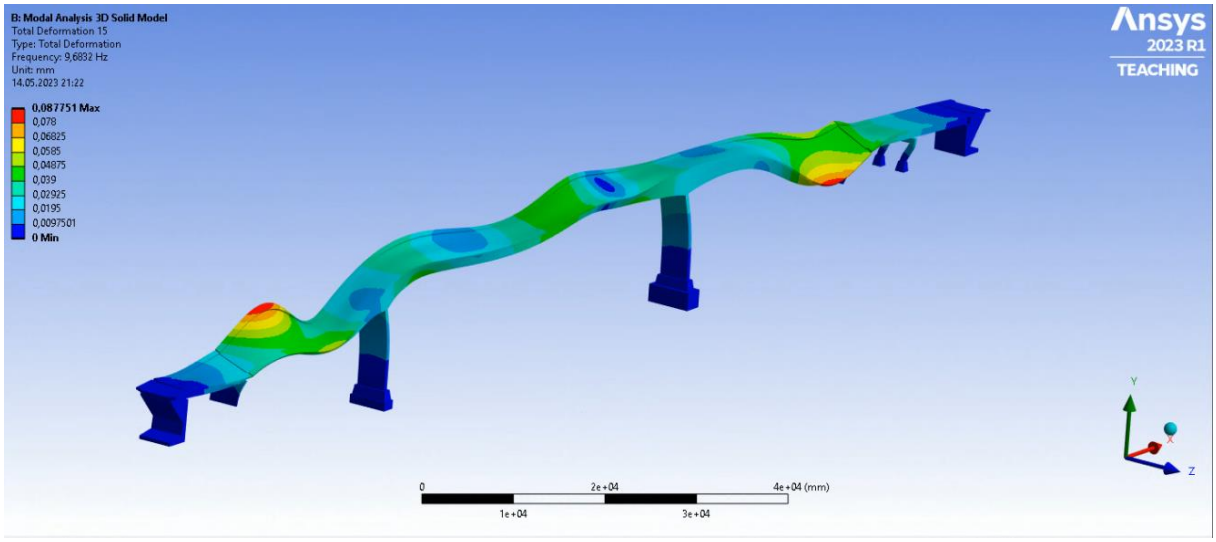

Mode 16

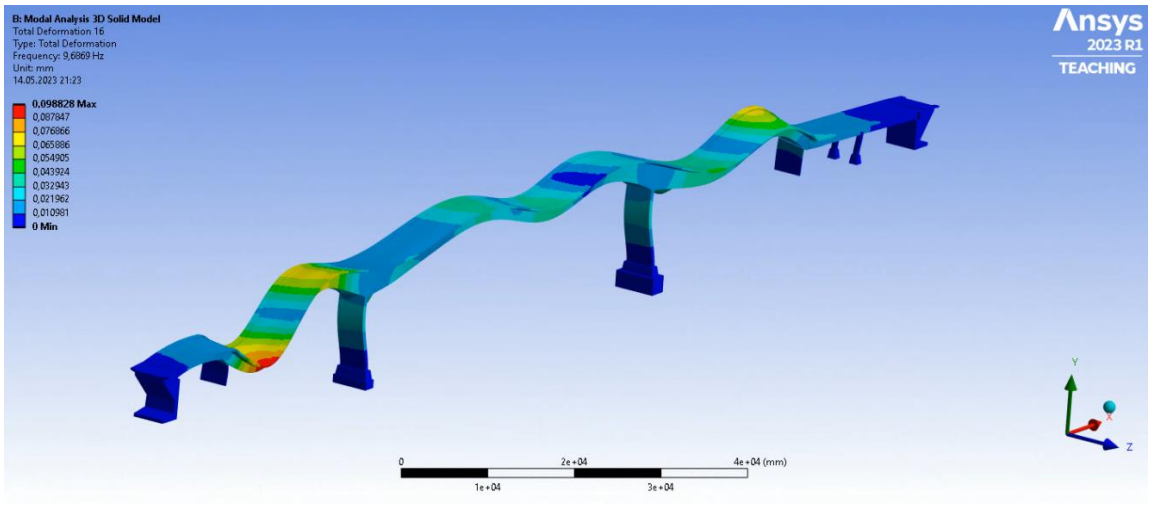

Mode 17

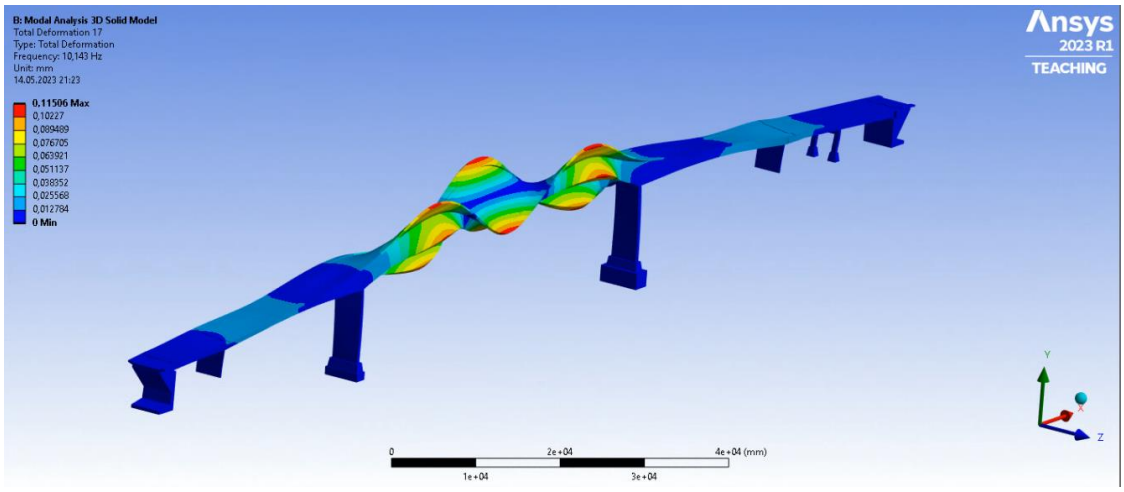

Mode 18

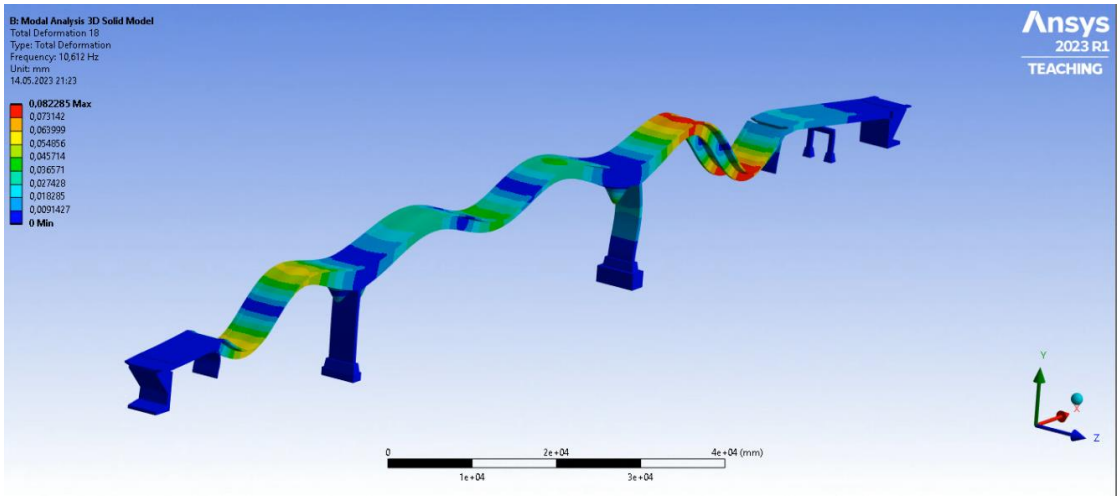

Mode 19

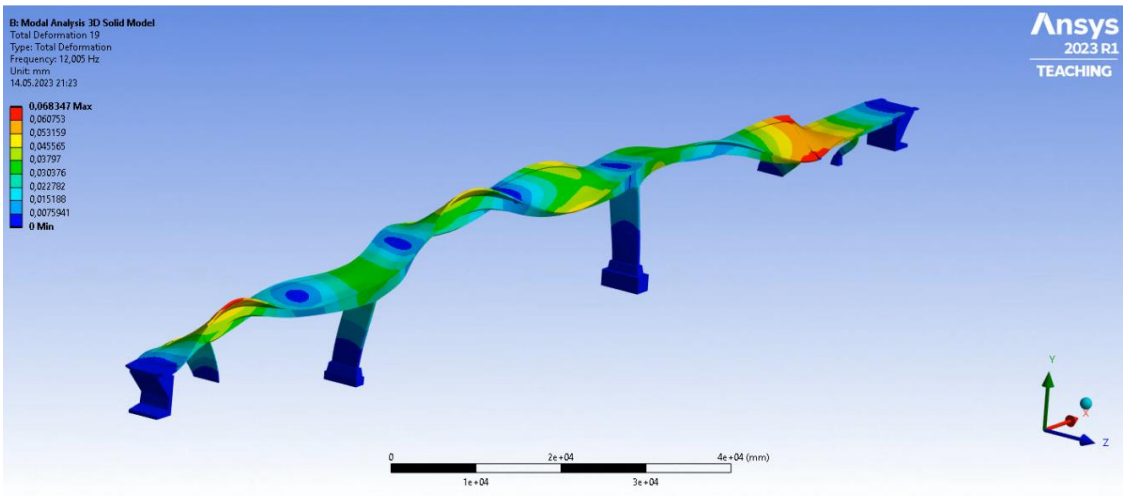
B: Modal Analysis 3D Solid Model
Total Deformation 19
Type: Total Deformation
Frequency: 12,005 Hz
Unit: mm
14.05.2023 21:23
0,068347 Max
0,060753
0,053159
0,045565
0,03797
0,030376
0,022782
0,015188
0,0075941
0 Min
Ansys
2023 R1
TEACHING
0
2e+04
4e+04 (mm)
1e+04
3e+04
Y
Z

Mode 20

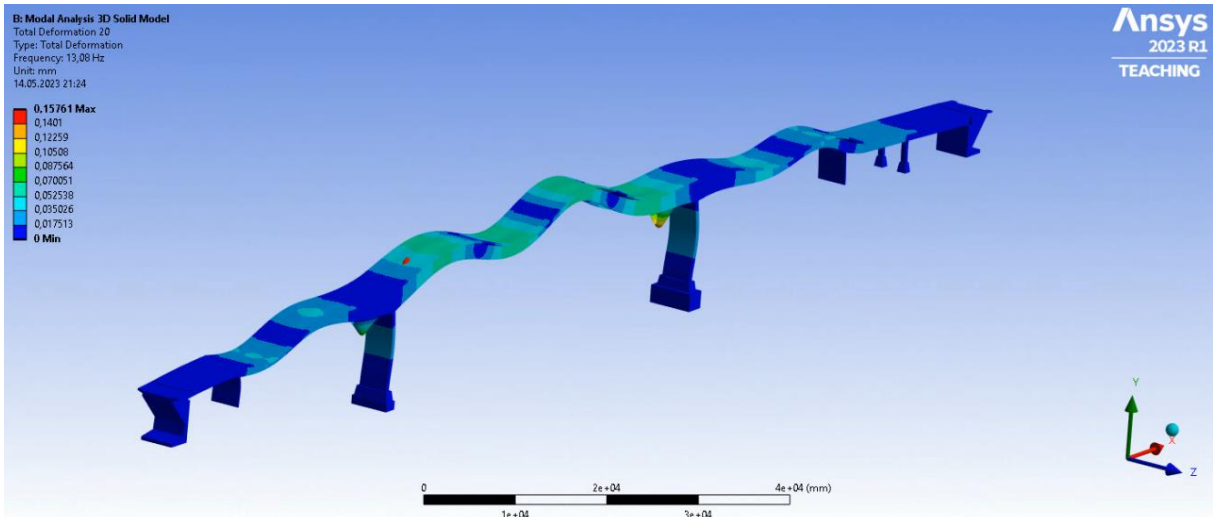
B: Modal Analysis 3D Solid Model
Total Deformation 20
Type: Total Deformation
Frequency: 13,08 Hz
Unit: mm
14.05.2023 21:24
0,15761 Max
0,1401
0,12259
0,10508
0,087564
0,070051
0,052538
0,035026
0,017513
0 Min
Ansys
2023 R1
TEACHING
0
2e+04
4e+04 (mm)
Y
Z

Shell model results

Normal stress

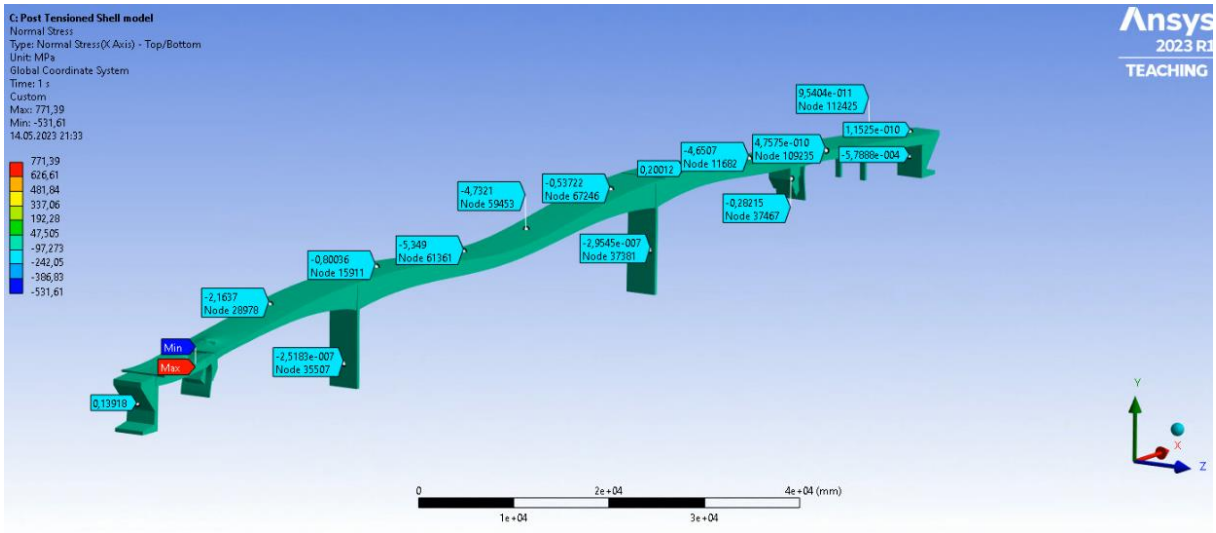

Shell model modes

Mode 7

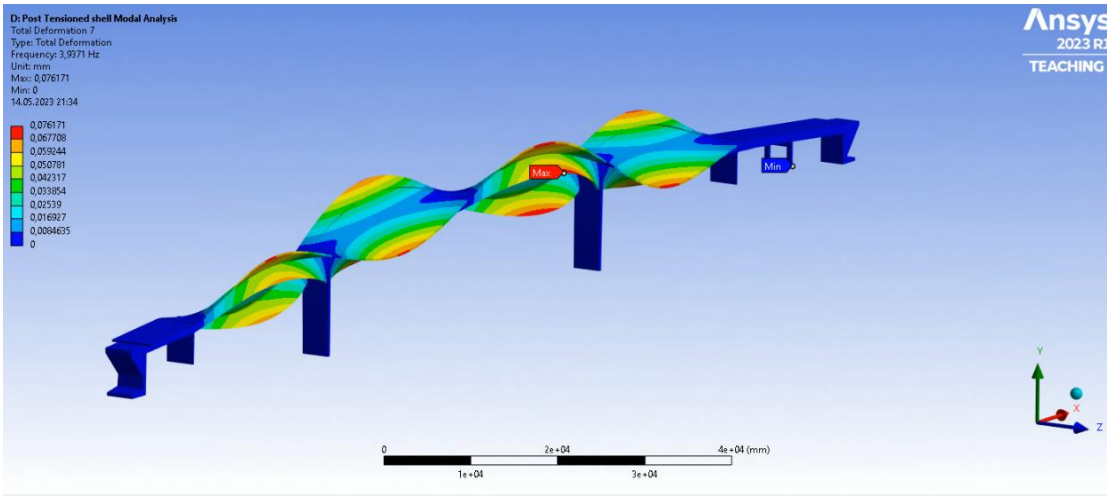

Mode 8

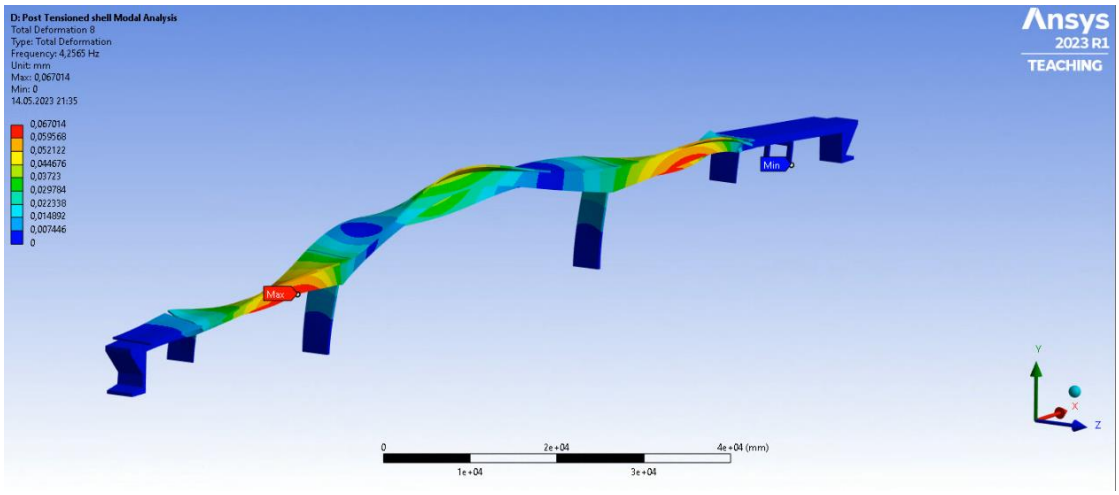

Mode 9

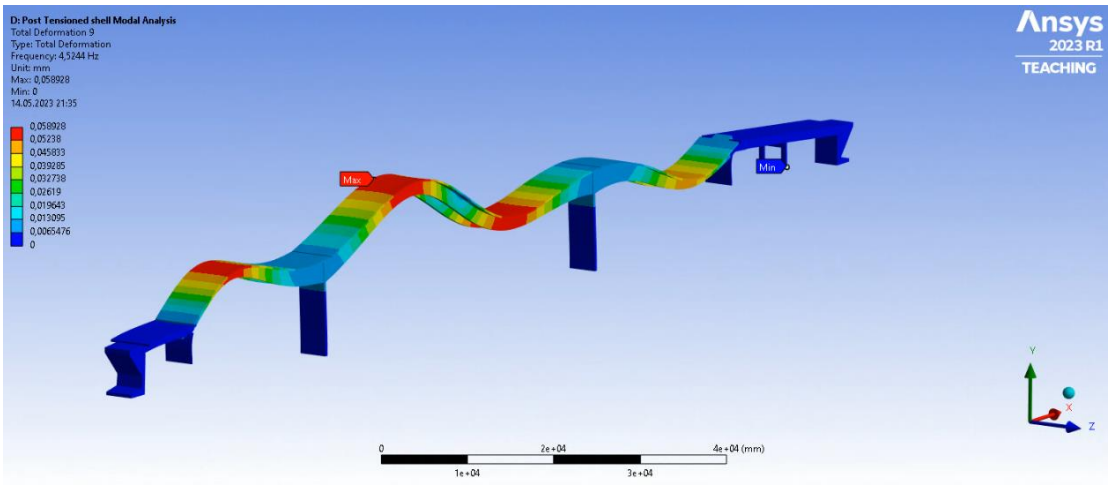

Mode 10

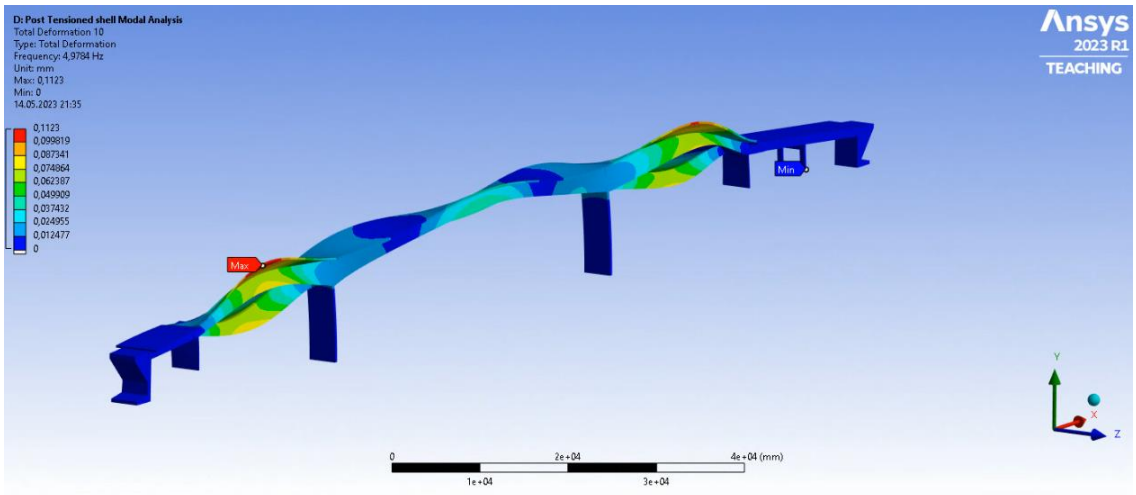

Mode 11

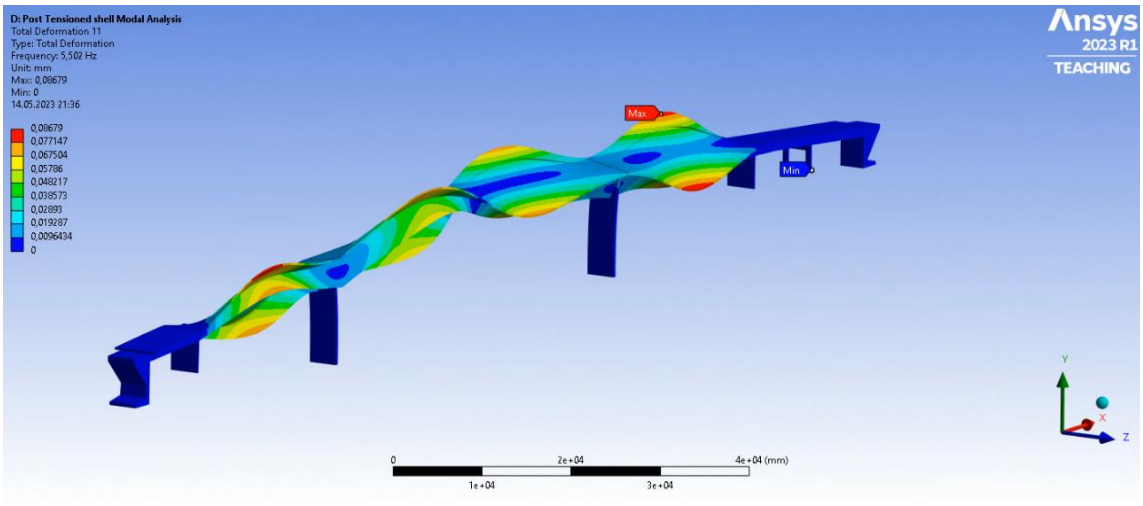

Mode 12

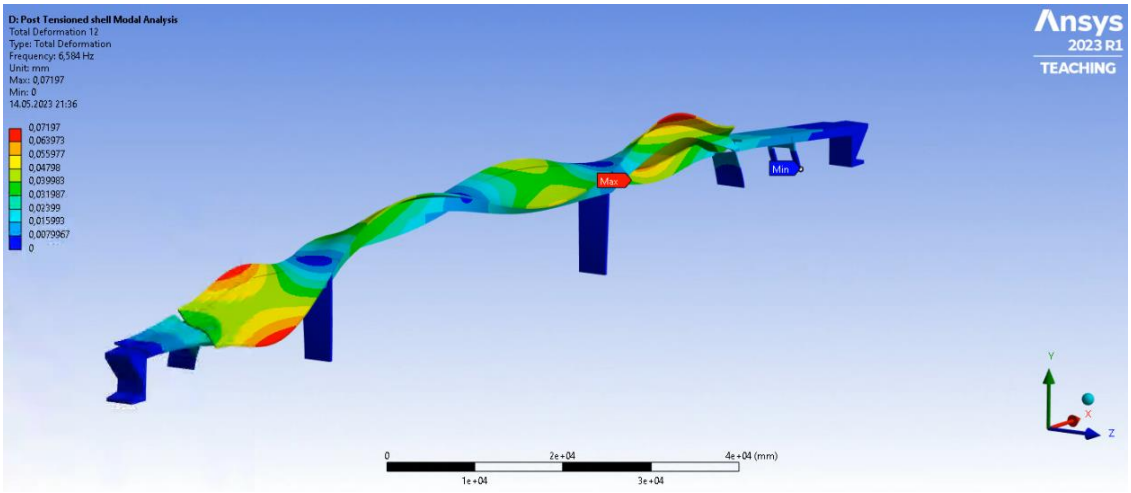

Mode 13

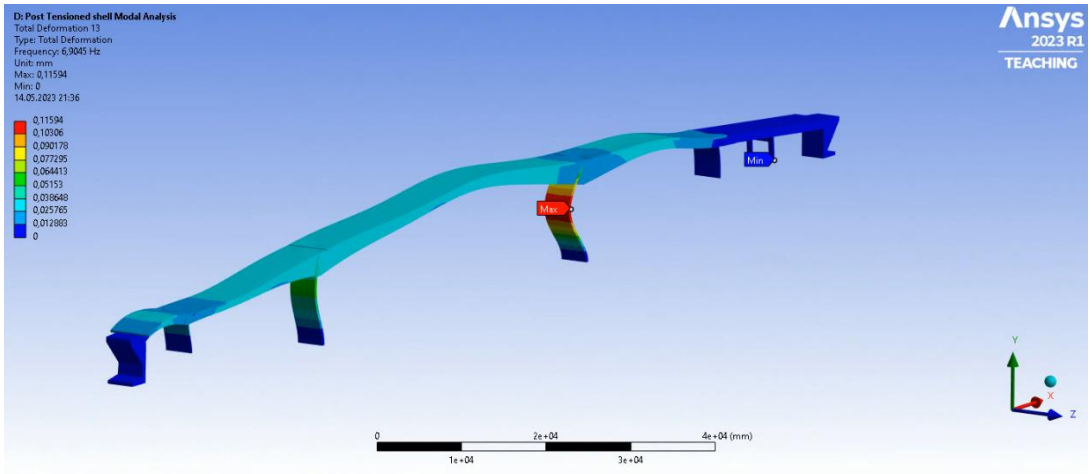

Mode 14

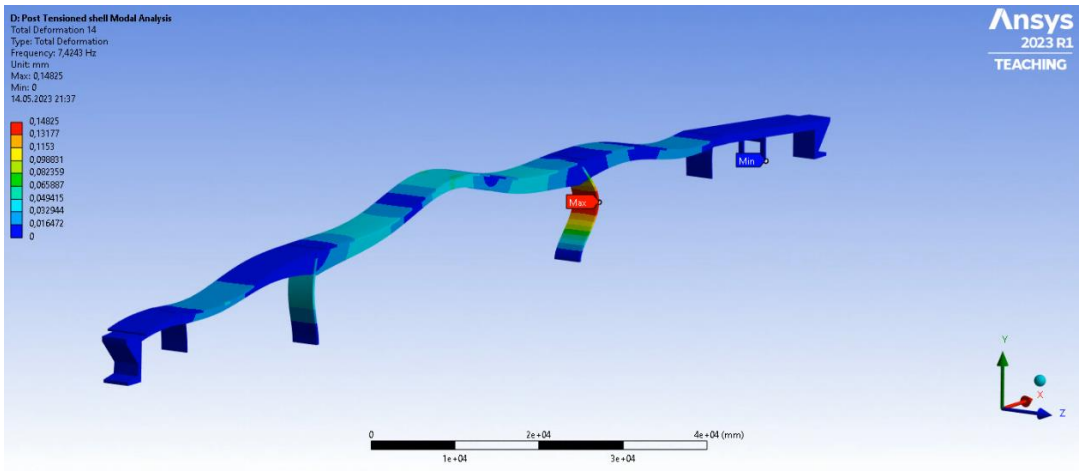

Mode 15

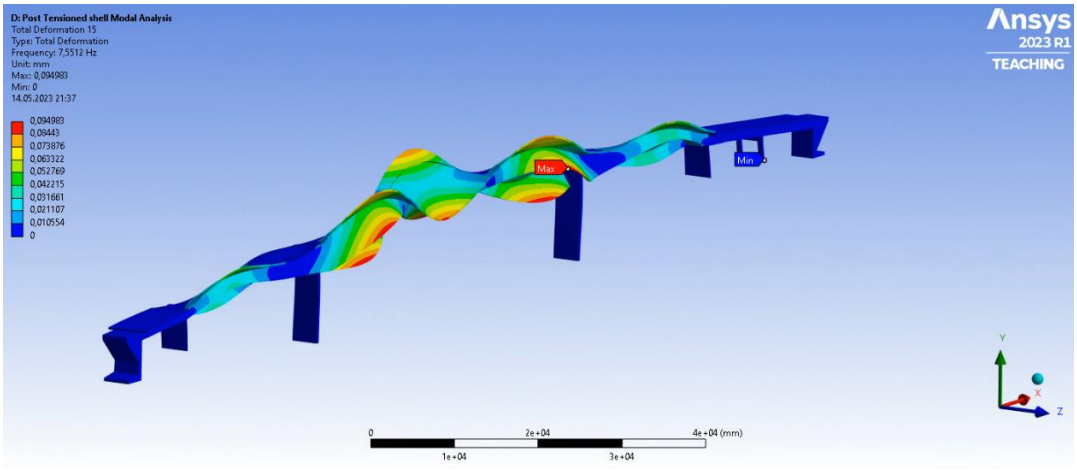

Mode 16

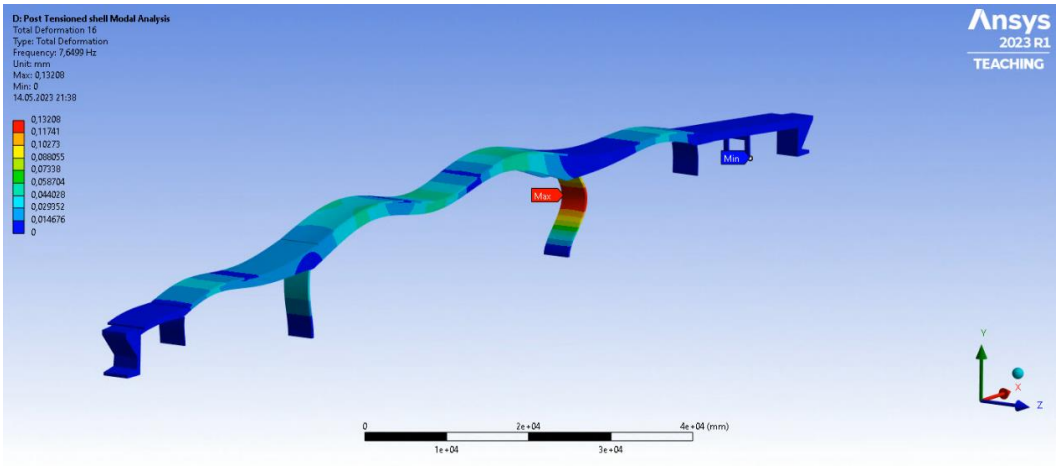

Mode 17

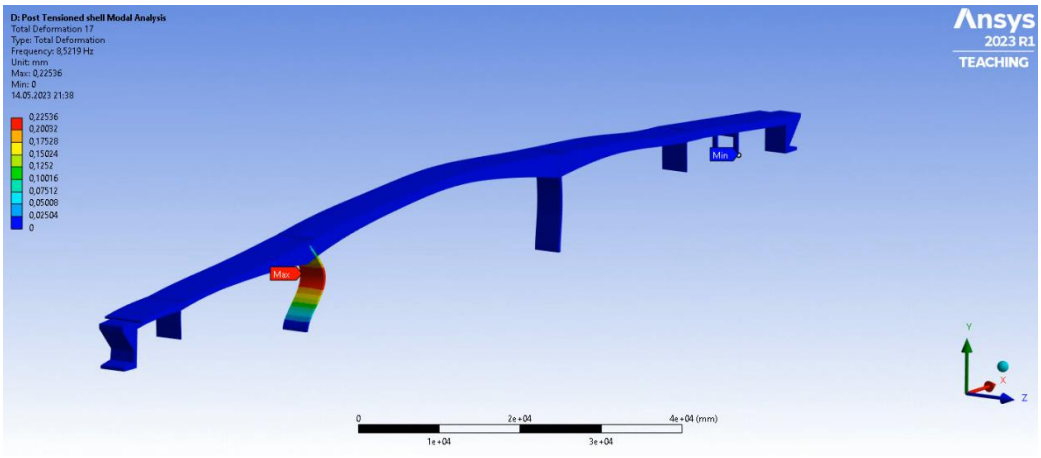

Mode 18

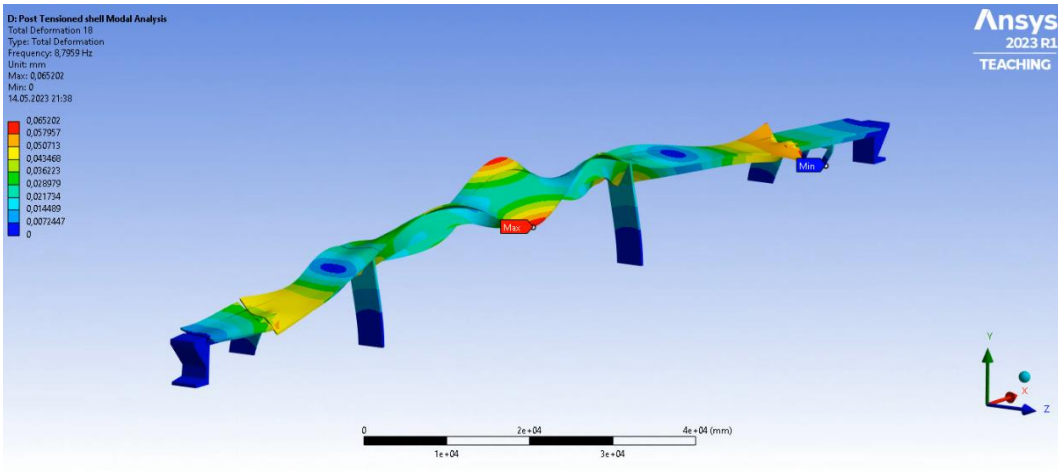

Mode 19

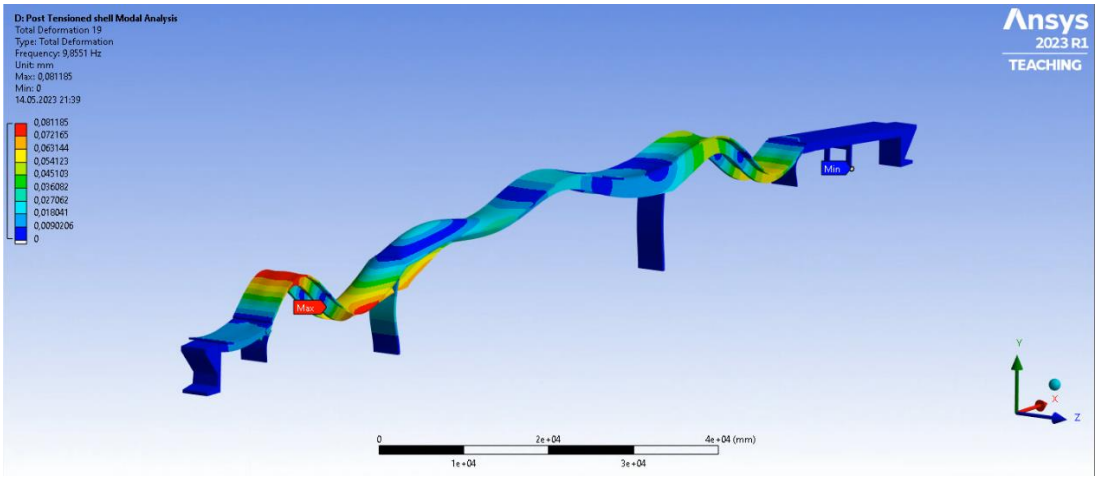

Mode 20

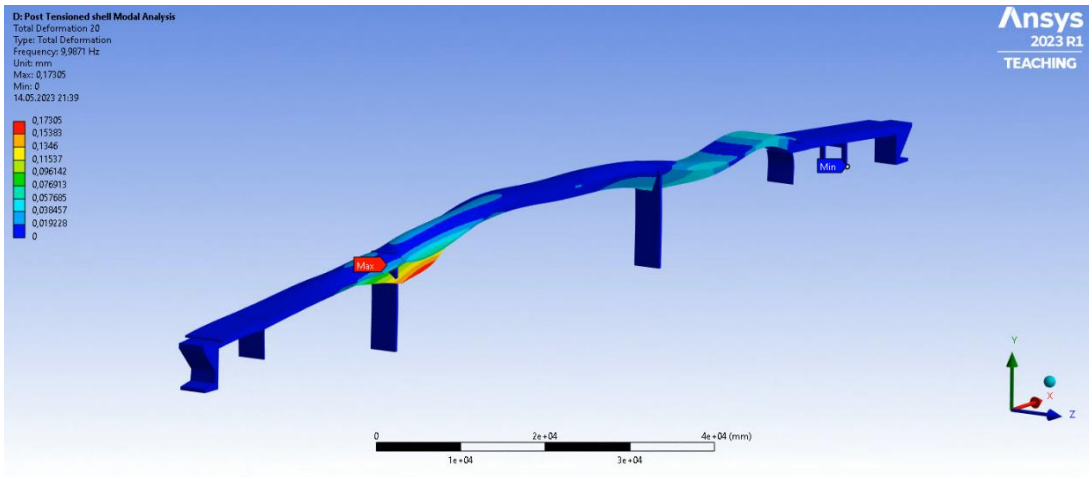

MAC for remaining modes solid vs shell model

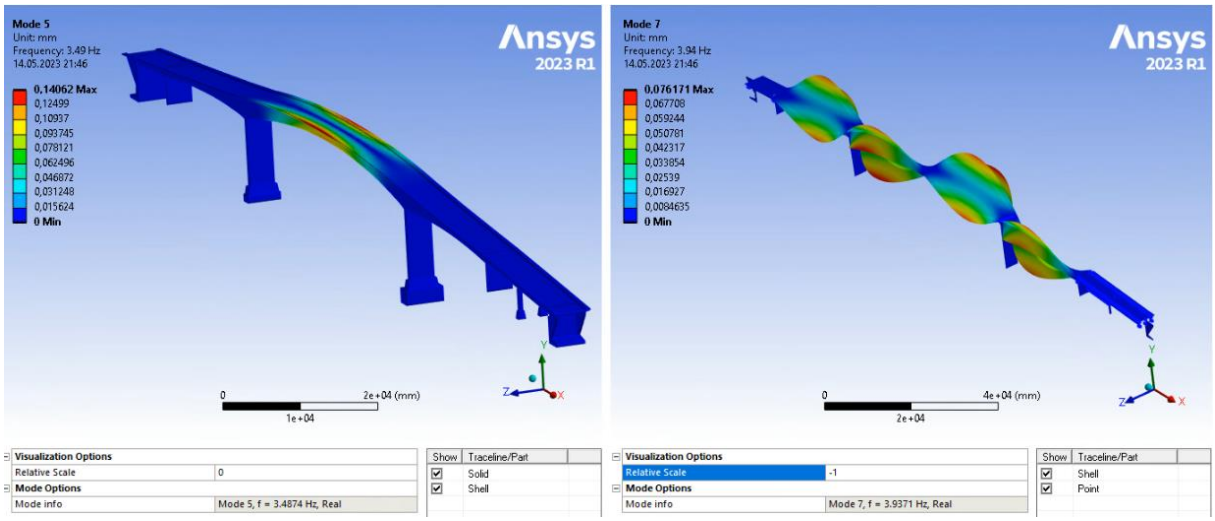

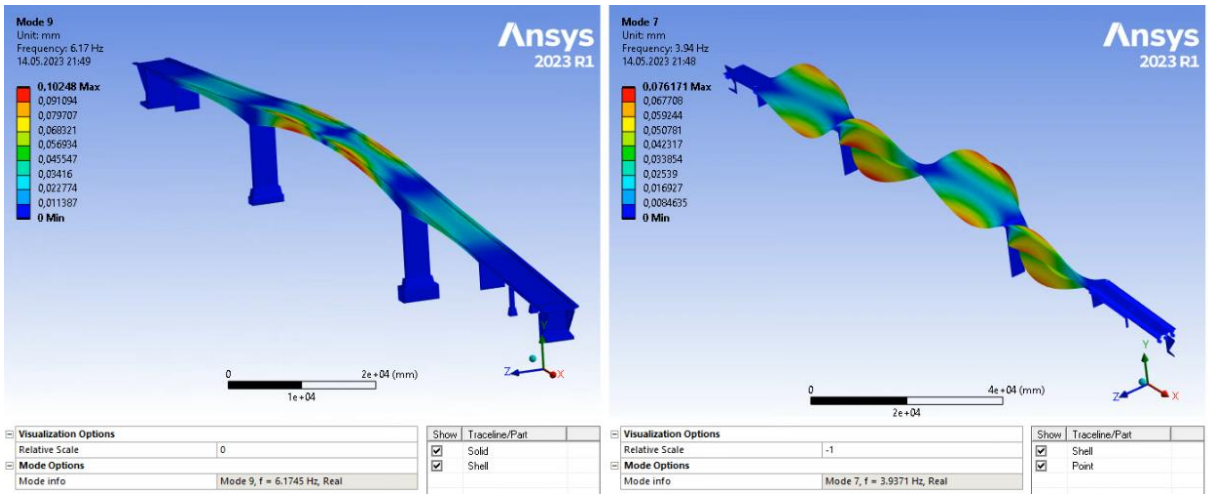

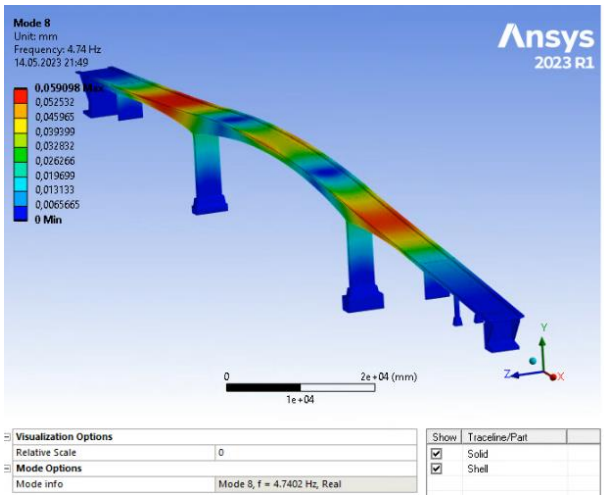
Mode 8
Unit: mm
Frequency: 4.74 Hz
14.05.2023 21:49
0,059098 Max
0,052532
0,045965
0,039399
0,032832
0,026266
0,019699
0,013133
0,0065665
0 Min
Ansys
2023 R1
0
2e+04 (mm)
1e+04
Visualization Options
Relative Scale
0
Mode Options
Mode info
Mode 8, f = 4.7402 Hz, Real
Show
Traceline/Part
Solid
Shell

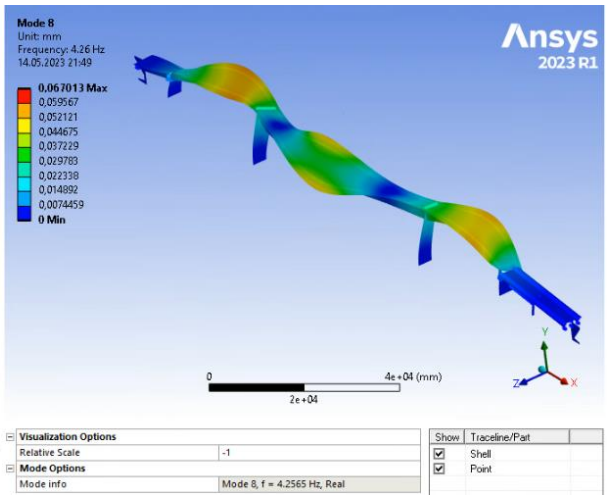
Mode 8
Unit: mm
Frequency: 4.26 Hz
14.05.2023 21:49
0,067013 Max
0,059567
0,052121
0,044675
0,037229
0,029783
0,022338
0,014892
0,0074459
0 Min
Ansys
2023 R1
0
4e+04 (mm)
2e+04
Visualization Options
Relative Scale
-1
Mode Options
Mode info
Mode 8, f = 4.2565 Hz, Real
Show
Traceline/Part
Shell
Point

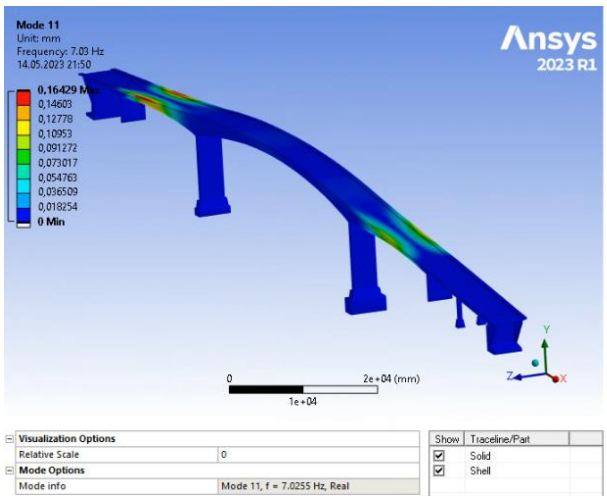
Mode 11
Unit: mm
Frequency: 7.03 Hz
14.05.2023 21:50
0,16429 Max
0,14603
0,12778
0,10953
0,091272
0,073017
0,054763
0,036509
0,018254
0 Min
Ansys
2023 R1
0
2e+04 (mm)
1e+04
Visualization Options
Relative Scale
0
Mode Options
Mode info
Mode 11, f = 7.0255 Hz, Real
Show
Traceline/Part
Solid
Shell

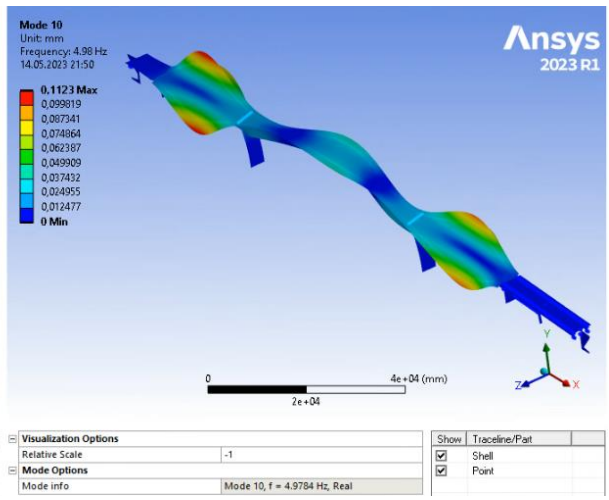
Mode 10
Unit: mm
Frequency: 4.98 Hz
14.05.2023 21:50
0,1123 Max
0,099819
0,087341
0,074864
0,062387
0,049909
0,037432
0,024955
0,012477
0 Min
Ansys
2023 R1
0
4e+04 (mm)
2e+04
Visualization Options
Relative Scale
-1
Mode Options
Mode info
Mode 10, f = 4.9784 Hz, Real
Show
Traceline/Part
Shell
Point

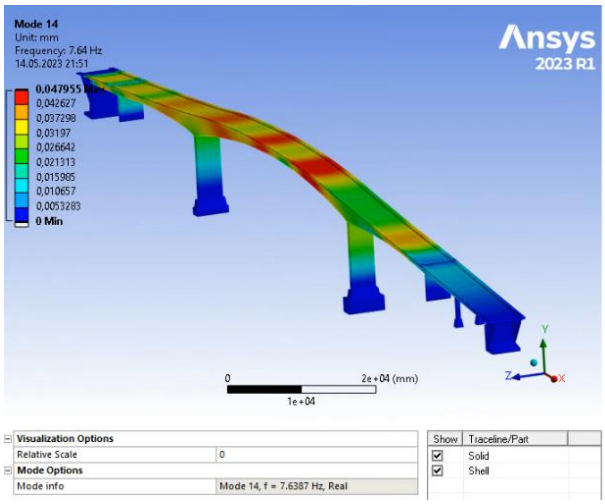
Mode 14
Unit: mm
Frequency: 7.64 Hz
14.05.2023 21:51
0,047955 Max
0,042627
0,037298
0,03197
0,026642
0,021313
0,015985
0,010657
0,0053283
0 Min
Ansys
2023 R1
0
2e+04 (mm)
1e+04
Visualization Options
Relative Scale
0
Mode Options
Mode info
Mode 14, f = 7.6387 Hz, Real
Show
Traceline/Part
Solid
Shell

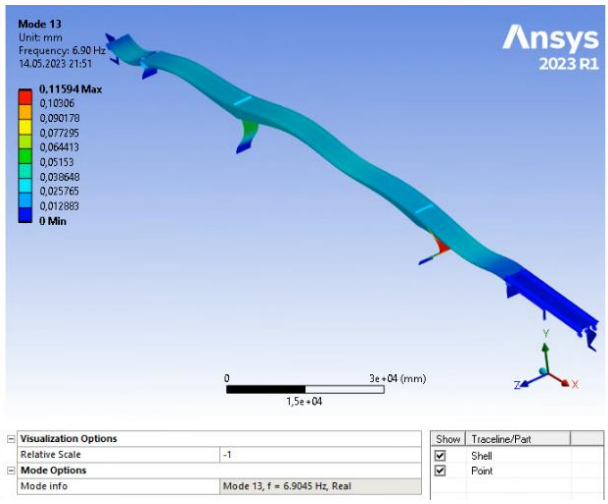
Mode 13
Unit: mm
Frequency: 6.90 Hz
14.05.2023 21:51
0,11594 Max
0,10306
0,090178
0,077295
0,064413
0,05153
0,038648
0,025765
0,012883
0 Min
Ansys
2023 R1
0
3e+04 (mm)
1,5e+04
Visualization Options
Relative Scale
-1
Mode Options
Mode info
Mode 13, f = 6.9045 Hz, Real
Show
Traceline/Part
Shell
Point

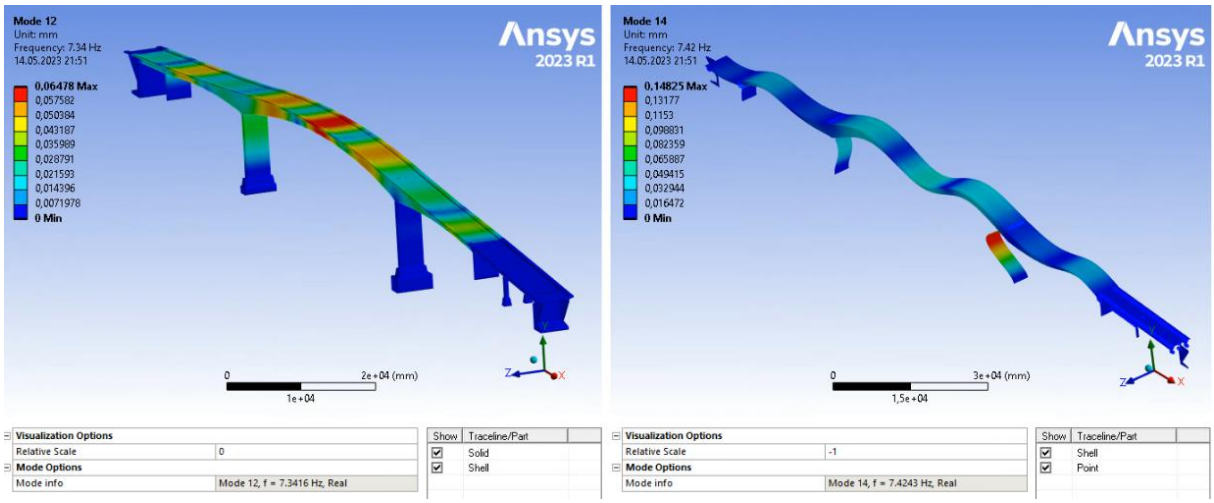

MAC chart for all twenty modes

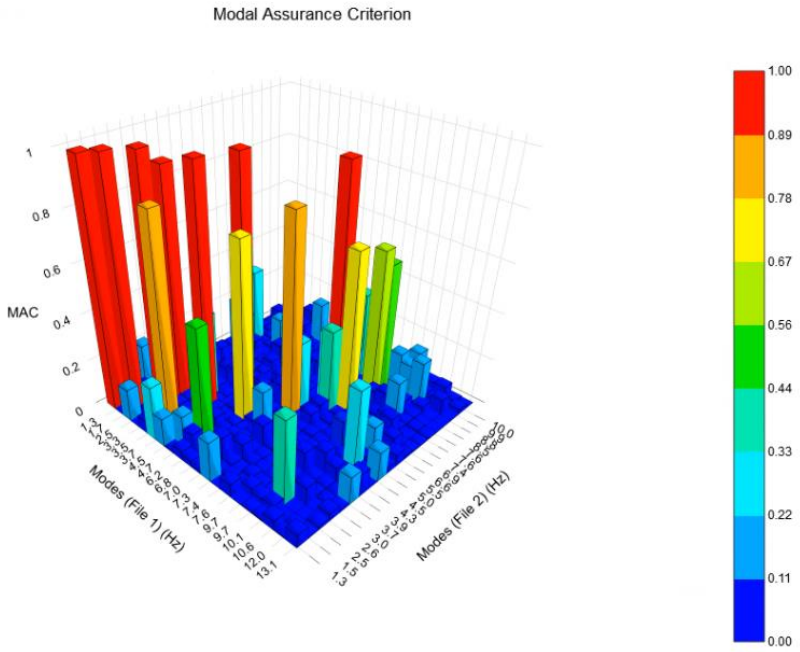

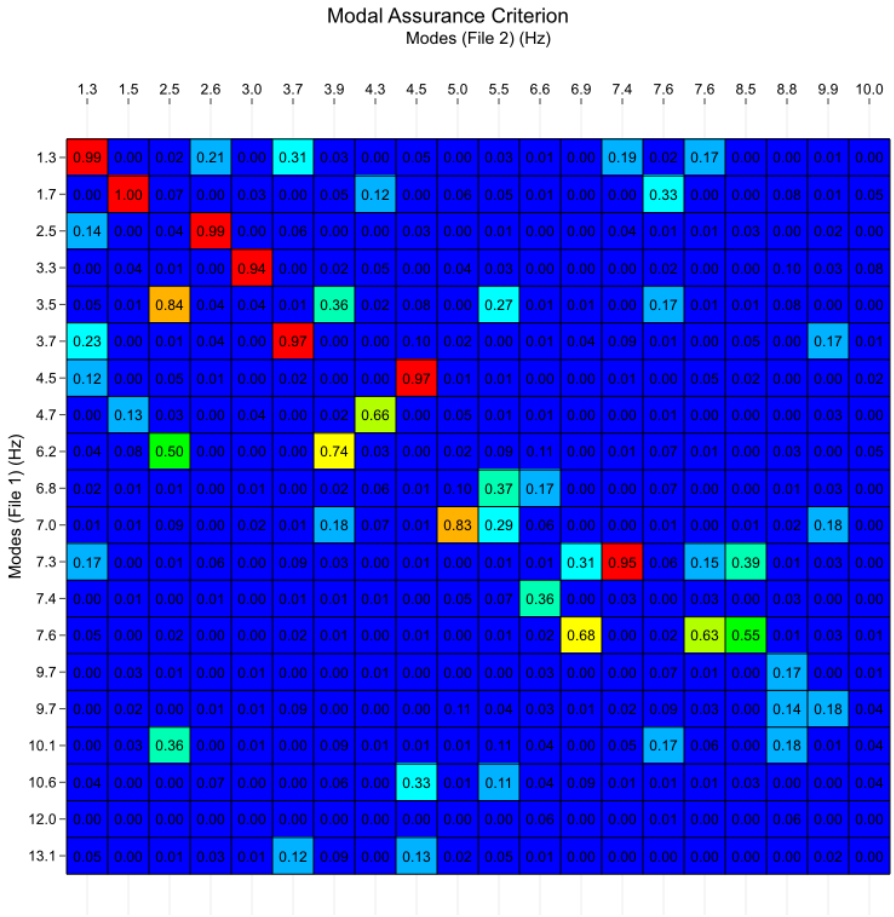
Modal Assurance Criterion
Modes (File 2) (Hz)
1.3 1.5 2.5 2.6 3.0 3.7 3.9 4.3 4.5 5.0 5.5 6.6 6.9 7.4 7.6 7.6 8.5 8.8 9.9 10.0
Modes (File 1) (Hz)
1.3 0.99 0.00 0.02 0.21 0.00 0.31 0.03 0.00 0.05 0.00 0.03 0.01 0.00 0.19 0.02 0.17 0.00 0.00 0.01 0.00
1.7 0.00 1.00 0.07 0.00 0.03 0.00 0.05 0.12 0.00 0.06 0.05 0.01 0.00 0.00 0.33 0.00 0.00 0.08 0.01 0.05
2.5 0.14 0.00 0.04 0.99 0.00 0.06 0.00 0.00 0.03 0.00 0.01 0.00 0.00 0.04 0.01 0.01 0.03 0.00 0.02 0.00
3.3 0.00 0.04 0.01 0.00 0.94 0.00 0.02 0.05 0.00 0.04 0.03 0.00 0.00 0.00 0.02 0.00 0.00 0.10 0.03 0.08
3.5 0.05 0.01 0.84 0.04 0.04 0.01 0.36 0.02 0.08 0.00 0.27 0.01 0.01 0.00 0.17 0.01 0.01 0.08 0.00 0.00
3.7 0.23 0.00 0.01 0.04 0.00 0.97 0.00 0.00 0.10 0.02 0.00 0.01 0.04 0.09 0.01 0.00 0.05 0.00 0.17 0.01
4.5 0.12 0.00 0.05 0.01 0.00 0.02 0.00 0.00 0.97 0.01 0.01 0.00 0.00 0.01 0.00 0.05 0.02 0.00 0.00 0.02
4.7 0.00 0.13 0.03 0.00 0.04 0.00 0.02 0.66 0.00 0.05 0.01 0.01 0.00 0.00 0.01 0.00 0.00 0.00 0.03 0.00
6.2 0.04 0.08 0.50 0.00 0.00 0.00 0.74 0.03 0.00 0.02 0.09 0.11 0.00 0.01 0.07 0.01 0.00 0.03 0.00 0.05
6.8 0.02 0.01 0.01 0.00 0.01 0.00 0.02 0.06 0.01 0.10 0.37 0.17 0.00 0.00 0.07 0.00 0.00 0.01 0.03 0.00
7.0 0.01 0.01 0.09 0.00 0.02 0.01 0.18 0.07 0.01 0.83 0.29 0.06 0.00 0.00 0.01 0.00 0.01 0.02 0.18 0.00
7.3 0.17 0.00 0.01 0.06 0.00 0.09 0.03 0.00 0.01 0.00 0.01 0.01 0.31 0.95 0.06 0.15 0.39 0.01 0.03 0.00
7.4 0.00 0.01 0.00 0.01 0.00 0.01 0.01 0.01 0.00 0.05 0.07 0.36 0.00 0.03 0.00 0.03 0.00 0.03 0.00 0.00
7.6 0.05 0.00 0.02 0.00 0.00 0.02 0.01 0.00 0.01 0.00 0.01 0.02 0.68 0.00 0.02 0.63 0.55 0.01 0.03 0.01
9.7 0.00 0.03 0.01 0.00 0.01 0.00 0.00 0.01 0.00 0.00 0.00 0.03 0.00 0.00 0.07 0.01 0.00 0.17 0.00 0.01
9.7 0.00 0.02 0.00 0.01 0.01 0.09 0.00 0.00 0.00 0.11 0.04 0.03 0.01 0.02 0.09 0.03 0.00 0.14 0.18 0.04
10.1 0.00 0.03 0.36 0.00 0.01 0.00 0.09 0.01 0.01 0.01 0.11 0.04 0.00 0.05 0.17 0.06 0.00 0.18 0.01 0.04
10.6 0.04 0.00 0.00 0.07 0.00 0.00 0.06 0.00 0.33 0.01 0.11 0.04 0.09 0.01 0.01 0.01 0.03 0.00 0.00 0.04
12.0 0.00 0.00 0.00 0.00 0.00 0.00 0.00 0.00 0.00 0.00 0.00 0.06 0.00 0.00 0.01 0.00 0.00 0.06 0.00 0.00
13.1 0.05 0.00 0.01 0.03 0.01 0.12 0.09 0.00 0.13 0.02 0.05 0.01 0.00 0.00 0.00 0.00 0.00 0.00 0.02 0.00

Appendix V

Eurocode regulations

Linear and non-linear FE analysis

Eurocode 2, CEN (2001) recommends approaches for determining the force distribution in a structure, which include linear elastic analysis, and non-linear analysis for concrete structures. When designing concrete structures in the serviceability limit state (SLS), it is recommended to use either linear elastic or non-linear analysis while considering the geometry and properties of each component [38]. Non-linear analysis accurately assesses the effects of cracking on concrete structures in the service state, while linear elastic analysis is applicable only to uncracked structures or those in the ultimate limit state(ULS) [52].

EN 1992-1-1 provide guidelines for both linear and non-linear analysis of concrete structures. In Eurocode 2, Section 5.2.1 offers guidance on using linear analysis to assess overall behavior, while Section 5.2.2 outlines requirements for non-linear analysis in extreme loading or non-linear behavior. Furthermore, Eurocode 2, Section 7.4 provides requirements for non-linear analysis of ULS, and Section 7.5 provides requirements for both linear and non-linear analysis of SLS [38].

3D-Solid and Shell elements

EN 1992-1-1 recommends 3D-Solid elements for FEM analysis of concrete structures, including bridges. This method accurately accounts for complex geometries, stress distributions, and non-linear material behavior such as cracking and crushing. However, 3D-Solid elements can be computationally expensive for large and complex structures. Therefore, the FEM method choice should balance accuracy and computational efficiency according to project requirements.

EN 1992-1-1 Annex B permits the use of 3D-Solid elements for FEM analysis of concrete structures. However, 3D Shell elements may be suitable for structures with thin or curved elements that require high-resolution modeling to reduce computational time and resources. 3D Shell elements offer accurate results but may not be suitable for complex geometries or highly non-linear structures [38].

Appendix VI

Modal analysis in concrete bridges

Modal analysis techniques

The vibration analysis of concrete girder bridges can be performed using various techniques, including analytical, numerical, and experimental methods. Here are some general methods that are commonly used in vibration analysis of concrete girder bridges.

Mode shapes and natural frequencies: The vibration of a concrete box girder bridge can be decomposed into a sum of sinusoidal waves, each with a different amplitude, frequency, and phase. These sinusoidal waves are called modes, and the frequency at which they vibrate naturally is called the natural frequency. The mode shapes and natural frequencies can be calculated analytically or numerically.

Modal superposition: Modal superposition is a technique used to calculate the response of a concrete box girder bridge to a complex input signal. It involves calculating the response of each mode individually and then adding them together to obtain the total response.

Response spectrum analysis: Response spectrum analysis is a method of analyzing the response of a concrete box girder bridge to an earthquake. It involves calculating the response of the bridge to a set of predefined ground motion records, known as the design spectra.

Finite element method (FEM): FEM is a numerical method used to solve the equations of motion for a concrete box girder bridge. It involves dividing the bridge into a finite number of small elements, each with its own stiffness and mass properties. The equations of motion are then solved for each element, and the results are combined to obtain the overall response of the bridge.

Linearity and non-linear case consideration

Modal analysis is a linear technique. This means that it assumes the behavior of the structure or system is linear, which is the case for small to moderate levels of displacement and deformation. In modal analysis, the dynamic characteristics of a structure or system are determined by solving linear equations of motion, and the response of the structure or system is assumed to be a linear combination of its mode shapes.

The linearity assumption makes modal analysis a powerful tool for analyzing and predicting the behavior of structures or systems under different loading conditions. It allows engineers to use the superposition principle to combine the effects of different loads and boundary conditions to obtain the total response of the system.

However, if the deformation and displacement levels become large, the linear assumptions may no longer hold, and the response of the structure or system may become nonlinear. In this case, more advanced techniques such as nonlinear modal analysis or finite element analysis may be required to predict the response of the structure or system accurately.

Mode shapes

In a box girder bridge, the modes of vibration can be classified into several types based on their mode shape and frequency. Some of the common modes of vibration in a box girder bridge include:

1. Longitudinal modes: These modes involve vibrations that occur along the length of the bridge, such as flexural vibrations in the box girder or the diaphragms that connect the girders.
2. Transverse modes: These modes involve vibrations that occur perpendicular to the longitudinal direction of the bridge, such as lateral vibrations in the box girder or the supports.
3. Torsional modes: These modes involve twisting deformations of the box girder or supports, which can occur due to torsional loads such as wind or earthquakes.
4. Vertical modes: These modes involve vibrations that occur in the bridge's vertical direction, such as in the box girder or supports.
5. Higher order modes: These are modes with higher frequencies and more complex mode shapes, which can involve multiple types of vibrations in the box girder.

Each type of mode can have multiple sub-modes or higher order modes with different frequencies and mode shapes. The natural frequencies and mode shapes of each mode can be determined using modal analysis techniques and can be used to evaluate the structural integrity and performance of the box girder bridge under different loading conditions.

Understanding the modes of vibration in a box girder bridge is important for ensuring its safety and structural integrity under dynamic loading conditions such as wind, earthquakes, and traffic. The results of modal analysis can be used to optimize the design of the bridge, mitigate

vibrations and resonance, and develop effective control strategies for improving its performance.

Appendix VII

Modal masses and Participation factors for Solid model

***** PARTICIPATION FACTOR CALCULATION ***** X DIRECTION

MODE	FREQUENCY	PERIOD	PARTIC.FACTOR	RATIO	EFFECTIVE MASS	CUMULATIVE MASS FRACTION	RATIO EFF.MASS TO TOTAL MASS
1	1.23209	0.81163	2.3754	0.080827	5.64230	0.484342E-02	0.407397E-02
2	1.69050	0.59154	-0.15911E-03	0.000005	0.253145E-07	0.484343E-02	0.182781E-10
3	2.56803	0.38940	4.6953	0.159767	22.0454	0.237675E-01	0.159177E-01
4	3.01474	0.33170	-29.388	1.000000	863.661	0.765146	0.623599
5	3.29068	0.30389	-0.17457E-01	0.000594	0.304744E-03	0.765146	0.220038E-06
6	3.45694	0.28927	-0.34424E-02	0.000117	0.118500E-04	0.765146	0.855621E-08
7	3.62910	0.27555	14.554	0.495241	211.825	0.946980	0.152947
8	4.69560	0.21297	-2.1089	0.071759	4.44735	0.950797	0.321117E-02
9	4.69763	0.21287	5.9114	0.201151	34.9451	0.980795	0.252318E-01
10	6.17547	0.16193	0.20447E-02	0.000070	0.418084E-05	0.980795	0.301874E-08
11	6.77591	0.14758	-0.28238E-02	0.000096	0.797366E-05	0.980795	0.575731E-08
12	7.06809	0.14148	0.55185E-03	0.000019	0.304538E-06	0.980795	0.219889E-09
13	7.32927	0.13644	-0.15314E-01	0.000521	0.234504E-03	0.980795	0.169321E-06
14	7.38449	0.13542	-1.7936	0.061032	3.21703	0.983556	0.232283E-02
15	9.31033	0.10741	-4.1350	0.140703	17.0982	0.998234	0.123456E-01
16	9.38137	0.10659	0.68357E-01	0.002326	0.467274E-02	0.998238	0.337392E-05
17	9.65510	0.10357	1.3944	0.047449	1.94446	0.999907	0.140398E-02
18	10.1367	0.98651E-01	0.17180E-03	0.000006	0.295143E-07	0.999907	0.213106E-10
19	10.6593	0.93815E-01	0.32937	0.011207	0.108482	1.00000	0.783287E-04
20	11.4920	0.87017E-01	0.36017E-04	0.000001	0.129725E-08	1.00000	0.936668E-12
sum					1164.94		0.841135

***** PARTICIPATION FACTOR CALCULATION ***** Y DIRECTION

MODE	FREQUENCY	PERIOD	PARTIC.FACTOR	RATIO	EFFECTIVE MASS	CUMULATIVE MASS FRACTION	RATIO EFF.MASS TO TOTAL MASS
1	1.23209	0.81163	9.8486	0.621086	96.9941	0.172193	0.700338E-01
2	1.69050	0.59154	-0.66209E-03	0.000042	0.438358E-06	0.172193	0.316513E-09
3	2.56803	0.38940	-0.45839	0.028908	0.210120	0.172566	0.151715E-03
4	3.01474	0.33170	-8.1362	0.513097	66.1976	0.290086	0.477974E-01
5	3.29068	0.30389	0.24854E-01	0.001567	0.617730E-03	0.290087	0.446027E-06
6	3.45694	0.28927	0.26632E-02	0.000168	0.709280E-05	0.290087	0.512130E-08
7	3.62910	0.27555	-15.857	1.000000	251.445	0.736474	0.181554
8	4.69560	0.21297	0.50243	0.031685	0.252432	0.736922	0.182267E-03
9	4.69763	0.21287	-1.3703	0.086418	1.87782	0.740256	0.135587E-02
10	6.17547	0.16193	0.10575E-01	0.000667	0.111839E-03	0.740256	0.807523E-07
11	6.77591	0.14758	-0.28212E-01	0.001779	0.795939E-03	0.740258	0.574701E-06
12	7.06809	0.14148	-0.42709E-02	0.000269	0.182404E-04	0.740258	0.131703E-07
13	7.32927	0.13644	0.11062	0.006976	0.122365E-01	0.740279	0.883525E-05
14	7.38449	0.13542	7.5581	0.476644	57.1255	0.841694	0.412470E-01
15	9.31033	0.10741	-3.0097	0.189804	9.05843	0.857775	0.654056E-02
16	9.38137	0.10659	-0.26555E-01	0.001675	0.705162E-03	0.857776	0.509156E-06
17	9.65510	0.10357	-0.61546	0.038813	0.378794	0.858449	0.273505E-03
18	10.1367	0.98651E-01	0.14499E-01	0.000914	0.210212E-03	0.858449	0.151782E-06
19	10.6593	0.93815E-01	8.9282	0.563041	79.7119	0.999961	0.575553E-01
20	11.4920	0.87017E-01	-0.14837	0.009357	0.220132E-01	1.00000	0.158944E-04
sum					563.288		0.406717

***** PARTICIPATION FACTOR CALCULATION ***** Z DIRECTION

MODE	FREQUENCY	PERIOD	PARTIC.FACTOR	RATIO	EFFECTIVE MASS	CUMULATIVE MASS FRACTION	RATIO EFF.MASS TO TOTAL MASS
1	1.23209	0.81163	0.90818E-03	0.000039	0.824790E-06	0.910429E-09	0.595533E-09
2	1.69050	0.59154	23.162	1.000000	536.501	0.592206	0.387376
3	2.56803	0.38940	-0.36729E-02	0.000159	0.134901E-04	0.592206	0.974039E-08
4	3.01474	0.33170	-0.50836E-05	0.000000	0.258431E-10	0.592206	0.186598E-13
5	3.29068	0.30389	0.98790E-01	0.004265	0.975948E-02	0.592217	0.704675E-05
6	3.45694	0.28927	-0.48920	0.021120	0.239316	0.592481	0.172796E-03
7	3.62910	0.27555	0.11366E-01	0.000491	0.129191E-03	0.592481	0.932816E-07
8	4.69560	0.21297	-15.599	0.673457	243.327	0.861072	0.175692
9	4.69763	0.21287	-5.5785	0.240841	31.1195	0.895423	0.224696E-01
10	6.17547	0.16193	-0.96116	0.041496	0.923831	0.896443	0.667045E-03
11	6.77591	0.14758	1.3552	0.058506	1.83643	0.898470	0.132598E-02
12	7.06809	0.14148	-2.4834	0.107218	6.16745	0.905278	0.445315E-02
13	7.32927	0.13644	-0.86014	0.037135	0.739837	0.906094	0.534193E-03
14	7.38449	0.13542	0.54046E-02	0.000233	0.292099E-04	0.906094	0.210908E-07
15	9.31033	0.10741	0.12441	0.005371	0.154784E-01	0.906111	0.111760E-04
16	9.38137	0.10659	8.0032	0.345525	64.0514	0.976813	0.462478E-01
17	9.65510	0.10357	-0.44526E-01	0.001922	0.198260E-02	0.976816	0.143152E-05
18	10.1367	0.98651E-01	-3.7488	0.161849	14.0537	0.992329	0.101473E-01
19	10.6593	0.93815E-01	-0.74981E-02	0.000324	0.562220E-04	0.992329	0.405946E-07
20	11.4920	0.87017E-01	2.6362	0.113815	6.94981	1.00000	0.501805E-02
sum					905.936		0.654123

***** MODAL MASSES, KINETIC ENERGIES, AND TRANSLATIONAL EFFECTIVE MASSES SUMMARY *****

MODE	FREQUENCY	MODAL MASS	KENE	EFFECTIVE MASS X-DIR	RATIO%	Y-DIR	RATIO%	Z-DIR	RATIO%
1	1.232	185.2	5550.	5.642	0.41	96.99	7.00	0.8248E-06	0.00
2	1.690	238.1	0.1343E+05	0.2531E-07	0.00	0.4384E-06	0.00	536.5	38.74
3	2.568	237.0	0.3085E+05	22.05	1.59	0.2101	0.02	0.1349E-04	0.00
4	3.015	565.7	0.1015E+06	863.7	62.36	66.20	4.78	0.2584E-10	0.00
5	3.291	404.9	0.8656E+05	0.3047E-03	0.00	0.6177E-03	0.00	0.9759E-02	0.00
6	3.457	51.29	0.1210E+05	0.1185E-04	0.00	0.7093E-05	0.00	0.2393	0.02
7	3.629	176.3	0.4583E+05	211.8	15.29	251.4	18.16	0.1292E-03	0.00
8	4.696	331.0	0.1441E+06	4.447	0.32	0.2524	0.02	243.3	17.57
9	4.698	242.2	0.1055E+06	34.95	2.52	1.878	0.14	31.12	2.25
10	6.175	119.8	0.9019E+05	0.4181E-05	0.00	0.1118E-03	0.00	0.9238	0.07
11	6.776	148.1	0.1343E+06	0.7974E-05	0.00	0.7959E-03	0.00	1.836	0.13
12	7.068	33.30	0.3284E+05	0.3045E-06	0.00	0.1824E-04	0.00	6.167	0.45
13	7.329	38.76	0.4110E+05	0.2345E-03	0.00	0.1224E-01	0.00	0.7398	0.05
14	7.384	201.0	0.2164E+06	3.217	0.23	57.13	4.12	0.2921E-04	0.00
15	9.310	247.3	0.4232E+06	17.10	1.23	9.058	0.65	0.1548E-01	0.00
16	9.381	323.9	0.5626E+06	0.4673E-02	0.00	0.7052E-03	0.00	64.05	4.62
17	9.655	99.82	0.1837E+06	1.944	0.14	0.3788	0.03	0.1983E-02	0.00
18	10.14	80.66	0.1636E+06	0.2951E-07	0.00	0.2102E-03	0.00	14.05	1.01
19	10.66	155.9	0.3497E+06	0.1085	0.01	79.71	5.76	0.5622E-04	0.00
20	11.49	319.8	0.8338E+06	0.1297E-08	0.00	0.2201E-01	0.00	6.950	0.50
sum				1165.	84.11	563.3	40.67	905.9	65.41

Modal masses and Participation factors for Shell model

***** PARTICIPATION FACTOR CALCULATION *****ROTX DIRECTION

MODE	FREQUENCY	PERIOD	PARTIC.FACTOR	RATIO	EFFECTIVE MASS	CUMULATIVE MASS FRACTION	RATIO EFF.MASS TO TOTAL MASS
1	1.27730	0.78290	0.16286E+06	0.398880	0.265220E+11	0.602435E-01	0.351415E-01
2	1.54149	0.64872	0.40828E+06	1.000000	0.166695E+12	0.438883	0.220870
3	2.54469	0.39298	-1642.3	0.004023	0.269723E+07	0.438889	0.357382E-05
4	2.56133	0.39042	12673.	0.031041	0.160615E+09	0.439254	0.212815E-03
5	3.03334	0.32967	231.27	0.000566	53483.7	0.439254	0.708657E-07
6	3.72803	0.26824	-0.36724E+06	0.899466	0.134863E+12	0.745589	0.178692
7	3.93706	0.25400	-4845.4	0.011868	0.234781E+08	0.745642	0.311083E-04
8	4.25655	0.23493	0.22338E+06	0.547133	0.499008E+11	0.858990	0.661184E-01
9	4.52441	0.22102	-17682.	0.043309	0.312662E+09	0.859700	0.414276E-03
10	4.97843	0.20087	-74257.	0.181877	0.551412E+10	0.872225	0.730619E-02
11	5.50196	0.18175	3197.8	0.007832	0.102257E+08	0.872248	0.135490E-04
12	6.58402	0.15188	-29089.	0.071247	0.846159E+09	0.874170	0.112116E-02
13	6.90455	0.14483	-30987.	0.075896	0.960191E+09	0.876351	0.127225E-02
14	7.42430	0.13469	0.11069E+06	0.271118	0.122529E+11	0.904183	0.162351E-01
15	7.55125	0.13243	-13547.	0.033181	0.183532E+09	0.904600	0.243179E-03
16	7.64992	0.13072	-0.15337E+06	0.375645	0.235222E+11	0.958030	0.311668E-01
17	8.52187	0.11735	-6488.3	0.015892	0.420978E+08	0.958125	0.557795E-04
18	8.79588	0.11369	0.12038E+06	0.294848	0.144916E+11	0.991042	0.192014E-01
19	9.85513	0.10147	44046.	0.107881	0.194004E+10	0.995449	0.257055E-02
20	9.98710	0.10013	44761.	0.109633	0.200356E+10	1.00000	0.265471E-02
sum					0.440246E+12		0.583325

***** PARTICIPATION FACTOR CALCULATION ***** Y DIRECTION

MODE	FREQUENCY	PERIOD	PARTIC.FACTOR	RATIO	EFFECTIVE MASS	CUMULATIVE MASS FRACTION	RATIO EFF.MASS TO TOTAL MASS
1	1.27730	0.78290	-8.7565	0.444137	76.6762	0.131273	0.567472E-01
2	1.54149	0.64872	-0.32764E-02	0.000166	0.107348E-04	0.131273	0.794471E-08
3	2.54469	0.39298	-0.28646E-02	0.000145	0.820619E-05	0.131273	0.607331E-08
4	2.56133	0.39042	-0.67687	0.034332	0.458158	0.132057	0.339077E-03
5	3.03334	0.32967	0.64402E-02	0.000327	0.414761E-04	0.132057	0.306959E-07
6	3.72803	0.26824	19.716	1.000000	388.711	0.797545	0.287680
7	3.93706	0.25400	0.78679E-02	0.000399	0.619045E-04	0.797545	0.458148E-07
8	4.25655	0.23493	0.70040E-02	0.000355	0.490556E-04	0.797545	0.363055E-07
9	4.52441	0.22102	0.93493	0.047421	0.874103	0.799041	0.646913E-03
10	4.97843	0.20087	0.11783E-02	0.000060	0.138832E-05	0.799041	0.102748E-08
11	5.50196	0.18175	0.17240E-03	0.000009	0.297207E-07	0.799041	0.219959E-10
12	6.58402	0.15188	0.11360E-01	0.000576	0.129040E-03	0.799042	0.955012E-07
13	6.90455	0.14483	1.6568	0.084033	2.74492	0.803741	0.203148E-02
14	7.42430	0.13469	-5.9445	0.301513	35.3376	0.864240	0.261530E-01
15	7.55125	0.13243	0.13307E-01	0.000675	0.177084E-03	0.864241	0.131058E-06
16	7.64992	0.13072	8.2335	0.417612	67.7910	0.980301	0.501713E-01
17	8.52187	0.11735	0.34598	0.017549	0.119705	0.980506	0.885921E-04
18	8.79588	0.11369	0.26723E-02	0.000136	0.714124E-05	0.980506	0.528515E-08
19	9.85513	0.10147	-2.3689	0.120153	5.61174	0.990114	0.415319E-02
20	9.98710	0.10013	-2.4030	0.121883	5.77451	1.00000	0.427365E-02
sum					584.100		0.432285

***** PARTICIPATION FACTOR CALCULATION ***** Z DIRECTION

MODE	FREQUENCY	PERIOD	PARTIC.FACTOR	RATIO	EFFECTIVE MASS	CUMULATIVE MASS FRACTION	RATIO EFF.MASS TO TOTAL MASS
1	1.27730	0.78290	-0.10463E-01	0.000433	0.109471E-03	0.115253E-06	0.810184E-07
2	1.54149	0.64872	24.159	1.000000	583.646	0.614471	0.431950
3	2.54469	0.39298	0.88340	0.036566	0.780396	0.615293	0.577562E-03
4	2.56133	0.39042	0.23831E-02	0.000099	0.567934E-05	0.615293	0.420321E-08
5	3.03334	0.32967	0.53570	0.022174	0.286975	0.615595	0.212387E-03
6	3.72803	0.26824	-0.11938E-01	0.000494	0.142519E-03	0.615595	0.105476E-06
7	3.93706	0.25400	-0.30547	0.012644	0.933123E-01	0.615694	0.690593E-04
8	4.25655	0.23493	16.578	0.686217	274.835	0.905044	0.203402
9	4.52441	0.22102	-0.21681E-01	0.000897	0.470070E-03	0.905045	0.347893E-06
10	4.97843	0.20087	-3.5697	0.147759	12.7426	0.918460	0.943061E-02
11	5.50196	0.18175	0.36144	0.014961	0.130640	0.918598	0.966848E-04
12	6.58402	0.15188	-1.7805	0.073702	3.17034	0.921936	0.234633E-02
13	6.90455	0.14483	-0.97480E-02	0.000403	0.950228E-04	0.921936	0.703252E-07
14	7.42430	0.13469	-0.24350E-03	0.000010	0.592905E-07	0.921936	0.438802E-10
15	7.55125	0.13243	0.47590	0.019699	0.226480	0.922174	0.167615E-03
16	7.64992	0.13072	-0.89800E-02	0.000372	0.806404E-04	0.922174	0.596810E-07
17	8.52187	0.11735	-0.32573E-02	0.000135	0.106101E-04	0.922174	0.785244E-08
18	8.79588	0.11369	8.5978	0.355886	73.9216	1.00000	0.547085E-01
19	9.85513	0.10147	-0.35502E-02	0.000147	0.126042E-04	1.00000	0.932820E-08
20	9.98710	0.10013	0.10639E-02	0.000044	0.113179E-05	1.00000	0.837626E-09
sum					949.835		0.702961

***** PARTICIPATION FACTOR CALCULATION *****ROTZ DIRECTION

MODE	FREQUENCY	PERIOD	PARTIC.FACTOR	RATIO	EFFECTIVE MASS	CUMULATIVE MASS FRACTION	RATIO EFF.MASS TO TOTAL MASS
1	1.27730	0.78290	0.57153E+06	0.447565	0.326644E+12	0.110275	0.397537E-01
2	1.54149	0.64872	215.88	0.000169	46602.1	0.110275	0.567163E-08
3	2.54469	0.39298	-766.97	0.000601	588240.	0.110275	0.715908E-07
4	2.56133	0.39042	-0.33870E+06	0.265234	0.114716E+12	0.149003	0.139613E-01
5	3.03334	0.32967	-459.55	0.000360	211186.	0.149003	0.257020E-07
6	3.72803	0.26824	-0.12770E+07	1.000000	0.163066E+13	0.699511	0.198457
7	3.93706	0.25400	-567.64	0.000445	322213.	0.699511	0.392144E-07
8	4.25655	0.23493	-1179.8	0.000924	0.139202E+07	0.699512	0.169414E-06
9	4.52441	0.22102	-0.51931E+06	0.406676	0.269687E+12	0.790558	0.328218E-01
10	4.97843	0.20087	-158.17	0.000124	25019.2	0.790558	0.304492E-08
11	5.50196	0.18175	-128.02	0.000100	16389.5	0.790558	0.199466E-08
12	6.58402	0.15188	-100.71	0.000079	10142.3	0.790558	0.123436E-08
13	6.90455	0.14483	0.44545E+06	0.348833	0.198426E+12	0.857546	0.241491E-01
14	7.42430	0.13469	0.48667E+06	0.381113	0.236849E+12	0.937506	0.288253E-01
15	7.55125	0.13243	-161.58	0.000127	26109.0	0.937506	0.317756E-08
16	7.64992	0.13072	-0.34185E+06	0.267701	0.116860E+12	0.976958	0.142222E-01
17	8.52187	0.11735	75008.	0.058739	0.562625E+10	0.978857	0.684734E-03
18	8.79588	0.11369	-1176.0	0.000921	0.138290E+07	0.978857	0.168303E-06
19	9.85513	0.10147	0.14588E+06	0.114235	0.212797E+11	0.986041	0.258981E-02
20	9.98710	0.10013	0.20334E+06	0.159235	0.413468E+11	1.00000	0.503204E-02
sum					0.296210E+13		0.360497